ANALYSIS AND SIMULATION OF SALIENT POLE SYNCHRONOUS GENERATOR WITH FINITE ELEMENT METHOD AND BLONDEL THEORY TO ENHANCE PERFORMANCE

BY

PAUL EDET OKON

BSc.(Eng.), M.Eng.

Reg. No. 20094704868

Presented to:

The Postgraduate School,

Federal University of Technology, Owerri.

IN PARTIAL FULFILMENT OF THE REQUIREMENTS FOR THE AWARD OF DOCTOR OF PHILOSOPHY (PHD.) DEGREE IN POWER SYSTEMS ENGINEERING IN THE DEPARTMENT OF ELECTRICAL AND ELECTRONIC ENGINEERING, SCHOOL OF ELECTRICAL SYSTEMS ENGINEERING AND TECHNOLOGY (SESET), FEDERAL UNIVERSITY OF TECHNOLOGY OWERRI, IMO STATE, NIGERIA

DECEMBER, 2022

Analysis and Simulation of Salient Pole Synchronous Generator with Finite Element Method and Blondel Theory to Enhance Performance

BY

PAUL EDET OKON

BSc., M.Eng.

Reg. No. 20094704868

Presented to:

The Postgraduate School,

Federal University of Technology, Owerri.

In partial fulfilment of the requirements for the award of Doctor of Philosophy (PhD.) Degree in Power System Engineering in the Department of Electrical and Electronic Engineering, School of Electrical Systems Engineering and Technology (SESET), Federal University of Technology Owerri, Imo State, Nigeria

SUPERVISORS:
Engr. Prof. E. N. C. Okafor
Engr. Dr. O. J. Onojo
Engr. Dr. N. Chukwuchekwa

December 2022

CERTIFICATION

I, OKON, PAUL EDET (**20094704868**), hereby certify that this research proposal, "Analysis and Simulation of Salient-Pole Synchronous Generator with Finite Element Method and Two-Reaction Theory to Enhance Performance" is original to me and has not been submitted elsewhere for the award of any degree.

Signature: 12/12/22
Engr. Prof. E. N. C. Okafor — Date
Principal Supervisor

Signature: 12/12/22
Engr. Dr. O. J. Onojo — Date
Co. Supervisor

Signature: 12/12/22
Engr. Dr. N. Chukwuchekwa — Date
Co. Supervisor

Signature: 12/12/22
Engr. Dr. N. Chukwuchekwa — Date
HOD Electrical/Electronic Engineering

Signature: ....
Engr. Prof. M. C. Ndinechi — Date
Dean School of Electrical System Engineering and Technology

Signature..... .....
Prof. C. C Eze — Date
Dean Post Graduate School

DEDICATION

This research is dedicated to God Almighty, the giver of life, knowledge; and the sole mentor of this PhD. program, my spiritual mother Virgin Mary, Mother of Perpetual Help and to my beloved family.

ACKNOWLEDGEMENTS

I express my sincere thanks to Late Professor T. C. Nwodo who introduced me into application of electromagnetic field to electrical systems especially rotating machinery during my Master's programme; also Late Professor C. C. Okoro who took over from him after his death. I am grateful to him as my mentor, lecturer, and former project supervisor who encouraged and contributed to this PhD. programme.

My sincere thanks go to my current supervisor, Engr. Prof. E. N. C. Okafor of Department of Electrical and Electronic Engineering, Federal University of Technology, Owerri, cosupervisors Engr. Dr. O. J. Onojo and Engr. Dr. N. Chukwuchekwa of the same Department for accepting to guide me in modifying this work to what it is now. My interactions with them motivated and gave me a desire for further work on electrical machines modelling and analysis. Also want to sincerely extend my thanks to the Dean, School of Electrical Systems Engineering and Technology (SESET), Engr. Prof. M. C. Ndinechi. I cannot wait to mention my former Head of Department, Engr. Prof. I. E. Achumba, whose encouragement added value to this work. I will also like to appreciate all the senior lectures of the Department of Electrical Engineering in persons of Engr. Prof. (Mrs.) G. A. Chukwudebe, Engr. Prof. F. K. Opara, Engr. Prof. (Mrs) G. N Ezeh, Engr. Prof. D. O. Dike, Engr. Prof. F. I. Izuegbunam, Eng. Dr.

C. C. Mbaocha, Engr. Dr. L. O. Uzoechi, Engr. Dr. C. K. Agubor, Engr. I. O. Akwukwaegbu, Engr. Dr. M. Olubiwe, Engr. Dr. O. C. Nosiri, Engr. Dr. S. O. Okozi and other lecturers of the same Department for their moral and individual supports in making this research work a success.

I also want to thank my friends, Mr. Kubiat Akpan and Mr. Idongesit Oduok, for all their supports in form of typing and formatting the work as many times I was asked to update to the level it is now. Many thanks go to my late parents, Mr. Chad Okon Udoh and Mrs. Anthonia O. Udoh whose prayers and those of my entire family aided me to accomplish this feat. I am indebted to my dear wife, Mrs. Cecilia Paul Okon and all my children, Genevieve, Chad, Maryann, and Celine Paul Okon, upon all odds, they stood by me especially during the period

I was left without a Supervisor as a result of Professor C. C. Okoro's death. They all gave me moral support that strengthened me to continue with this work.

My heartfelt gratitude goes to Professor Umana Itaketo for going through the work with useful comments and feedback.

TABLE OF CONTENTS

LIST OF TABLES

LIST OF FIGURES

LIST OF ABBREVIATIONS AND SYMBOLS

A - Magnetic Vector Potential

A.C. - Alternating Current

abc - Three Phase System

AutoCAD – Autodesk Computer Aided Design

B - Magnetic Flux Density

BEM - Boundary Element Method

BP - Blondel-Pasle D.C

- Direct Current d-axis

- Direct Axis

dq0 - Direct, Quadrature and Zero System

E - Electric Field Intensity

E□ - Phase Voltage

E_c - Instantaneous Coil Voltage

FDM - Finite Difference Method

FEA - Finite Element Analysis

FEM - Finite Element Method

FEMM - Finite Element Method Magnetics

H - Magnetic Field Intensity

J - Current Density l_g -

Length of air gap

MMF (**F**) - Magneto-motive Force

mvp - magnetic vector potential n -

Normal unit vector N - Number of

turns p - Pole Pair

p.f - Power Factor
q-axis - Quadrature Axis

R - Reluctance

RMxprt – Rotating Machine Expert

SCR - Short Circuit Ratio

SPSG - Salient-Pole Synchronous Generator

T - Torque

WFM – Winding Function Method αβ - Alpha-Beta System Ψ - Magnetic Flux Linkage
ω - Angular Frequency - Flux Linkage
 - Magnetic Flux

 - Permeability

 - Vector Operator

θ_e - Electrical Degrees

θ_m - Mechanical Degrees

K - Output coefficient

B_{ar} - Specific magnetic loading

N_s - Speed of generator (rps)

L - Gross length of the armature D -

Diameter of armature q - Specific electric

loading X_l – Leakage reactance X_{ad} –

Armature direct - axis reactance X_{aq} –

Armature quadrature – axis reactance

X_m – Magnetizing Reactance

ABSTRACT

Synchronous generators are the only means of converting mechanical energy to electrical energy for bulk electrical power generation. As a result of saturation in its electromagnetic structure, prediction of its performance often involves approximations that seek to account for the effect of saturation. Therefore, it is necessary to develop an accurate method for prediction of the field patterns in magnetic structure to ensure precise performance evaluation. In order to compute the magnetizing reactance of salient-pole synchronous generator apart from using finite element method, a modified winding function approach was developed in this reseach, which utilize the actual winding distribution and the shape of the pole arc. This research seeks to utilize the finite element variational method (finite element method magnetics) for magnetostatic computation for magnetic field distribution in the air gap for cylindrical and salient-pole type generator. The comparative analysis of the magnetic field distribution is used to illustrate the Two Reaction Theory. The obtained results indicate magneto-motive force comparison of salient 4-pole and cylindrical rotor generator, which clearly demonstrate Andrew Blondel Theory (Two-Reaction Theory). ANSYS Maxwell also is utilized in this research to simulate and analyze salient-pole synchronous generator in order to evaluate the generator performance through electromagnetic field computation. The ANSYS Maxwell results include, moving torque, winding currents, magnetic flux linkages, induced voltages, self and mutual inductances, damper bar voltage/current and others characteristic of synchronous generator under no-load, load and three phase short circuit conditions. The results obtained agreed with the conventional acceptable parameters for the salient-pole synchronous generator.

Keywords: Salient – pole, Inductance, Generator, Air-gap and Andrew Blondel Theory.

CHAPTER ONE

INTRODUCTION

1.1 Background of Study

Synchronous generators have become sources for bulk power generation. They are classified into two different types:

i. Round or non-salient pole rotor structure – High-speed generator (commonly called Cylindrical Rotor or Turbo Synchronous Generator) ii. Salient pole rotor – Low speed generator (Hydroelectric Synchronous Generator) In a secure power system, synchronous generators must operate within stability limits to maintain its synchronism. This is steady state operation. It is therefore expedient to predict and investigate the behaviour of these generators during the abnormal or transient phenomena for better analysis and design.

The non-uniform air gap of Salient pole generators makes air-gap inductances a timevarying quantity with respect to the rotor angular position. This makes the analysis of such generators more complex than cylindrical rotor synchronous generators of a uniform air-gap. Therefore, the inductances of salient-pole generators can be resolved into two different components based on Two Reaction Theory propounded by Andrew Blondel in 1913 (Ghanim, D., 2012). The principle behind the Two Reaction Theory is for the armature magneto-motive force (MMF) and fluxes in a salient-pole synchronous generator to be resolved into two different space components. The Direct-Axis (d-axis) is the magnetic axis of the field winding while the Quadrature Axis (q-axis) is at the interpolar space that lags the direct axis by 90°.

Analysis of Salient Pole Synchronous Generators steady state and transient performance anchor on the prediction of the reactances and flux patterns within the generator inner structure especially at the air gap between rotor and stator. Therefore, precise identification and computation of these parameters are essential. In the past, they have been many advancements

in predicting these parameters through analytical computation and tests. Presently, modern numerical methods have been deployed through the use of electromagnetic field analysis with boundary value equation based on actual geometrical configuration of the generator structure. This research uses Finite Element Method Magnetic (FEMM) and ANSYS Maxwell to obtain salient four-pole synchronous generator reactances under steady and transient states. The analytical method has not been very accurate due to approximation of the flux pattern within the region of computation, irregular geometry and non-linear magnetic materials associated with the generator. Therefore, the advent of Advanced Numerical Method and Software (ANSYS Maxwell and Finite Element Method Magnetic) give the computational capability to analyse and compute the parameters of electrical machines more accurately and timely.

Different methods have been deployed over the years to handle this task. These are the Finite Difference Method (FDM), Boundary Element Method (BEM), Winding Function Method (WFM), and Finite Element Method (FEM). Winding Function Method and others use geometrical parameters without considering generator core saturation and geometrical configuration. However, designers due to its ability to handle the complex internal structure and non-linear materials present in the generator are increasingly using the FEM, which is based on magnetic field computation using generator geometry dimensions and materials.

The Finite Element Method has its origin in the field of structural analysis. Although the earlier mathematical treatment of the method was provided by a Mathematician, R. Courant in 1943 (Brauer, J. R. 1993), the method was not applied to electromagnetic problem until 1968 when he proposed breaking continuum problem into triangular regions and replacing the field with piecewise approximation within the triangles. This method is applied to other fields of engineering such as heat transfer (mechanical), structural mechanics (civil) and fluid flow

(hydraulic), (Sadiku, 1989). Many credits are attributed to people like Turner et al in application of FEM to aerodynamic problems on aircrafts, (Brauer, J. R. 1993). Professor Ray Clough at the

University of California – Berkley's Civil Engineering Department developed this method and in his paper presentation in 1960 coined the term "Finite Element Method". Recent trends in the design of electrical machinery and electromagnetic structures for increased power densities at the same time improve reliability of operation called for stringent specifications and a demand for economy in the size and weight of these machines have been expressed, (Chari, 1980). This in turn, has necessitated the development of accurate methods for predicting the performance characteristics of these machines during the design stage. The performance indicators for synchronous generators under steady state and transient conditions are the reactance obtained at transient and steady state periods. Other parameters considered under these two conditions are the moving torque, winding currents, magnetic flux linkages, induced voltages, currents, leakages, self and mutual inductances, which play a dominant role in electrical machine performance and stability. In order to evaluate these quantities with precision, accurate and detailed electromagnetic field mapping will be carried out under various operating conditions.

Classical analysis methods and analogue technique have proved unsatisfactory except for simplified geometrical structures and boundary conditions, (Chari, 1980). Therefore, the need for numerical solution was recognized even in the early stages of the design art. Nevertheless, only the advent of large-scale digital computers has enabled the development and extensive use of such methods for solving the field distribution in electrical machinery and apparatus with details and accuracy. As already mentioned, there are two principal methods currently used for modelling and determining these critical parameters of salient pole synchronous generators. This research utilizes Finite Element Method Magnetic (FEMM) and ANSYS

Maxwell, which uses variational formulation of partial differential equations of the field problem in terms of an energy function and minimizing the function to obtain approximate solutions.

1.2 Statement of Problem

Synchronous generators as important as they are, have analysis and modelling setbacks especially for the Salient-Pole Synchronous type. Unlike Cylindrical-rotor type where the airgap geometry is uniform, the Salient-Pole type has non-uniform gap, which cause the air-gap inductances, and reactances to be time varying based on rotor angular position with regard to armature magneto-motive force (Ghanim, D 2012).

Scanty research work had been carried out in this area of Two-Reaction Theory without application of trigonometric derivation of armature magneto-motive force components around

the air gap geometry from the orthogonal rotor axis, also demonstrating magnetic density distribution with finite element analysis.

In the past, modelling and analysis of Salient-Pole Synchronous Generator had been carried out using Cylindrical-rotor theory approximation (McPherson, G 1981). Due to the complexity of its analysis, Andrew Blondel came up with the Two-Reaction Theory formulation where all the generator variables will be separated into two orthogonal components acting along two different axes on the Salient-Pole rotor.

The Two-Reaction Theory is therefore, mathematically proven and magnetically illustrated to convey Andrew Blondel's concept. The realization of this illustration is to adopt an advanced numerical method called Finite Element Method to magnetically demonstrate this theory through magneto-motive force (MMF) field mapping, display the computational region and plots at various rotor angular positions.

The applicable softwares to illustrate this are Finite Element Method Magnetic (FEMM) and ANSYS Maxwell which perform magneto-static and transient time-stepping computation in the analyzed region of the Salient-pole Synchronous Generator respectively.

1.3 Objectives of Study

The aim of this research is to analyse and simulate Salient Pole Synchronous Generator with Finite Element Method and Two-Reaction Theory to Enhance Performance. The specific objectives are:

(i) To obtain or provide detail design specification for Salient-Pole Synchronous Generator

(ii) To develop and prove a mathematical relationship between generated armature, MMF and orthogonal (d-axis & q-axis) MMF of the rotor.

(iii) To obtain physical data of the Salient-Pole Synchronous Generator geometry from AutoCAD and ANSYS Maxwell (RMxprt).

(iv) To simulate, plot and analyse generated Salient-Pole Synchronous Generator parameters (i.e. Moving Torque, Winding Current, Self and Mutual Inductances,

Magnetic Flux Linkages, Induced Voltages and Current, Inductances, Torque, Winding Phase Currents and Voltages and Induced Voltage and Current with FEMM and ANSYS Maxwell) for performance analysis.

(v) To collect simulated data of a Salient-Pole Synchronous Generator (SPSG) for performance analysis

(vi) To illustrate magnetically the Two-Reaction Theory through magnetic field density spatial distribution around air gap at various rotor angles

(vii) To validate the results obtained through Magneto-static and Transient Time – Stepping Finite Element Method with other relevant methods such as Winding Function Method and compare the results with recommended generator design standards.

Results obtained from these objectives will be used to predict the synchronous generator behaviour and performance through Magneto-static and Magneto-dynamic Finite Element

Methods.

1.4 Significance of Study

Modelling and analysis of Electrical Machines were carried out by analytical method in the past and this process has been cumbersome especially the salient pole synchronous machine. Data obtained for modelling salient pole synchronous machine were all approximated based on cylindrical or round rotor synchronous machines. This challenge brought about the emergence

of the Two Reaction Theory by Andrew Blondel in 1913, to facilitate the analysis of salient pole synchronous machines.

In practice, electrical machine systems are saturated making its behaviour nonlinear. Consequently, electrical machines calculations are based on approximations that typify the operating point. Inaccuracies resulting from these approximations make it necessary to employ high precision analytical tool – the finite element method. With the advent of high-speed computing system, the advanced numerical method: the finite element method was introduced to deal with nonlinear, irregular structure and predominate saturation nature of magnetic materials of the electrical machines in solving this complex electromagnetic field problem. The combined finite element method and Two Reaction Theory was accomplished by obtaining the more accurate results.

Therefore, this study is aimed at obtaining steady state, transient and fault behaviour of synchronous generators with the help of magnetic flux distribution at the air gap.

The ultimate purpose of the study is to demonstrate the practical application of Two Reaction Theory and obtain generator reactance under steady state and transient condition from TimeStepping Finite Element Method for appreciation by Electrical Power System Students and Engineers. The advantage of this reactance plays a vital role in generator behaviour analysis and modelling.

1.5 Scope of Study

The scope of this research is limited to the use of Finite Element Method Magnetics (FEMM) and ANSYS Maxwell software for the analysis and simulation of the Salient-Pole

Synchronous Generator.

It also covers the mathematical derivation of Andrew Blondel – Two Reaction Theory from first principles using trigonometry functions. Winding Function form part of this research for the computation of generator reactance in order to validate the results.

CHAPTER TWO

LITERATURE REVIEW

2.1 Historical Overview of Finite Element Method and Two-Reaction Theory of Salient-Pole Synchronous Generator

Tandon et al, (1980) used Finite Element Method with considerable success in the areas of structural mechanics, fluid flow, and heat conduction and now serves as a basis for many of today's large general-purpose structural and aero elasticity computer programs, (Ferrari *et.al*, 1996). The extension of the usage into solving electromagnetic field problems was first carried out in 1968 (Sadiku, M 1989). Tandon et al, (1980) affirmed that F. W. Carter, who analyzed the magnitude of flux fringing in an open slot facing a smooth pole face, first determined the magnetic field distribution in the air gap of an electrical machine. Chari, (1980) also confirmed that a general and topologically unrestricted variational formulation of the electromagnetic field problem in electrical machine. (Reece and Preston, 2000) also presented this in their book recently. Many electrical machines field problems involving the solution of magneto-static and magneto-dynamic fields are taking into account the geometric complexity and non-linearity of the iron part of the machine. Wang and Demerdash, (1991) mentioned in their paper how the problem of electrical machines was solved successfully and accurately using two dimensional and Cartesian geometries with a single component vector potential formulation.

Traditionally, electrical machine parameters will be evaluated from formulae based on approximations, to account for saturation in the actual flux distributions in the machine. A more accurate prediction of the machines flux pattern and performance characteristics using ANSYS Maxwell and Finite Element Magnetic Method will be employed to enhance one's skill to design and understand the electromagnetic behaviour of synchronous generator. This is possible with the advent of modern digital computer systems where many unknowns forming the discretized regions of the cross section of the synchronous generator are numerically solved to

obtain magnetic vector potential at these regions. The results are displayed in the form of magnetic flux distribution along the magnetic path in the cross section. The analysis of the magneto dynamic and static field mapping of electrical machines involve field computation of the iron part and the air gap of the machines under static and physical rotational conditions.

Hameyer and Belmans, (1999) explained "Time-Stepping Finite Element Method", as applied to this research, to solve elliptic and diffusion equations expressed as Poisson's Equation derived from electromagnetic field Maxwell's equation. The equations relate magnetic vector potential **A**, magnetic flux density **B**, magnetic field intensity, **H**, electric field intensity **E** and current density **J** to obtain steady state time harmonic equation in order to solve transient magnetic field problem. The following areas are previously executed work done about the research topic. Most of the mathematical equations used in simulating the electric and dynamic behaviour of a salient pole synchronous machine are highly nonlinear as a result of time-varying inductances due to rotor position. This leads to more complexity in the analysis of these machines. Salient Pole Synchronous Machine variables (flux linkages, currents, and voltages) are changed in order to eliminate the time varying inductances from voltage equations of synchronous machine. This technique is referred to as *Reference Frame Theory*.

Andrew Blondel suggested a new technique in 1913, which helped facilitate the analysis of Salient-Pole Synchronous Machine. This is referred to *Blondel Two Reaction Theory*. This theory has opened doors to several new research areas especially in synchronous machines analysis and design.

AIEE member, Doherty and Nickle, who included effect of MMF harmonics in both direct and quadrature axis, further exploited additional elucidation on Two Reaction Theory,

i. Park, R. et al (1929) developed a new means of analyzing synchronous machine and simplified the analysis by proposing a mathematical transformation that refers three phase stator variables into new variables in a frame of reference fixed on a salient-pole rotor whose imaginary axis are known as direct, quadrature and zero axis (dq0 coordinate system). This transformation is now known as *Park's Transformation*. ii. Zhang Liu et al (1989) also proposed another extension of the Blondel-Park (BP) transformation that was referred to in their work as the *Extension Blondel Park Transformation*. The new transformation is trying to not only consider electric subsystem of the ac machine as Park's transformation did, but also consider the dynamics of mechanical variables in the machine's analysis.

iii. Finite Element Method Magnetic (FEMM) is customized Finite Element Analysis software used in this work. It gives the computational capability to analyse and compute from electrical machine geometry, parameters more accurately and, timely. Finite Element Analysis has gained more grounds in the areas of electrical machine simulation and design especially in commercial design of ac machines.

iv. A Mathematician, Courant, R. L in 1943 provided earlier mathematical treatment of the method (Brauer, J. R 1993). Finite Element Analysis has been used in many electromagnetic field problems using Maxwell equations to optimize, simulate and analyze electric machines. The method was not applied to electromagnetic problems until 1968 (Sadiku, M 1989). Courant in his paper proposed breaking the continuum problem into triangular regions and replacing the field with piecewise approximation within the triangles (Brauer, J. R 1993).

2.2 Major Contributions on the Topic

Many of the provided literature form parts of this research review, other scholars in area of synchronous machine performance prediction, analysis and design are also summarized in the Table 2.1:

Table 2.1: Major contributions on the topic

Author(s)	Title of Paper	Findings/Result	Gap
Deng and Demerdas (1996)	A Couple FiniteElement State-Space Approach for Synchronous Generators	Generator performance obtained from Time Stepping Finite Element Model with effect of space harmonic to magnetic saturation	Couple circuit was not clearly defined and simulated
Xiao, Zhou, Wang and Yang (2017)	Finite Element Computation of Transient Parameters of a Salient-Pole Synchronous Machine	A novel method was used with Finite Element Analysis to compute leakage inductances in d-q model with external circuit	Additional software PYTHON and Visual Basic were used to control FE but algorithm for computation was not explained.

Liu, Xu, Mingzhu Shangguan1	Finite Element Method Simulation of a High Speed Wound-Rotor Synchronous Machine	Synchronous machine parameters were obtained from analytical method and the result validated/consolidated using finite element method.	The obtained parameters were few. Only self / mutual inductances and torque were plotted.

Author(s)	Title of Paper	Findings/Result	Gap
TANG, K.Y., Cosgriff, Robert L., AIEE Rotating Machinery	Two-Axis Method of Analyzing Electric Machines	Demonstrate the basic 2-pole machine which will be analyzed. It consists of a stator with two windings displaced by an angle alpha.	The Two Reaction Theory concept was not addressed.
Kolondzovski International PhDseminar Computation of Electromagnetic Fields, 23-28 September 2004	Evaluation methods for calculating synchronous generator reactances	Magneto-statics finite element simulation was conducted. Magnetic field plotting of various transient stages was presented.	Magneto-dynamics was not presented in the work.
Misir, Raziee, and Ponick	Determination of the Inductances of Salient Pole Synchronous Machines Based on the Voltage Equation of a Single Coil in the Stator	Analytical method was adopted to computer self and mutual inductances between the stator and field windings, also between damper and field windings.	Time-stepping finite element method was not used for result comparison.

	Winding		
Aiberto Tessarolo, Cristina Bassi, and Davide Giulivo. **IEEE, (June 2012)**	Time-Stepping Finite-Element Analysis of a 14MVA Salient-Pole Shipboard Alternator for Different Damper Winding Design Solutions	A time-stepping FE was used to simulate a 14MVA salient pole alternator with damper winding	Numerous results were obtained without application of external circuits.

Author(s)	**Title of Paper**	**Findings/Result**	**Gap**
Nabeta, Dietrich, Rocco IEEE (1999)	Harmonic Analysis of a Synchronous Machine Feeding a Non-Linear Load by Time-Stepping Finite Element Simulation	The time stepping finite element simulation was carried out in synchronous machine feeding a fully controlled rectifier. The harmonic waveforms were plotted and harmonic content measured.	Scanty results were presented and with no significant plots to illustrate the work

Nabeta IEEE Transaction on Magnetics Vol. 31 (1995)	A Non-Linear Time-Stepped Finite-Element Simulation of a Symmetrical Short-Circuit in a Synchronous Machine	2-Dimensional, nonlinear, time-stepped finite element simulation on symmetrical short circuit in a synchronous machine. Computed current and torque result were presented.	Only currents and torque results were presented. No other parameters were shown.
Shieng, L. Ching PhD Thesis, University of Edinburgh (October 1948)	The Two-Reaction Theory of Salient – Pole Synchronous Machines	Analytical explanation of the theory was completely laid out. Phasor diagram plotted form the result. Park's transformation and equations were also presented.	Some computation results were based on various assumptions. Finite element technique was not applied to the analysis.

Author(s)	Title of Paper	Findings/Result	Gap
Bargallo, Llaverias, J. De Blas, A., Martín, H., Piqué, R.	Main inductance determination in rotating machines using analytical and numerical calculation	Electrical machines inductances were obtained through analytical and numerical methods of finite element method.	Magneto-statics finite element was used as the only numerical technique instead of magnetodynamic method.

Shieng, L. Ching PhD Thesis, University of Edinburgh (October 1948)	The Two-Reaction Theory of Salient – Pole Synchronous Machines	Analytical explanation of the theory was completely laid out. Phasor diagram plotted form the result. Park's transformation and equations were also presented.	Some computation results were based on various assumptions. Finite element technique was not applied to the analysis.
Doherty, R, E and Nickle C. A, AIEE Trans., Vol. 45, pp. 912-947, June 1926	Synchronous Machine – Part 1 – An Extension of Blondel's Two Reaction Theory	Further modification the Two Reaction Theory and include new consideration to include the effect of MMF harmonics in both direct and quadrature axis.	No exposition of magnetic field illustration by Boundary Value Method.
Onah, C. O. and Reuben, J. , 2016	Dynamic n of Modelling and Simulation of Salient Pole Synchronous Motor Using Embedded MATLAB	MATLAB/Simulink model is used to develop and simulate the synchronous machine model. The result produced all the machine state variable both in transient and steady state. This approach can also be used to obtain feasible solution of any electrical machines.	The model is using MATLAB/Simulink architecture which does not explicitly demonstrate the behaviour of the machine under steady and transient state. The electromagnetic field presentation will generate real time and physical demonstration.

Author(s)	**Title of Paper**	**Findings/Result**	**Gap**

Prentice B. R. AIEE Trans., May 1937	**Synchronous Machine Reactance**	The paper has Part I, II & III which deals with concept of flux and inductances to application to synchronous machines and finally formation of differential equations and expression to reactance in terms of self and mutual inductances ending with machine equations.	Utilizing analytical method to derive these equations which makes the process cumbersome instead of using modern numerical method of Finite Element Method.
Helmer, R., Duck, P., and Ponick, B., 2010	**Determination of Transient Reactances of Salient Pole Synchronous Machines with Analytical and Numerical Methods**	Computation of transient reactances for Salient Pole Synchronous Machines were numerically obtained using Finite Element Method process. The calculation for transient analysis was faster than timestepping methods where the complete differential equation system of the machine will be solved for different field situations.	The work employed FEM tool – FEMAG without much emphasis on the two reaction theory and Park's transformation process of converting three phase to two phase variable.

2.3 Maxwell's Equations

Three basic Maxwell's (electromagnetic) equations are expressed in differential form as in Equations 2.1, 2.2 and 2.3.

$\nabla \times \mathbf{H} = \mathbf{J}$ 2.1

$\nabla \cdot \mathbf{B} = 0$ 2.2

$\nabla \times \mathbf{E} = -\frac{\partial \mathbf{B}}{\partial t}$ 2.3

and the relationship

$\mathbf{B} = \mu\mathbf{H}$

Where **B** is the magnetic flux density, **H** is the magnetic field intensity, **J** is the current density and μ is the material absolute permeability. If a vector field has no divergence, that vector field is the curl of some other vector fields (Prentice, B., 1937). Therefore,

$\nabla \cdot \mathbf{B} = 0$ means that **B** is the curl of another vector field.

Let that other vector field be **A**.

Since $\nabla \cdot \mathbf{B} = 0$, it implies that there exists a magnetic vector **A** such that $\mathbf{B} = \nabla \times \mathbf{A}$.

2.3.1 Vector Magnetic Potential Formation

It is a well-known fact that any vector field that has no divergence is a curl of some other vector field. In this case, that vector is referred to as vector magnetic potential, **A**. A current in the *z* direction produces $\mathbf{A}_z$ only, and *x* and *y* component of **B**. $\mathbf{A}_z$ is then related to the flux circulating in the *x*, *y* plane, per unit length in the *z* direction: it has the units of Webers per metres.

Thus, for a two-dimensional field, **A** can be treated as a scalar quantity. The magnetic flux flowing in a conducting material carrying current has its permeability μ greater than that of copper conductor of permeability μ_o. Solving for the magnetic vector potential **A**, the components of the magnetic flux density are obtained by finding the derivatives $\frac{\partial \mathbf{A}}{\partial y}$ and $\frac{\partial \mathbf{A}}{\partial x}$ as shown below.

$\mathbf{B} = \nabla \times \mathbf{A}$ 2.4

$$\mathbf{B} = u_x \frac{\partial \mathbf{A}}{\partial y} - u_y \frac{\partial \mathbf{A}}{\partial x} \quad 2.5$$

With current density $\mathbf{J}_z$ only, and hence $\mathbf{A}_z$ only, and no variation of these quantities in the *z* direction,

$$\mathbf{B}_x = \frac{\partial \mathbf{A}_z}{\partial y}, \quad \mathbf{B}_y = -\frac{\partial \mathbf{A}_z}{\partial x} \quad 2.6$$

$$\nabla \times \mathbf{H} = \mathbf{J}_z \quad 2.7$$

$\mathbf{J}_x$ and $\mathbf{J}_y = 0$, do not exist

Therefore, only $\mathbf{J}_z = \frac{\partial \mathbf{H}}{\partial x} - \frac{\partial \mathbf{H}}{\partial y}$ exist 2.8 Using

$\mathbf{B} = \mu\mathbf{H}$ and substituting equation 2.8 into the above equation gives

$$\frac{\partial}{\partial x}\left(\frac{1}{\mu}\frac{\partial A_{\hat{z}}}{\partial x}(x,y)\right) + \frac{\partial}{\partial y}\left(\frac{1}{\mu}\frac{\partial A_{\hat{z}}}{\partial y}(x,y)\right) = J_{\hat{z}}(x,y) \quad 2.9$$

And so, for fixed μ,

$$\frac{\partial^2 A_{\hat{z}}}{\partial x^2}(x,y) + \frac{\partial^2 \partial A_{\hat{z}}}{\partial y^2}(x,y) = -\mu J_{\hat{z}}(x,y)$$(Bastos J. P. A. and Sadowski, N. 2003).

In general, non-linear and time-dependent equations for 2-D simulation model of synchronous machine is given by

$$\frac{\partial}{\partial x}\left(\frac{1}{\mu}\frac{\partial A_{\hat{z}}}{\partial x}(x,y)\right) + \frac{\partial}{\partial y}\left(\frac{1}{\mu}\frac{\partial A_{\hat{z}}}{\partial y}(x,y)\right) = J_{\hat{z}}(x,y) + \sigma\frac{\partial A_{\hat{z}}}{\partial t}(x,y)$$(Bastos J. P. A. and Sadowski, N. 2003). 2.10

Which is **Poisson's Equation**

2.4 Finite Element Method

Finite Element Method appears to be a widely used method for solving partial differential equations with complex geometry. This is possible by transforming a problem of a complicated form in a continuous region into one in which the region is discretized and an

approximate solution is obtained for the field quantity at the discretized point (the nodes). The potential function is approximated in those finite elements by simple shape functions mainly linear or quadratic. The results are a large linear system of equations (Hameyer, K and Belmans, R 1999). Thus, a large set of algebraic equations has to be derived to replace the governing differential equation. Using triangular elements for two-dimensional field problems and tetrahedral in three dimensions, a very good approximation of the geometry is obtained. The Finite Element Method is the most flexible method when compared to other techniques like finite difference method mentioned before.

2.4.1 Mathematical Formation

Finite Element Method as applied in this research is used to solve a derived electromagnetic field problem of Poisson's equation from basic magneto-static and transient time-dependent Maxwell equations. The equations relate magnetic vector potential **A**, magnetic flux density **B** and magnetic field intensity **H**, electric field intensity E and current density J to obtain the Poisson's equation. The basic steps used in solving these magnetic equations have been numerated in vector magnetic potential formulation discussed above.

2.4.2 Field Computation and Numerical Method

Partial differential equations such as elliptic parabolic or hyperbolic equations are commonly used in different fields of engineering. For this work, elliptic equations will be applied for the computational process and are classified into magneto-static and transient timestepping problems as explained below.

2.4.2.1 Magneto-static Problem

A Partial Differential Boundary Equation expressed in a magnetic vector form as Twodimensional Poisson Equations of Finite Element Method derived from Maxwell's Equations formulation as presented in equations 2.11 and 2.12 as magneto-static problem of the

magnetic field mapping and distribution in the analysed region (computational region) of a Salient-Pole Synchronous machine.

$$\frac{\partial}{\partial x}\left(\frac{1}{\mu}\frac{\partial A}{\partial x}(x,y)\hat{z}\right)+\frac{\partial}{\partial y}\left(\frac{1}{\mu}\frac{\partial A}{\partial y}(x,y)\hat{z}\right)=-J(x,y)\hat{z} \quad 2.11$$

$$\frac{\partial^2 A}{\partial x^2}(x,y)\hat{z}+\frac{\partial^2 A}{\partial y^2}(x,y)\hat{z}=-\mu J(x,y)\hat{z} \text{(Bastos J. P. A. and Sadowski, N. 2003)} \quad 2.12$$

2.4.2.2 Transient Time-Stepping Problem

In general, non-linear and time-dependent equation for 2-D simulation model of synchronous machine is given by equation 2.13.

$$\frac{\partial}{\partial x}\left(\frac{1}{\mu}\frac{\partial A}{\partial x}(x,y)\hat{z}\right)+\frac{\partial}{\partial y}\left(\frac{1}{\mu}\frac{\partial A}{\partial y}(x,y)\hat{z}\right)=-J(x,y)\hat{z}+\sigma\frac{\partial A}{\partial t}(x,y)\hat{z} \quad \text{(Bastos J. P. A. and Sadowski, N. 2003)} \quad 2.13$$

Where:

μ_0 = permeability of free space

μ_r = relative permeability

μ = absolute permeability = $\mu_0\mu_r$

$A(x,y)\hat{z}$ = magnetic vector potential normal to the section of the machine

$J(x,y)\hat{z}$ = current density vector normal to the region

σ = conductivity of the studied region under transient time-stepping simulation.

Reece and Preston, (2000) in their paper showed how vector magnetic potential is of great value when solving two-dimensional problems containing current carrying areas. This equation, though reformulated by variational calculus, in the finite element method, and firstorder triangular elements are used to discretize the field region, resulting in a set of linear algebraic equations. These linear simultaneous equations are solved using Newton-Raphson technique to obtain the magnetic vector potential.

Bastos and Sadowski, (2003) in their book explained a two-dimensional

electromagnetic field mapping, where the excitation current is time-dependent where there are existing conducting materials. A non-conducting magnetic circuit (i.e., a laminated core of the rotor) and copper conductor generate eddy currents in the direction perpendicular to the plane of the stator core housing the winding.

Two dimensional problems will be considered and solved. The analytical way for solving these problems often has to face complicated mathematical process. Hence, the numerical way is preferred as there are powerful means of carrying out this computational process using software.

Hoole, (1989) explained that electromagnetic devices such as electrical machines have their behaviour governed by the electromagnetic field which flow in them; and in turn obey

Maxwell's equations. In order to predict the performance characteristics, it is necessary in the design of these devices to solve the Maxwell equations governing the fields.

In the real world, which involves complex geometries and electromagnetic configurations numerical techniques yield far more accurate solutions than are possible by classical analysis, in view of the latter methods dependence on simplifying assumptions. To solve a technical field problem numerically, an appropriate method has to be chosen. The two most important groups of numerical methods are the finite difference and finite element methods, but for this work, finite element methods will be considered.

Poisson equation is commonly met in different field of engineering such as temperature distribution, electric current flow etc. The analytical method for solving these equations often has to face complicated mathematical obstacles. Hence, the numerical method is preferred due to availability of powerful calculation using digital computers.

2.5 Finite Element Method Magnetics (FEMM)

Finite Element Method Magnetics (FEMM) is a suite of programs for solving low frequency electromagnetic problem on two-dimensional planar and axi-symmetric domain (Brauer, N 1993). The software deals with linear/non-linear magneto static problems, liner/nonlinear time harmonic magnetic problems, and linear electrostatic problems. This program is specifically used in this research for illustration of Two Reaction Theory by comparing the magnetic flux density of the Salient-Pole and Cylindrical type Synchronous

Generator generated from FEMM at various rotor angles.

Finite Element Method Magnetic is divided into three parts (Meeker, D 2004):

2.5.1 Pre-Processing

i. Creation of model from AutoCAD ii. Addition of materials to the geometry of the generator model iii. Definition of materials for each region of the geometry iv. Creation of boundary conditions on the model

v. Mesh generation

2.5.2 Processing

Solving the computational space problem by relevant Maxwell's equations and obtaining the field distribution in the analyzed domain of the salient pole synchronous generator at arbitrary chosen excitations and loading conditions.

2.5.3 Post-Processing

Presentation of the characteristics, as well as parameters, of the analyzed salient pole synchronous generator. Finite Element Method Magnetic discretizes the problem domain using triangular elements. Over each element, the solution is approximated by a linear interpolation

of the values of potential at the three vertices of the triangle. The linear algebra problem is forced by minimizing a measure of the error between the exact differential equation and the approximation differential equation as written in terms of the linear trial functions. The finite element method magnetic 4.0 application software used in this work agrees with the other

Finite Element Analysis software like ANSYS Maxwell software based on FEMM's algorithms discussed above.

2.6 ANSYS Maxwell

This high-performance interaction software uses finite element analysis (FEA) to solve electromagnetic field problems in either two or three dimensions. The problems are solved by using Maxwell's equations in finite region of space with appropriate boundary conditions and user-specified initial conditions in order to obtain solution with minimum error.

Like any other finite element software, the process of achieving the solution are the same as stated below:

i. Pre-processing: (Model the required geometry, assign maternal boundary conditions, load and constraints).

ii. Processing: Analysis solver; (Assembles and solves the computational space equations).

iii. Post Processing: (Sort and display the results).

ANSYS Maxwell software can be used to achieve the desired result by utilizing different products built into the program. Under electrical machine design platform, the following:

i. Maxwell design types can be added to a Maxwell project to achieve the expected result.

ii. Rotating Machinery Expert (RMxprt): An interactive analytical tool used for electrical machines design and analyses in ANSYS Domain.

iii. Maxwell Two-Dimension (Maxwell 2D): Uses Finite Element Analysis to simulate and solve 2D electromagnetic fields in XY or RZ planes.

iv. Maxwell Three Dimension (Maxwell 3D): Uses Finite Element Analysis to simulate and solve 3-D electromagnetic fields.

2.7 The Basic Andrew Brondel (Two-Reation) Theory

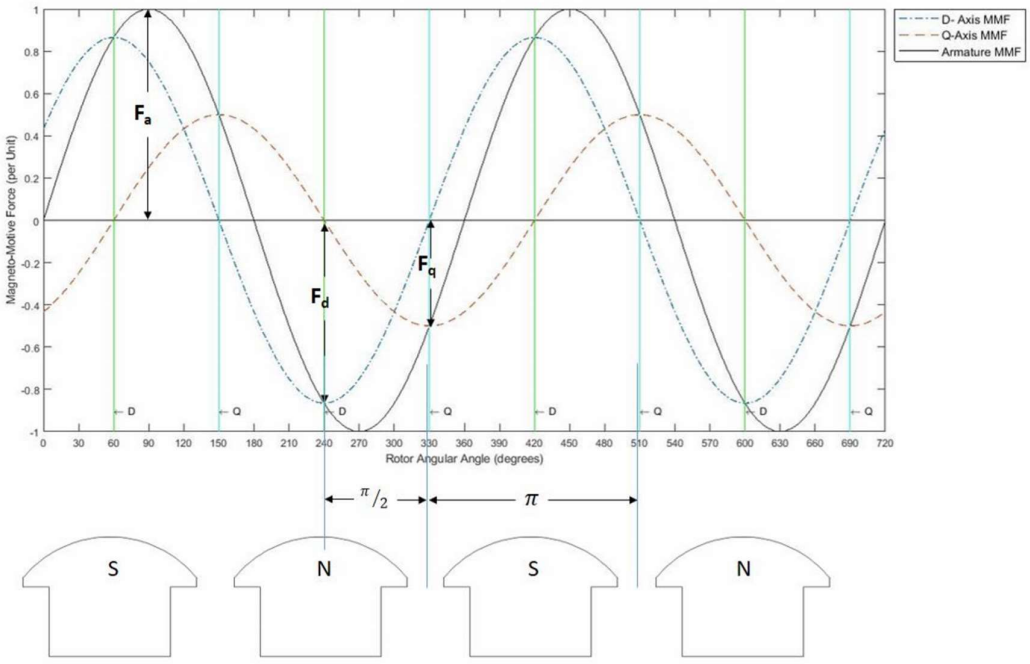

Figure 2.1: Armature-Reaction MMF of Salient-Pole Generator

The pole-shape of salient-pole generator makes the reluctance presented to the armature-reaction magneto-motive force (MMF) not constant along the machine air gap periphery. Non-salient pole synchronous machine has its field flux axis shifted by the air nature reaction and modified its strength without producing any significant amount of field distortion with salient

pole synchronous machine; however, the armature reaction not only modifies the strength, but also distorts the field by crowding the flux towards one of the pole tips.

Figure 2.1 shows the armature-reaction MMF of a salient-pole generator assuming the total armature magneto-motive force (MMF) is sinusoidally distributed along the air gap. This magneto-motive force, under steady state condition, revolves in synchronism with the rotor field and may be resolved into two sinusoidal components. In order to account for the two effect of the armature, reaction of salient-pole synchronous generator, Blondel suggested the two-reaction theory. The armature reaction of an alternator according to two reaction theory, is resolved into two orthogonal components one producing only distortion and the other producing only a change in the field strength (Rajendra Prasad, 2015). The two components are designated as direct-axis MMF component with peak on the same axis as the main poles, and with either an aiding or an opposing effect on the field own MMF. The quadrature-axis

MMF component has a "cross-magnetizing effect in the field as it strengthens the existing field MMF at one pole tip and weakens it at the other".

2.8 Application of Two-Reaction Theory to Salient-Pole Synchronous Generator

The Two Reaction Theory illustrated above form a conduit through which Salient-Pole Synchronous Generator is effectively modelled and analyzed with the application of Park's Transformation. The process involves transformation of three phase (**a**, **b**, **c**) stator variable to two phase (**d**, **q**) rotor variable in order to simplify the generator's performance computation by:

(i) Reducing a balanced three phase quantity to a two-phase quantity (ii)
Transform the time varying inductance to a dc quantity.

The following basic equations are applied to realize Two Reaction Theory.

$$\text{Metic flux } (\Phi) = \frac{\text{MMF}}{\text{Reluctance}} \qquad 2.14$$

$$\text{Reluctance} = \frac{\text{Length of air gap}}{\mu_o \times \text{Area of the flux linkage}} \quad 2.15$$

$$\text{Magneticflux linkage } (\psi) = N\Phi$$

$$\text{Magneto} - \text{motive force (MMF)} = F$$

MMF = NI

Number of coils turns = N

Induced current = I

$$\text{Reluctance} = R$$

$$\text{Length of air gap} = l_g$$

$$\text{Area of the flux linkage} = A$$

$$\text{Differential area } (dA) = rld\alpha$$

Length of the generator = l

$$\text{Differential flux } (d\phi) = d\left[\frac{F_d(\alpha 1)}{R_{gd}} + \frac{F_q(\alpha 2)}{R_{gq}}\right] \quad 2.16$$

$$\text{Differential flux linkage } (d\psi) = N(d\Phi) \quad 2.17$$

Magnetic flux linkage is computed with the help of equations 2.16 and 2.17, equation 2.19 is obtained by substituting equations 4.5 and 4.7 into equation 2.18

$$\psi_s = \int_0^{\pi} N d\Phi_s \quad 2.18$$

$$\psi_s = N_s \int_0^{\pi} \left[\frac{\mathbf{F}_a \cos\theta_r \sin(\alpha+\theta_r)}{R_{gd}} - \frac{\mathbf{F}_a \sin\theta_r \cos(\alpha+\theta_r)}{R_{gq}}\right] d\alpha \quad 2.19$$

$$\psi_s = N_s \mu_0 rl \int_0^{\pi} \left[\frac{\mathbf{F}_a \cos\theta_r \sin(\alpha+\theta_r)}{l_{gd}} - \frac{\mathbf{F}_a \sin\theta_r \cos(\alpha+\theta_r)}{l_{gq}}\right] d\alpha \quad 2.20$$

$$\psi_s = N_s \mathbf{F}_a \mu_0 rl \left\{ - \left[\frac{\cos\theta_r \cos(\alpha+\theta_r)}{l_{gd}}\right]_0^{\pi} - \left[\frac{\sin\theta_r \sin(\alpha+\theta_r)}{l_{gq}}\right]_0^{\pi} \right\} \quad 2.21$$

$$\psi_s = N_s \mathbf{F}_a \mu_0 rl \left\{\frac{\cos^2\theta_r}{l_{gd}} + \frac{\sin^2\theta_r}{l_{gq}}\right\} \quad 2.22$$

From trigonometric identities in equation A.2 and A.3 equation, 2.23 and 2.24 could be obtained.

$$2\cos^2\theta = 1 + \cos 2\theta \quad 2.23$$

$2\sin^2\theta = 1 - \cos 2\theta$ 2.24 Equation 2.21 is obtained

by substituting equation 2.19 and 2.20.

$$\psi_s = N_s \mathbf{F}_a \mu_o rl \left[\frac{(1+\cos 2\theta_r)}{2l_{gd}} + \frac{(1-\cos 2\theta_r)}{2l_{gq}}\right] \quad 2.25$$

The magneto-motive force (MMF) is expresses in equation 2.26

$$\text{MMF (F)} = \frac{4}{\pi}\frac{N_s I_s}{2} \quad 2.26$$

$$\psi_s = N_s \left(\frac{4}{\pi}\frac{N_s i_s}{2}\right) \mu_o rl \left[\left(\frac{1}{2l_{gd}} + \frac{1}{2l_{gq}}\right) + \cos 2\theta_r \left(\frac{1}{2l_{gd}} - \frac{1}{2l_{gq}}\right)\right] \quad 2.27$$

$\frac{\psi_s d}{i_s} = L_d$(Direct axis Inductance)

$\frac{\psi_s q}{i_s} = L_q$(Quadrature axis Inductance)

$$\psi_s = i_s \left[\left(\frac{L_d}{2} + \frac{L_q}{2}\right) + \left(\frac{L_d}{2} - \frac{L_q}{2}\right)\cos 2\theta_r\right] \quad 2.28$$

$$L_s = \frac{\psi_s}{i_s} = \frac{L_d + L_q}{2} + \frac{(L_d - L_q)}{2}\cos 2\theta_r \Rightarrow \textbf{Two-Reaction Theory Concept}$$

A detailed analysis of self and mutual inductance derivation is deduced in 2.8.1 and 2.8.2.

2.8.1 Self-Inductance of Armature Phases

Self Inductance of the Stator (L_s)

$$L_s = L_{ls} + \frac{L_d + L_q}{2} + \frac{(L_d - L_q)}{2}\cos 2\theta_r \quad 2.29$$

Direct Axis Inductance of the Stator (L_{aad})

Leakage inductance = L_{ls}

$$L_{aad} = \frac{L_d + L_q}{2}$$

Quadrature Axis Inductance of the Stator (L_{aaq})

$$L_{aaq} = \frac{L_d - L_q}{2}$$

$l_{aa} = L_{ls} + L_{aad} + L_{aaq}\cos 2\theta_r$

$l_{aa} = L_{ls} + L_1 + L_2 \cos 2\theta_r$ 2.30

$$l_{bb} = L_{ls} + L_1 + L_2 \cos(2\theta_r + \frac{2\pi}{3}) \quad 2.31$$

$$l_{cc} = L_{ls} + L_1 + L_2 \cos(2\theta_r - \frac{2\pi}{3}) \quad 2.32$$

θ_r = Angle of rotor in electrical degrees

2.8.2 Mutual Inductance of Armature Phases

The magneto-motive force of the direct and quadrature axis generated in phase '*a'* are resolved along phase '*b*' axis to obtain the mutual magnetic flux between phases *a* and *b* as shown in figure 4.9(a).

Therefore, the direct and quadrature axis magnetic flux components can be projected onto the surface of phase 'b' to find the flux linkage of phase 'b' due to current in phase 'a'.

This can be exemplified as follows:

$$\Phi_{ba} = -\Phi_{ad} \cos(\theta_r - \frac{2\pi}{3}) - \Phi_{aq} \sin(\theta_r - \frac{2\pi}{3}) \quad 2.33$$

$$\Phi_{ad} = \frac{F_{ad}}{R_{gd}}, \ \Phi_{aq} = \frac{F_{aq}}{R_{gd}} \quad 2.34$$

Substitute equation 2.34 into equation 2.33 to obtain equation 2.35.

$$\Phi_{ba} = -\frac{F_{ad}}{R_{gd}} \cos(\theta_r - \frac{2\pi}{3}) - \frac{F_{aq}}{R_{gd}} \sin(\theta_r - \frac{2\pi}{3}) \quad 2.35$$

$F_{ad} = \mathbf{F}_a \cos\theta_r, \quad F_{aq} = \mathbf{F}_a \sin\theta_r$ 2.36 Substitute equation 2.34 into equation 2.36 to obtain equation 2.37.

$$\Phi_{ba} = -\frac{F_a}{R_{gd}} \cos\theta_r \cos(\theta_r - \frac{2\pi}{3}) - \frac{F_a}{R_{gd}} \sin\theta_r \sin\left(\theta_r - \frac{2\pi}{3}\right) \quad 2.37$$

$\psi_{ba} = N\Phi_{ba}$ 2.38

Recalling equation 2.22, 2.25 and 2.26 into equation 2.37 and equation 2.39 is obtained.

$$\psi_{ba} = N_s \mathbf{F}_a \mu_0 r l \left\{ \frac{-\cos^2\theta_r \cos(\frac{2\pi}{3})}{l_{gd}} + \frac{\cos\theta_r \sin\theta_r \sin(\frac{2\pi}{3})}{l_{gd}} - \frac{-\sin^2\theta_r \cos\left(\frac{2\pi}{3}\right)}{l_{gq}} + \frac{\cos\theta_r \sin\theta_r \sin\left(\frac{2\pi}{3}\right)}{l_{gq}} \right\} \quad 2.39$$

Substituting equation 2.23, 2.24 and 2.26 into equation 2.39; hence equation 2.40

$$\psi_{ba} = N_s\left(\frac{4}{\pi}\frac{N_s i_a}{2}\right)\mu_o rl\left[-\frac{1}{2} - \left(\frac{1}{2l_{gd}} + \frac{1}{2l_{gq}}\right) - \left(\frac{1}{2l_{gd}} - \frac{1}{2l_{gq}}\right)\cos(2\theta_r - \frac{2\pi}{3})\right] \quad 2.40$$

$$\psi_{ba} = N_s\left(\frac{4}{\pi}\frac{N_s i_a}{2}\right)\mu_o rl\left[-\frac{1}{2}\left(\frac{1}{2l_{gd}} + \frac{1}{2l_{gq}}\right) + \left(\frac{1}{2l_{gd}} - \frac{1}{2l_{gq}}\right)\cos(2\theta_r - \frac{2\pi}{3})\right] \quad 2.41$$

$$l_{ba} = l_{ab} = \frac{\psi_{ba}}{i_a} = -\frac{L_1}{2} + L_2\cos(2\theta_r - \frac{2\pi}{3}) \quad 2.42$$

Similarly, other inductances are space shifted by $\frac{2\pi}{3}$. Hence,

$$l_{bc} = l_{cb} = -\frac{L_1}{2} + L_2\cos 2\theta_r \quad 2.43$$

$$l_{ac} = l_{ca} = -\frac{L_1}{2} + L_2\cos\left(2\theta_r + \frac{2\pi}{3}\right) \quad 2.44$$

Details of this derivation of Mutual Inductance of Armature Phases is illustrated below.

2.8.3 Mutual Inductance Between Field Winding and the Armature Phases

In salient-pole synchronous generators, the inductances for the rotor; and between rotor and armatures phases can be obtained as follows.

(i) Rotor Self Inductance is constant as l_{rr}

(ii) The mutual inductances between rotor and the armature phases vary between maximum and minimum valve of magneto-motive force of each of the axis of the phases.

They are obtained as follows:

$$l_{ra} = l_{ar} = L_M\cos\theta_r \quad 2.45$$

$$l_{rb} = l_{br} = L_M\cos\left(\theta_r - \frac{2\pi}{3}\right) \quad 2.46$$

$$l_{rc} = l_{ar} = L_M\cos\left(\theta_r + \frac{2\pi}{3}\right) \quad 2.47$$

$$l_{rr} = \text{constant} \quad 2.48$$

In all the above formulas, the angle θ_r represent electrical angles. This is expressed as a function of mechanical angle in the form below.

$\theta_{r(elect)} = \frac{P}{2}\theta_{r(mech)}$, where P is the number of poles.

2.9 The General Salient-Pole Generator Equation

The generator contains four basic windings: the three identical and symmetrically placed distributed stator windings (identified by the subscripts a, b and c) and rotor or field winding (subscript r).

The practical generator may be equipped in addition with damper windings consisting of a short-circuited squirrel cage winding placed in slots on the rotor surface. Each of the four winding is characterized by resistance, self-inductance and mutual inductances relative to the other three windings.

Mathematical analysis of the general salient-pole synchronous generator equation are given in the voltage equation as:

The voltage equation is expressed as:

$$V = -Ri - \frac{d(Li)}{dt} = -Ri - L\frac{di}{dt} \quad 2.49$$

$$V = -Ri - \frac{d\psi}{dt} \quad 2.50$$

Expanding the differential equation, we have:

$$V_a = -i_a r_s - \frac{d(l_{aa}i_a)}{dt} - \frac{d(l_{ab}i_b)}{dt} - \frac{d(l_{ac}i_c)}{dt} + \frac{d(l_{ar}i_r)}{dt} \quad 2.51$$

$$V_b = -i_b r_s - \frac{d(l_{ba}i_a)}{dt} - \frac{d(l_{bb}i_b)}{dt} - \frac{d(l_{bc}i_c)}{dt} + \frac{d(l_{br}i_r)}{dt} \quad 2.52$$

$$V_c = -i_c r_s - \frac{d(l_{ca}i_a)}{dt} - \frac{d(l_{cb}i_b)}{dt} - \frac{d(l_{cc}i_c)}{dt} + \frac{d(l_{cr}i_r)}{dt} \quad 2.53$$

$$V_r = i_r r_r - \frac{d(l_{ra}i_a)}{dt} - \frac{d(l_{rb}i_b)}{dt} - \frac{d(l_{rc}i_c)}{dt} + \frac{d(l_{rr}i_r)}{dt} \quad 2.54$$

These equations can also be expressed in terms of magnetic flux linkage as below.

$$V_a = -i_a r_s - \frac{d\psi_{aa}}{dt} - \frac{d\psi_{ab}}{dt} - \frac{d\psi_{ac}}{dt} + \frac{d\psi_{ar}}{dt} \quad 2.55$$

$$V_b = -i_b r_s - \frac{d\psi_{ba}}{dt} - \frac{d\psi_{bb}}{dt} - \frac{d\psi_{bc}}{dt} + \frac{d\psi_{br}}{dt} \quad 2.56$$

$$V_c = -i_c r_s - \frac{d\psi_{ca}}{dt} - \frac{d\psi_{cb}}{dt} - \frac{d\psi_{cc}}{dt} + \frac{d\psi_{cr}}{dt} \quad 2.57$$

$$V_r = i_r r_r - \frac{d\psi_{ra}}{dt} - \frac{d\psi_{rb}}{dt} - \frac{d\psi_{rc}}{dt} + \frac{d\psi_{rr}}{dt} \quad 2.58$$

$$V_s = \begin{bmatrix} V_a \\ V_b \\ V_c \end{bmatrix}, i_s = \begin{bmatrix} i_a \\ i_b \\ i_c \end{bmatrix} \quad 2.59$$

$$R_s = \begin{bmatrix} r_s & 0 & 0 \\ 0 & r_s & 0 \\ 0 & 0 & r_s \end{bmatrix}, \quad r_r \quad 2.60$$

$$l_{aa} \quad l_{ab} \quad l_{ac}$$

$$L_s = [l_{ba}\ l_{bb}\ l_{bc}] \quad 2.61 \quad l_{ca}\ l_{cb}\ l_{cc}$$

$$l_{ar}$$

$$l_{rs} = [l_{br}], \quad l_{rr} \quad 2.62$$

$$l_{cr}$$

The total matrices V, i, R and L are composed of the submatrices in the following pattern:

$$V = \begin{bmatrix} V_S \\ V_r \end{bmatrix}, \quad i = \begin{bmatrix} i_s \\ -i_r \end{bmatrix} \quad 2.63$$

$$R = \begin{bmatrix} R_s & 0 \\ 0 & r_r \end{bmatrix} \qquad L = \begin{bmatrix} L_s & l_{rs} \\ l_{rs}^{\ T} & l_{rr} \end{bmatrix}$$

$$\begin{bmatrix} V_S \\ V_r \end{bmatrix} = -\begin{bmatrix} R_s & 0 \\ 0 & r_r \end{bmatrix} \begin{bmatrix} l_s \\ -i_r \end{bmatrix} - \frac{d}{dt}\left\{ \begin{bmatrix} L_s & l_{rs} \\ l_{rs}^{\ T} & l_{rr} \end{bmatrix} \begin{bmatrix} i_s \\ -i_r \end{bmatrix} \right\} \quad 2.64$$

$$2.65$$

2.9.1 The General Machine Equation

The voltage equation for machine modelling and analysis is expressed as:

$$\mathbf{v} = -\mathbf{Ri} - \frac{d}{dt}\mathbf{(Li)} \quad 2.66$$

$$\mathbf{L(Inductance\ Matrix)} = \begin{bmatrix} \mathbf{l_{aa}\ l_{ab}\ l_{ac}\ l_{ar}} \\ \mathbf{l_{ba}\ l_{bb}\ l_{bc}\ l_{br}} \\ \mathbf{l_{ca}\ l_{cb}\ l_{cc}\ l_{cr}} \\ \mathbf{l_{ra}\ l_{ra}\ l_{ra}\ l_{rr}} \end{bmatrix} \qquad 2.67$$

The performance of three-phase AC machines is described by their voltage equations and inductances in equation 2.66. It is well known that some machine inductances are functions of rotor speed. The coefficients of the differential equations, which describes the behaviour of these machines, are time varying except when the rotor is at standstill. A change of variables is often used to reduce the complexity of these differential equations. Park's transformation, a revolution in machine analysis, has the unique property of eliminating all time varying inductances from the voltage equations of three-phase ac machines due to the rotor spinning through the following:

Formulating a change of variables associated with fictitious windings rotating with the rotor.

i. Referring the stator and rotor variables to a reference frame fixed on the rotor.

ii. From the rotor point of view, all the variables can be observed as constant values.

$$\begin{bmatrix} i_d \\ i_q \\ i_o \end{bmatrix} = \frac{2}{3}\begin{bmatrix} \cos\theta_r & \cos\left(\theta_r - \frac{2\pi}{3}\right) & \cos\left(\theta_r + \frac{2\pi}{3}\right) \\ -\sin\theta_r & -\sin\left(\theta_r - \frac{2\pi}{3}\right) & -\sin\left(\theta_r + \frac{2\pi}{3}\right) \\ \frac{1}{2} & \frac{1}{2} & \frac{1}{2} \end{bmatrix}\begin{bmatrix} i_a \\ i_b \\ i_c \end{bmatrix} \qquad 2.68$$

$$i_{dq0} = \mathbf{T}i_{acb} = \mathbf{T}i_s \qquad 2.69$$

$$i_{dq0} = \begin{bmatrix} i_d \\ i_q \\ i_0 \end{bmatrix} \qquad 2.70$$

$$i_s = \mathbf{T^{-1}}i_{dq0} \qquad 2.71$$

The stator voltage will also be transformed similarly by applying the transformation.

$$V_{dq0} = \mathbf{T}V_s \qquad 2.72$$

With the associated inverse transformation

$V_s = \mathbf{T}^{-1}V_{dq0}$ 2.73

From the voltage equation 2.65, equation 2.74 and 2.75 are obtained

$$V_s = -R_s i_s - \frac{d}{dt}(L_s i_s - l_{rs} i_r) \quad 2.74$$

$$V_r = -r_r i_s - \frac{d}{dt}\left(L_{rs}{}^{T} i_s - l_{rr} i_r\right) \quad 2.75$$

Substitute $V_s = \mathbf{T}^{-1}V_{dq0}$ and $i_s = \mathbf{T}^{-1}i_{dq0}$ into above equations 2.74 and 2.75, equations 2.76 and 2.77 are obtained.

$$\mathbf{T}^{-1}V_{dq0} = R_s\mathbf{T}^{-1}i_{dq0} - \frac{d}{dt}\left(L\mathbf{T}^{-1}i_{dq0} - l_{rs} i_r\right) \quad 2.76$$

$$V_r = r_r\mathbf{T}^{-1}i_{dq0} - \frac{d}{dt}\left(l_{rs}{}^{T}\mathbf{T}^{-1}i_{dq0} - l_{rr} i_r\right) \quad 2.77$$

Multiply equation 2.76 by $\mathbf{T}$ to obtain equation 2.78

$$V_{dq0} = -\mathbf{T}R_S\mathbf{T}^{-1}i_{dq0} - \mathbf{T}\frac{d}{dt}\left(L_s\mathbf{T}^{-1}i_{dq0} - l_{rs} i_r\right) \quad 2.78$$

2.9.2 Direct Axis, Quadrature Axis and Zero Sequence Inductance

The direct, quadrature axis and zero sequence inductances are obtained below:

$$\begin{bmatrix} L_d \\ L_q \\ L_0 \end{bmatrix} = [\mathbf{T}][L_s][\mathbf{T}^{-1}] \quad 2.79$$

$$\mathbf{T} = \frac{2}{3}\begin{bmatrix} \cos\theta_r & \cos\left(\theta_r - \frac{2\pi}{3}\right) & \cos\left(\theta_r + \frac{2\pi}{3}\right) \\ -\sin\theta_r & -\sin\left(\theta_r - \frac{2\pi}{3}\right) & -\sin\left(\theta_r + \frac{2\pi}{3}\right) \\ \frac{1}{2} & \frac{1}{2} & \frac{1}{2} \end{bmatrix}$$

$$L_s = \begin{bmatrix} l_{aa} & l_{ab} & l_{ac} \\ l_{ba} & l_{bb} & l_{bc} \\ l_{ca} & l_{cb} & l_{cc} \end{bmatrix}$$

$$\left.\begin{aligned} L_{aa} &= L_1 + L_2\cos 2\theta_r \\ L_{ab} = L_{ba} &= -L_3 + L_2\cos\left(2\theta_r - \frac{2\pi}{3}\right) \\ l_{bb} &= L_1 + L_2\cos\left(2\theta_r + \frac{2\pi}{3}\right) \\ l_{bc} = l_{cb} &= -L_3 + L_2\cos\left(2\theta_r + \frac{2\pi}{3}\right) \end{aligned}\right\} \quad 2.80$$

2.81

2.82

Inverse transformation of equation 2.80 is expressed below.

$$\mathbf{T}^{-1} = \begin{bmatrix} \cos\theta_r & \sin\theta_r & 1 \\ \cos\left(\theta_r - \frac{2\pi}{3}\right) & \sin\left(\theta_r - \frac{2\pi}{3}\right) & 1 \\ \cos\left(\theta_r + \frac{2\pi}{3}\right) & \sin\left(\theta_r + \frac{2\pi}{3}\right) & 1 \end{bmatrix} \quad 2.83$$

The first step in the development of a suitable model is to transform the winding variables to a coordinate system in which the rotor is stationary. This process will map the stator currents, fluxes and the rest into direct and quadrature axes using Park Transformation, which helps in the study of transient behaviour of synchronous machines.

At this moment, the stator parameters will be transformed into the rotor reference that will be seen rotating with the rotor rotational reference frame. Therefore, being on the rotor will make the parameters to be seen as stationary.

The rotating angle $\theta_r$will be seen as not changing hence, $\theta_r = 0$ This

will transform equation 2.79 to equation 2.84 at standstill.

$$\begin{bmatrix} L_d \\ L_q \\ L_0 \end{bmatrix} = \frac{2}{3}\begin{bmatrix} 1 & -\frac{1}{2} & -\frac{1}{2} \\ 0 & \frac{\sqrt{3}}{2} & -\frac{\sqrt{3}}{2} \\ \frac{1}{2} & \frac{1}{2} & \frac{1}{2} \end{bmatrix}\begin{bmatrix} L_1 + L_2 & -\frac{L_2}{2} + L_3 & -\frac{L_2}{2} + L_3 \\ -\frac{L_2}{2} + L_3 & L_1 - \frac{L_2}{2} & L_2 + L_3 \\ \frac{L_2}{2} + L_3 & L_2 + L_3 & L_1 - \frac{L_2}{2} \end{bmatrix}\begin{bmatrix} 1 & 0 & 1 \\ -\frac{1}{2} & \frac{\sqrt{3}}{2} & 1 \\ -\frac{1}{2} & -\frac{\sqrt{3}}{2} & 1 \end{bmatrix} \quad 2.84$$

$$= \begin{bmatrix} \frac{2L_1+3L_2-2L_3}{2} & 0 & 0 \\ 0 & \frac{2L_1-3L_2-2L_3}{2} & 0 \\ 0 & 0 & L_1 + 2L_3 \end{bmatrix} \quad 2.85$$

$$\begin{bmatrix} L_d \\ L_q \\ L_0 \end{bmatrix} = \frac{2}{3}\begin{bmatrix} L_1 - L_3 + \frac{3}{2}L_2 & 0 & 0 \\ 0 & L_1 - L_3 - \frac{3}{2}L_2 & 0 \\ 0 & 0 & L_1 + 2L_3 \end{bmatrix} \quad 2.86$$

$$L_d = L_1 - L_3 + \frac{3}{2}L_2 \quad 2.87$$

$$L_q = L_1 - L_3 - \frac{3}{2}L_2 \quad 2.88$$

$$L_0 = L_1 + 2L_3 \quad 2.89$$

2.9.3 Stator to Rotor Mutual Inductance Computation

The inductances between stator and rotor are computed below.

$$l_{rs} = [\mathbf{T}]\begin{bmatrix} l_{ar} \\ l_{br} \\ l_{cr} \end{bmatrix} \quad 2.90$$

$$l_{rs} = \frac{2}{3}\begin{bmatrix} 1 & \frac{-1}{2} & \frac{-1}{2} \\ 0 & \frac{\sqrt{3}}{2} & \frac{-\sqrt{3}}{2} \\ \frac{1}{2} & \frac{1}{2} & \frac{1}{2} \end{bmatrix}\begin{bmatrix} l_{ar} \\ l_{br} \\ l_{cr} \end{bmatrix} = \frac{2}{3}\begin{bmatrix} 1 & \frac{-1}{2} & \frac{-1}{2} \\ 0 & \frac{\sqrt{3}}{2} & \frac{-\sqrt{3}}{2} \\ \frac{1}{2} & \frac{1}{2} & \frac{1}{2} \end{bmatrix}\begin{bmatrix} L_5\cos\theta_r \\ L_5\cos\left(\theta_r - \frac{2\pi}{3}\right) \\ L_5\cos\left(\theta_r + \frac{2\pi}{3}\right) \end{bmatrix} \quad 2.91$$

For $\theta_r = 0$

$$l_{rs} = \frac{2}{3}\begin{bmatrix} 1 & \frac{-1}{2} & \frac{-1}{2} \\ 0 & \frac{\sqrt{3}}{2} & \frac{-\sqrt{3}}{2} \\ \frac{1}{2} & \frac{1}{2} & \frac{1}{2} \end{bmatrix}\begin{bmatrix} L_5 \\ -\frac{L_5}{2} \\ -\frac{L_5}{2} \end{bmatrix} = \begin{bmatrix} L_5 \\ 0 \\ 0 \end{bmatrix} \quad 2.92$$

$$l_{rs}^{\,T} = [l_{ar} \quad l_{br} \quad l_{cr}][\mathbf{T}] = \left[L_5 \quad -\frac{L_5}{2} \quad -\frac{L_5}{2}\right]\frac{2}{3}\begin{bmatrix} 1 & \frac{-1}{2} & \frac{-1}{2} \\ 0 & \frac{\sqrt{3}}{2} & \frac{-\sqrt{3}}{2} \\ \frac{1}{2} & \frac{1}{2} & \frac{1}{2} \end{bmatrix}^{-1} \quad 2.93$$

$$= \left[L_5 \quad -\frac{L_5}{2} \quad -\frac{L_5}{2}\right]\begin{bmatrix} 1 & 0 & 1 \\ -\frac{1}{2} & \frac{\sqrt{3}}{2} & 1 \\ -\frac{1}{2} & -\frac{\sqrt{3}}{2} & 1 \end{bmatrix} = \left[\frac{3}{2}L_5 \quad 0 \quad 0\right] \quad 2.94$$

2.9.4 Rotor Self Inductance

Rotor self induces remain constant throughout the rotor angle.

Rotor Self Inductance (l_{rr}) = constant

Voltage Equation Relationship

Ignoring the armature resistance, the armature voltage is:

$$V_{ph} = V_{abc} = \frac{d}{dt}\psi_{ph} \qquad 2.95$$

$\psi_{ph} =$

$$\mathbf{T}^{-1}\psi_{dq0} \qquad 2.96$$

$$V_{ph} = \frac{d}{dt}\mathbf{T}^{-1}\psi_{dq0} \qquad 2.97$$

$$V_{dq0} = \mathbf{T}V_{ph} \qquad 2.98$$

$$V_{dq0} = \mathbf{T}\frac{d}{dt}\mathbf{T}^{-1}\psi_{dq0} \qquad 2.99$$

$$= \mathbf{T}\left[\mathbf{T}^{-1}\frac{d}{dt}\psi_{dq0} + \psi_{dq0}\frac{d}{dt}T^{-1}\right] \qquad 2.100$$

$$= \mathbf{T}.\mathbf{T}^{-1}\frac{d}{dt}\psi_{dq0} + \mathbf{T}\psi_{dq0}\frac{d}{dt}\mathbf{T}^{-1} \qquad 2.101$$

$$= \frac{d}{dt}\psi_{dq0} + \psi_{dq0}T.\frac{dT^{-1}}{dt} \qquad 2.102$$

$$= \frac{d}{dt}\psi_{dq0} + \psi_{dq0}\mathbf{T}.\frac{d\theta_r}{dt}.\frac{d\mathbf{T}^{-1}}{d\theta_r} \qquad 2.103$$

$$= \frac{d}{dt}\psi_{dq0} + \psi_{dq0}\mathbf{T}.\omega.\frac{d\mathbf{T}^{-1}}{d\theta_r} \qquad 2.104$$

$$= \frac{d}{dt}\psi_{dq0} + \psi_{dq0}.\omega.\mathbf{T}\frac{d\mathbf{T}^{-1}}{d\theta_r} \qquad 2.105$$

Resolving the term: $\mathbf{T}\frac{d}{d\theta_r}\mathbf{T}^{-1}$

$$\mathbf{T} = \frac{2}{3}\begin{bmatrix} \cos\theta_r & \cos\left(\theta_r - \frac{2\pi}{3}\right) & \cos\left(\theta_r + \frac{2\pi}{3}\right) \\ -\sin\theta_r & -\sin\left(\theta_r - \frac{2\pi}{3}\right) & -\sin\left(\theta_r + \frac{2\pi}{3}\right) \\ \frac{1}{2} & \frac{1}{2} & \frac{1}{2} \end{bmatrix} \qquad 2.106$$

$$\mathbf{T}^{-1} = \begin{bmatrix} \cos\theta_r & -\sin\theta_r & 1 \\ \cos\left(\theta_r - \frac{2\pi}{3}\right) & -\sin\left(\theta_r - \frac{2\pi}{3}\right) & 1 \\ \cos\left(\theta_r + \frac{2\pi}{3}\right) & -\sin\left(\theta_r + \frac{2\pi}{3}\right) & 1 \end{bmatrix} \quad 2.107$$

$$\mathbf{T}\frac{d}{d\theta_r}\mathbf{T}^{-1} = [\mathbf{T}]\omega\frac{d}{d\theta_r}\begin{bmatrix} \cos\theta_r & -\sin\theta_r & 1 \\ \cos\left(\theta_r - \frac{2\pi}{3}\right) & -\sin\left(\theta_r - \frac{2\pi}{3}\right) & 1 \\ \cos\left(\theta_r + \frac{2\pi}{3}\right) & -\sin\left(\theta_r + \frac{2\pi}{3}\right) & 1 \end{bmatrix}$$

$$= [\mathbf{T}]\omega\begin{bmatrix} -\sin\theta_r & -\cos\theta_r \\ -\sin\left(\theta_r - \frac{2\pi}{3}\right) & -\cos\left(\theta_r - \frac{2\pi}{3}\right) \\ -\sin\left(\theta_r + \frac{2\pi}{3}\right) & -\cos\left(\theta_r + \frac{2\pi}{3}\right) \end{bmatrix} \quad 2.108$$

2.109

Therefore,

$$V_{dq0} = \frac{d\psi_{dq0}}{dt} + \psi_{dq0}[\mathbf{T}]\omega\begin{bmatrix} -\sin\theta r & -\cos\theta r \\ -\sin\left(\theta r - \frac{2\pi}{3}\right) & -\cos\left(\theta r - \frac{2\pi}{3}\right) \\ -\sin\left(\theta r + \frac{2\pi}{3}\right) & -\cos\left(\theta r + \frac{2\pi}{3}\right) \end{bmatrix} \quad 2.110$$

Hence, $V_{dq0} = \frac{d\psi_{dq0}}{dt} + \psi_{dq0}\begin{bmatrix} 1 & -\frac{1}{2} & -\frac{1}{2} \\ \frac{2}{3} & 0 & \frac{\sqrt{3}}{2} & -\frac{\sqrt{3}}{2} \\ \frac{1}{2} & \frac{1}{2} & \frac{1}{2} \end{bmatrix}\omega\begin{bmatrix} 0 & -1 \\ \frac{\sqrt{3}}{2} & \frac{1}{2} \\ -\frac{\sqrt{3}}{2} & \frac{1}{2} \end{bmatrix}$

$$= \frac{d\psi_{dq0}}{dt} + \psi_{dq0}\begin{bmatrix} 0 & -\omega \\ \omega & 0 \\ 0 & 0 \end{bmatrix} \quad 2.111$$

This expresses the speed voltage that arises from a coordinate transformation. The two voltage/flux relationship that are affected are:

$$V_d = \frac{d\psi_d}{dt} - \omega\psi_q \quad 2.112$$

$$V_q = \frac{d\psi_q}{dt} + \omega\psi_d \quad 2.113$$ Where $\omega = \frac{d\theta_r}{dt}$

2.9.5 Power and Torque Equation

The instantaneous power is given as:

$p = V_a i_a + V_b i_b + V_c i_c$ in a 3ϕ system 2.114

In a three-phase stationary frame instantaneous power is expressed as

$p = V_s i_s$ 2.115

Where $i_s = [i_a, i_b, i_c]$; $V_s = [V_a, V_b, V_c]$ Looking at

the two-rotating frame

$i_s = \mathbf{T}^{-1} i_{dq0}$ 2.116

$$i_s{}^{T} = (\mathbf{T}^{-1})^{T}\left(i_{dq0}\right)^{T} \quad 2.117$$

Substitute in power equation $p = i_s v_s$

$p = (i_{dq0})\ (T^{T} \quad {}^{-1})^{T} T^{-1} V_{dq0}$ 2.118

$$= (\mathbf{T}^{-1})^{T}(\mathbf{T}^{-1}) = \begin{bmatrix} \frac{3}{2} & 0 & 0 \\ 0 & \frac{3}{2} & 0 \\ 0 & 0 & 3 \end{bmatrix} \quad 2.119$$

$$p = [i_d \quad i_q \quad i_0] \begin{bmatrix} \frac{3}{2} & 0 & 0 \\ 0 & \frac{3}{2} & 0 \\ 0 & 0 & 3 \end{bmatrix} \begin{bmatrix} V_d \\ V_q \\ V_0 \end{bmatrix} \quad 2.120$$

$$p = \frac{3}{2} V_d i_d + \frac{3}{2} V_q i_q + 3 V_0 i_0 \quad 2.121$$

Substituting V_d and V_q in power equation,

$$p = \frac{3}{2}\left(\frac{d\psi_d}{dt} - \omega\psi_q\right) i_d + \frac{3}{2}\left(\frac{d\psi_q}{dt} + \omega\psi_d\right) i_q + 3\frac{d\psi_0}{dt} i_0 \quad 2.122$$

With the equation for the flux linkage, the stator voltage equations, and the torque equation of the salient-pole synchronous machine is completely described in a coordinate system rotating in synchronism with the rotor (Gerling, 2015).

Starting from these equations in space vector rotation (for the computation of the dynamic behaviour) firstly as a special case the steady-state operation, there is no timedependent change of the flux linkage $\frac{d\psi}{dt}$ is zero and the speed is constant. From equation 2.110

$\frac{d\psi_d}{dt} = \frac{d\psi_q}{dt} = \frac{d\psi_0}{dt} = 0$ steady-state operation.

$$p = -\frac{3}{2}\omega\psi_q i_d + \frac{3}{2}\omega\psi_d i_q \qquad 2.123$$

2.9.6 Electromagnetic Torque

Torque can be calculated from mechanical power as

$$P_{mechanical} = \frac{T(t)\omega_{mechanical\ speed}}{pole\ pair} \qquad 2.124$$

$$= T(t)\frac{1}{P}\frac{d\theta_r}{dt} \qquad 2.125$$

Therefore,

$$T = \frac{Power_{mech} \times Pole\ Pair}{\omega} \qquad 2.126$$

$$= \frac{3}{2}P\left(-\psi_q I_d + \psi_d I_q\right) \qquad 2.127$$

or

$$= \frac{3}{2}P\left(-L_q I_q I_d + L_d I_d I_q\right)$$

$$= \frac{3}{2}P\left(L_d - L_q\right)I_d I_q \qquad 2.128$$

2.10 Winding Function Method

A. W. Ranlui first defined the winding function method in 1965 (Lipo, T. A. 2012). The modified winding function was developed to take care of saliences in case of non-uniform air

gap machines. The purpose of the winding function method is to take the winding arrangement and the air gap geometry into account in order to compute self and mutual inductances in a simplify way, without considering the current in the system, but with the assumption of infinite core permeability.

Electrical machines can be reviewed as a combination of windings that are embedded in slots covered by a magnetic circuit such that the current flowing through them will perform electromechanical energy conversion process. Evidently, the magnetic flux established by a winding may, through the magnetic material and air, link not only the winding itself but also other windings of the machine (Filizadeh, Shaahin, 2013). The linkage of the fluxes generated by various windings leads to the development of self and mutual inductances.

Computation of the inductances of electric machine windings is an important step in the formation of electrical machine models and in the analysis of their operation. Apart from the finite element method that is widely used for these inductances computation, traditionally, winding function method was also deployed due to its computational simplicity and less time consuming.

This work also demonstrates the process of inductances computation of the stator windings of a four-pole synchronous generator using winding function method.

2.10.1 Basic formulation

Every electrical machine depends upon the magneto-motive force (MMF) produced by the current flowing in the winding placed in the stator slots to achieve a useful goal of efficient energy conversion. Therefore, one approach to model and analyze electrical machine is by direct analysis of the winding configuration and the air gap MMF produced by the current flow in the windings. Consider the simplest form of the stator phase winding and it is a single concentrated

coil of only one side as shown in Figure 2.2. Assuming uniform air-gap length i.e., neglecting existence of stator and rotor slots, also infinite permeability of iron is assumed.

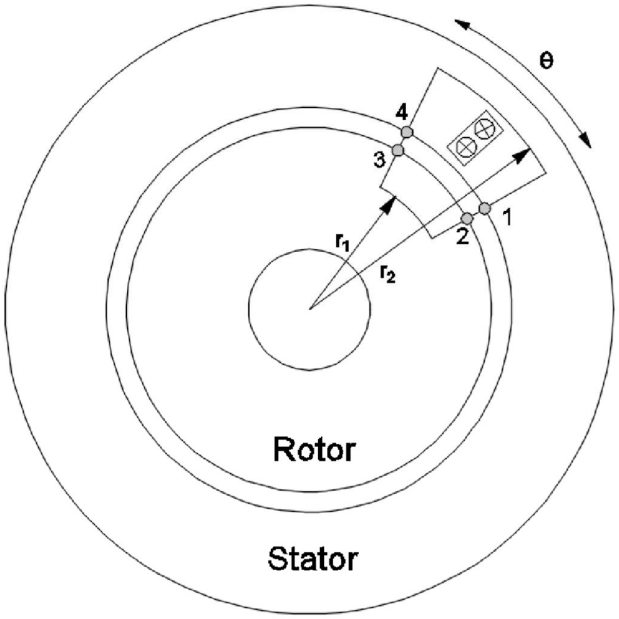

Figure 2.2: Cross-section of Generation Schematic with Winding and Air Gap

Ampere's circuital law can be expressed as following the geometry of the figure 2.2 shown

$\oint_c \mathbf{H}.\mathrm{dl} = \int_s \mathbf{J}.\mathrm{ds}$ 2.129

Where **H** and **J** are the magnetic field intensity and current density respectively. S represents the surface enclosed by the depicted path 12341.

Therefore equation 2.129 can be expressed as

$\oint_{12341} \mathbf{H}.\mathrm{dl} = \int_s \mathbf{J}.\mathrm{ds}$ 2.130

Since all the current on the surface is concentrated in the winding equation 2.130 can be rewritten as

$\oint_{12341} \mathrm{H}.\mathrm{dl} = n(\theta)i$ 2.131

Where n(θ) is the number of terms enclosed by the path, this is called turns function and i is the winding current while θ shows the rotor angle.

Equation 2.131 can therefore by expressed in terms of MMF as

$$F_{12} + F_{23} + F_{34} + F_{41} = n\ (\theta)\ i \qquad 2.132$$

Neglecting the MMF drop in the ferromagnetic core regions (rotor, F_{23} and stator, F_{41}) and considering the path from 1 to 2 at zero angle equation 2.132 can be expressed as

$$F_{12}\ (0) + F_{34}\ (\theta) = n(\theta)i \qquad 2.133$$

F_{12} and F_{34} indicate the MMF drop in the air gap at zero and θ degree respectively.

$F_{12}\ (\theta)$ and $F_{34}\ (\theta)$ are also expressed in term of radial and rotor angle components.

$$F_{12}\ (0) = -g\mathbf{H}_r(r,0) \qquad 2.134$$

$$F_{34}\ (\theta) = g\mathbf{H}_r(r,\theta) \qquad 2.135$$

H_r represents the radial component of magnetic field intensity in the air gap at a specific angle and r shows the radius of the air gap, while g is the air gap function.

Equation 2.133 and 2.134 combined can be written equivalently as equation 2.137

$$\int_0^{2\pi} F_{34}\ (\theta)d\theta = 0 \qquad 2.136$$

Equation 2.136 states that in order for the net flux linking the rotor to be zero, the function $F_{34}\ (\theta)$ must have no average component. [Lipo, T. A., 2012]. The equation 2.131 can be utilized to solve for $F_{34}\ (\theta)$ and $F_{12}\ (0)$.

Integrating equation 2.133 from 0 to 2π

$$\int_0^{2\pi} F_{12}\ (0)d\theta + \int_0^{2\pi} F_{34}\ (\theta)d\ \theta = \int_0^{2\pi} n(\theta)i\ d\ \theta \qquad 2.137$$

Gauss's law of magneto-statics field states that, the net flux leaving any closed surface is zero or

$\int_S \mathbf{B}.ds = 0$

Therefore $\int_0^{2\pi} F_{34}\ (\theta)d\ \theta = 0$

$$F_{12} = \left[\frac{1}{2\pi}\int_0^{2\pi} n(0)d\theta\right] \quad 2.138$$

The quantity in the brackets is clearly the average value of the twin's function $n(\theta)$.

$$<n(\theta)> = \frac{1}{2\pi}\int_0^{2\pi} n(\theta)d\theta \quad 2.139\ F_{12} = <n(\theta)>i$$

From equation 2.139, the MMF at any point along the air gap is

$$F_{34}(\theta) = (n(\theta) - <n(\theta)>)i \quad 2.140$$

The function in the bracket is a turn function $n(\theta)$ without its average value. This is used in machine analysis and named as the winding function.

$$N(\theta) = n(\theta) - <n(\theta)> \quad 2.141$$

2.10.2 Modification of Winding Function for Salient-Pole Generator

In the past, only machines with cylindrical configuration were considered using winding function analysis. This is because the radial air gap between the rotor and the stator is independent of the angle θ measure along the stator-rotor periphery (Lipo, T. A., 2012); hence, the air gap between the rotor outer radius and stator inner radius becomes a function of radial position. Therefore, the air gap length must be expressed as a function of radial angle θ. Consider Figure 2.2 where various points between the stator and rotor are indicated as point

1,2,3,4. Point 1 indicating θ = 0 and point 4 shown at angle θ on the stator.

Salient-pole machine unlike cylindrical type will make the flux lines assume an irregular shape in the air gap to continue to interact both the stator and rotor iron orthogonally.

Path 12 and 34 are in this case defined to lie among line of flux.

Using Ampere's Law

$$\int_{1234} H.dl = \int_{12} H.dl + \int_{34} H.dl = n(\theta)i \quad 2.142$$

Where dl is defined to be along flux lines originating (or terminating) at points 1 and 4. n(θ) is the turn function corresponding to the number of turns enclosed by path 12341. Since the line integral of **H** is by definition the MMF

$$F_{12}(0) + F_{34}(\theta) = n(\theta)i \qquad 2.143$$

Gauss' Law for magnetic fields states that

$$\oint_S \mathbf{B}.\, ds = 0 \qquad 2.144$$

Equation 2.144 can also be expressed in terms of machine deferential area ds which is $R_S(dl)(d\theta)$.

Since **B** does not vary with respect to the axial length.

$$\int_0^{2\pi} \int_o^l (\mu_0 H)\ R_S(dl)(d\theta) = 0 \qquad 2.145$$

R_S is the stator inner radius.

From equation 2.144,

$\int_0^{2\pi} \mathbf{H}(\theta)d\theta = 0$, after eliminating the constants.

The stator surface is where the magnetic field intensity **H**(θ) is evaluated.

Therefore, the equation 2.144 becomes

$$\int_0^{2\pi} \frac{F(\theta)}{g(\theta)} d\theta = 0 \qquad 2.146$$

Equation 2.143 can be divided by g(θ) to give

$$\int_0^{2\pi} \frac{F_{34}(\theta)}{g(\theta)} d\theta = 0$$

Therefore

$$2\pi F_{12}(0) < g^{-1} > = \int_0^{2\pi} \frac{n(\theta)I}{g(\theta)} d\theta \qquad 2.147$$

This is further expressed as

$2\pi F_{12}(0) < g^{-1} > = 2\pi < n > < g^{-1} > I$ or $F_{12}(0) = < n > I$

the winding function is now established as in Equation 1.141

The mutual inductance is therefore

$$\frac{\lambda}{i}AB = L_{AB} = \mu_0 rl \int_0^{2\pi} n_A(\theta) N_B(\theta)\, g^{-1}(\theta) d\theta$$

For the flux linking the B winding due to current in the A winding is considered also as

$$L_{BA} = \mu_0 rl \int_0^{2\pi} N_A(\theta)\, n_B(\theta)\, g^{-1}(\theta) d\theta \qquad 2.148$$

Similarly, the magnetizing inductance is given by

$$L_{AA} = \mu_0 rl \int_0^{2\pi} n_A(\theta)\, N_A(\theta)\, g^{-1}(\theta)\, d\theta \qquad 2.149$$

In the practical case considered here, the rotor is designed to have an even number of symmetrically shaped poles and an equal number of north and south poles [Lipo, T. A, 2012]. Hence, the inverse gap function $g^{-1}(\theta)$ consists of a constant term plus even harmonics of the form.

$$g^{-1}(\theta) = \frac{1}{g_0} + \left(\frac{1}{g_2}\right)\cos 2(\theta - \theta_0) + \left(\frac{1}{g_4}\right)\cos 4(\theta - \theta_0) + \ldots \qquad 2.150$$

Where θ_0 is the point of minimum gap and $g^{-1}(\theta)$ at maximum.

An equivalent expression for mutual inductance is

$$L_{BA} = \mu_0 rl \int_0^{2\pi} n_A(\theta)\, n_B(\theta)\, g^{-1}(\theta)\, d\theta \qquad 2.151$$

While, the magnetizing inductance is

$$L_{AA} = \mu_0 rl \int_0^{2\pi} n_A(\theta)\, N_A(\theta)\, g^{-1}(\theta)\, d\theta \qquad 2.152$$

2.10.3 Formulation of Magnetizing Inductance in Salient Pole Generator

The determination of inductances is the fundamental principle in the analysis and modelling of salient pole synchronous generator assuming the non-linear effects is neglected, the self and mutual inductances of the generators are established due to flux linkage in its own current and current following in another winding.

The differential flux passing through a differential volume of cross-sectional area $(rd\theta)l$ and air gap length g is given by

$$d\varphi = FdP = \frac{\mu_0 rlFd\theta}{g} \qquad 2.153$$

Integrating equation 2.153

$$\varphi = \frac{\mu_0 rl}{g} \int_0^{2\pi} Fd\,\theta \qquad 2.154$$

where P = Permeance, r = inner stator radius, l = axial length of the air gap and μ_0 = permittivity of free space.

Flux linkage ψ is also expressed as

$$\psi = N\,\varphi = iL \qquad 2.155$$

Where L is the inductance and i the current.

Therefore, the total flux linkage for a N_A turns winding due to current in a N_B turn winding can be expressed as

$$\psi_{AB} = \mu_0 rli \int_0^{2\pi} \frac{n_A(\theta) N_B(\theta) d\theta}{g(\theta)} \qquad 2.156$$

2.11 Synchronous Generator

Synchronous generators have been a major source of bulk power generation. They are classified into two different types. The essential difference between the two classes of the generator lies in the rotor construction. The dc excitation is supplied to the field winding. The armature winding stator is usually on the stator and is called stator winding. Stator winding is mostly a three-phase winding. The field winding is on the rotor, the field winding is call rotor winding.

2.11.1 Cylindrical or Round Rotor Structure: This machine has a uniformly cylindrical rotor that carries its excitation winding distributed over a number of slots around its periphery. The Round Rotor Synchronous machine has smaller diameter but long axial length. It is well adapted for the highest speed usually 1500 rpm to 3000 rpm and universally employed for steam or gas turbine as drivers. They are commonly called Turbo Synchronous Generator. The cylindrical pole is used for 2-pole or 4-pole turbine generators and damper windings are not required.

2.11.2 Salient-Pole Structure: Salient-Pole machine has poles that are physically separated and projected, each carrying a concentrated excitation winding. This machine is used for multipolar slow speed hydroelectric generators of speed between 100 rpm to 1500 rpm. They require damper windings to prevent rotor oscillation during operation.

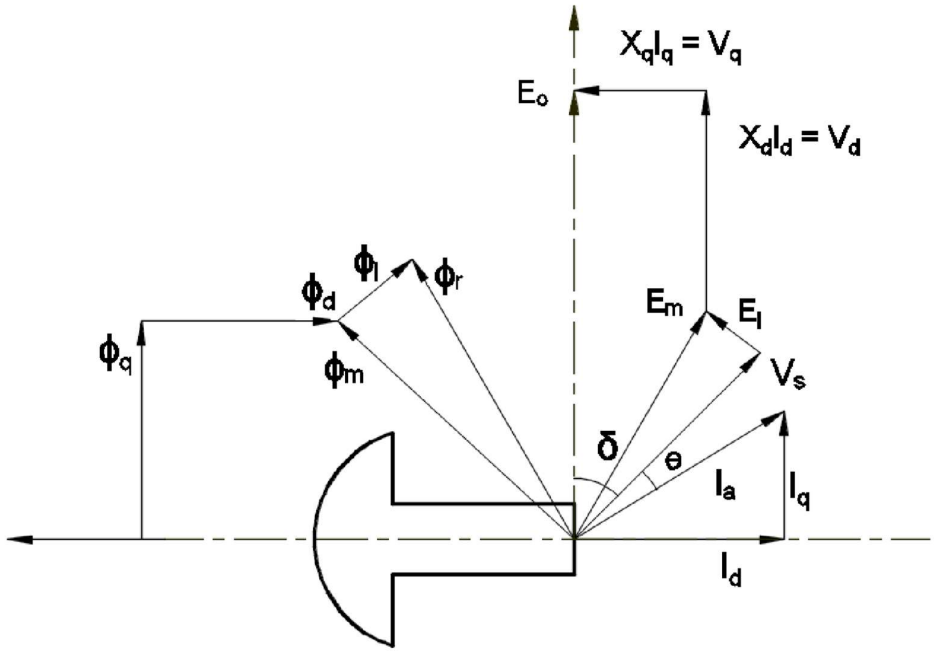

Figure 2.3: Phase Diagram of Steady State with an Inductive Load

2.12 Steady-State Salient-Pole Synchronous Generator Model

The vector diagram of salient-pole rotor synchronous generator is shown in Figure 2.3. Assuming the magnetic circuit is unsaturated with a non-uniform air gap. The effect of this non-uniform air gap is the flux produced by the armature reaction magneto-motive force (MMF) which depends on the rotor position and also determines the reluctance of the path the flux will travel along (Filizadeh, 2013). When the Salient-Pole direct axis is aligned with a particular phase axis MMF, the corresponding magnetic flux density is created, but when the quadrature axis is aligned with the phase axis MMF, a very severe distortion is setup. The difference is

treated by considering these two axes separately as Direct-Axis and Quadrature Axis or Inter-polar axis. The two-axis component of elements, flux density and magneticmotive force brought about a Two-Reaction Theory.

The phase diagram above shows over-excited generator with armature resistance R assume zero for the Salient-Pole Synchronous Generator illustrate the splits of the reactances and current into direct and quadrature components.

The synchronous reactance for the direct axis as

$X_d = X_{ad} + X_l$ while the quadrature axis is $X_q = X_{aq} + X_l$

The major components are expressed as

X_d= Direct axis reactance

X_l = Leakage reactance

X_q = Quadrature reactance

E_o = Internal voltage

V = Terminal voltage I_s =

Inductive load current δ =

Load angle θ = Power

factor

2.12.1 Synchronous Generator Steady State Model

In steady state, a synchronous generator will rotate at a speed directly dictated by the angular frequency of ω_e of its terminal voltage. This synchronous speed is the speed of the stators rotating magnetic field and is equal to the rotor speed. (Fitizadeh, S 2013)

The steady-state behavior is characterized by the mode of operations.

i) The generator at No-load ii) The generator under symmetrical loading conditions.

2.12.2 The Generator at No-load condition

Generator at No-load condition means the machine is subjected to the following conditions

i) Zero stator current
ii) Constant rotor current
iii) Constant speed $\frac{d\theta_r}{dt} = \omega_{mech}$

This type of operation is achieved when generator running is disconnected from the busbar or grid (running by itself).

If the stator current is zero, the electrical power and torque are also zero.

Let's recall the voltage equation for a typical synchronous generator.

$$V = -Ri - \frac{d}{dt}(Li) \qquad 2.157$$

Expressed in matrix form as:

$$\begin{bmatrix} V_s \\ V_r \end{bmatrix} = - \begin{bmatrix} R_s & 0 \\ 0 & r_r \end{bmatrix} \begin{bmatrix} i_s \\ -i_r \end{bmatrix} - \frac{d}{dt} \left\{ \begin{bmatrix} L_s & L_{rs} \\ L_{rs}^T & L_{rr} \end{bmatrix} \begin{pmatrix} i_s \\ -i_r \end{pmatrix} \right. \qquad 2.158$$

The emf in phase a can be expressed as

$$e_a = -\omega L_5 i_r^{\circ} \sin \omega t = \sqrt{2} I_m \{E_a e^{j\omega t}\}$$

where the emf phasor or E_a is defined by

$$\frac{\omega L_5 i_r^{\circ}}{E_a \triangleq -\sqrt{2}}$$

$|E_a|$ is proportional to the field current magnitude i_r° and rotor speed ω.

2.12.3 Salient-Pole Synchronous Generator d q Model

The analysis and modelling of salient-pole synchronous generator was considered by implementing cylindrical rotor theory where all the armature reactance were assumed constant, regardless of the rotor position, due to the uniform air-gap geometry. In a salientpole

synchronous generator, this cannot be the same due to saliency effect of the rotor. Thus the effect of non-uniform air gap of salient-pole generator will cause the air-gap reactance to be time-varying based on the rotor angular position. Therefore, the power angle curve model of salient-pole synchronous generator is expressed below.

2.12.4 Power Angle Curve with Saliency

Figure 2.4 shows the Power Angle Curve plotted from the Power-Angle equation given by

$$P_e = \frac{|E||V|}{X_d}\sin\delta + |V|^2\frac{X_d - X_q}{2X_dX_q}\sin 2\delta \qquad 2.159$$

Equation 2.159 is represented in power per unit.

Where,

E = No-load generated emf in pu.

V = Generator terminal voltage in pu.

X_d = Direct-axis reactance in pu.

X_q = Quadrature-axis reactance in pu.

δ = Power angle

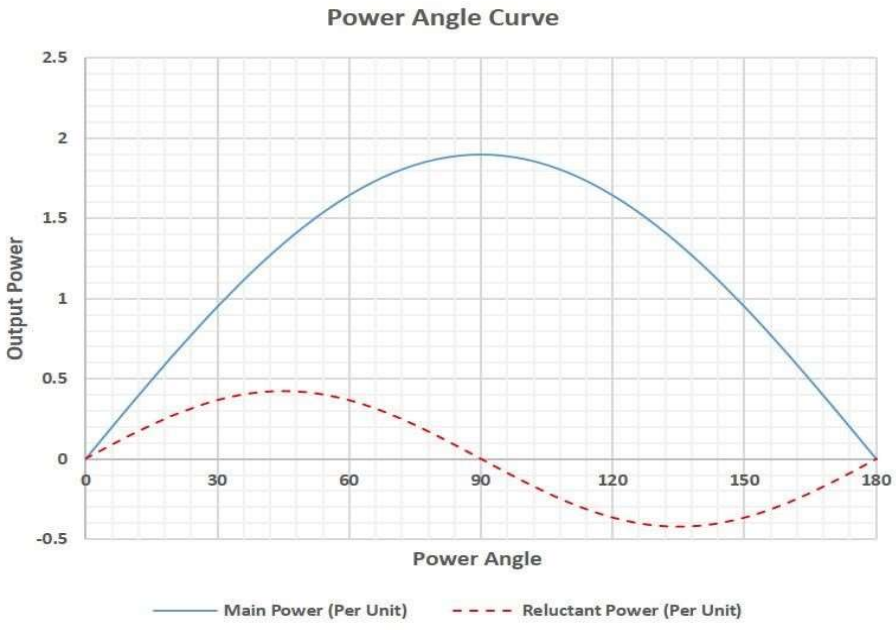

Figure 2.4: Power Angle Curve with Saliency

This power comprises the first term which represent power from non-salient rotor generator with synchronous reactance (X_s) equal to the direct axis reactance and constitute the major part in power transfer. The second term is the power delivered because of saliency of the rotor and it is called Reluctance Power.

Also, the power angle equation is expressed in equation 2.160 as

$$\delta = \tan^{-1}\frac{X_q|I_a|\cos\theta}{|V| + X_q|I_a|\sin\theta} \qquad 2.160$$

Where,

I_a is the armature current and θ

is the power factor

Under steady-state condition the dq0 components attain constant value and hence their time derivative tend to zero (Filizadeh, 2013)

That is

i) No time dependent change of flux linkage $\left(\frac{d\psi}{dt} = 0\right)$ ii)

The speed of the rotor is constant $\left(\frac{d\theta_r}{dt} = \omega_e\right)$

Also, in a balance operation, it is assumed that 0-component is equal to zero.

The following steady state equations are obtained

i) The steady state flux linkages are

$$\psi_d = L_d i_d + L_{dF} i_F \qquad 2.161$$

$$\psi_q = L_q i_q \qquad 2.162$$

$$\psi_F = L_F i_F + L_{dF} i_d \qquad 2.163$$

ii) Steady state stator voltage components

$V_d = \omega_e L_q i_q$ 2.164

$V_q = -\omega_e(L_d i_d + L_{dF} i_F)$ 2.165

$V_F = -i_F R_F$ 2.166

Since the damper current is zero, the steady state torque becomes

$T_e = [L_d I_F I_q + (L_d - L_q) I_d I_q]$ 2.167 Torque produced by the field winding is

Reaction Torque $= \frac{3}{2}\frac{P}{2} L_d I_F I_q$ 2.168

Reluctance Torque $= \frac{3}{2}\frac{P}{2}(L_d - L_q) I_d I_q$ 2.169 **CHAPTER THREE**

MATERIALS AND METHOD

3.1 Research Materials

Materials used in this research include the following:

3.1.1 Finite Element Method Magnetic (FEMM)

(a) Two Reaction Theory demonstration or illustration

(b) Magneto-statics Analysis

3.1.2 ANSYS Maxwell

(a) Magneto-statics, Transient and Time Harmonic Analysis

(b) Time-Stepping Simulation

3.1.3 MATLAB

(a) Data from FEMM & ANSYS Maxwell for analysis.

(b) Data Plotting

3.2 Research Method

3.2.1 Basic Design Method and Specification for Salient-Pole Synchronous Generator

The design of any generator involves determination of each part of the generator's specification, with prepared drawings and supply to production units. The design carried out has to be in view of cost optimization, volume and weight at the same time achieving the desired performance as per specification.

The design of synchronous generators involves the following:

i. Dimension of the stator frame ii.

Complete detail of the stator windings iii.

Design detail of the rotor and rotor winding iv.

Performance details of the generator

Apart from the above, other targets of the design are:

i. Specification of the synchronous generator ii.

Information regarding the choice of design parameters iii.

Knowledge on the availability of the materials iv.

Limiting value of the performance parameters

v. Details of design equations

3.2.2 Design Specification without Values

Other important specifications required to initiate the design procedure are as follows:

a) Rated output of the generator in kVA or MVA

b) Rated voltage of the generator in kV

c) Rated speed (N_s) rpm

d) Frequency (Hz)

e) Generator type

f) Type of rotor

g) Stator winding connection

h) Temperature limit

i) Detail of prime mover

The parameters and dimensions for the design are specified Table 3.3, Table 3.4, Table 3.5 and Table 3.6.

3.2.3 Main dimension of stator frame

The internal diameter and the gross length of the stator frame are the main dimensions of the generator. It is important to develop an equation relating the output of the synchronous generator with its main dimensions, in order to estimate them. Linking the dimensions of the generator with magnetic and electrical parameters of the generator using the output equation

3.1, will result in equation 3.2.

Output of the generator, $Q = 3V_{ph}I_{ph} \times 10^{-3}$ kVA 3.1

$Q = (11B_{av}q\ k_w)D^2Ln_s$ kVA 3.2

Where output coefficient (k) = $11\ B_{av}q\ k_w \times 10^{-3}$

The starting point of the generator design is by utilization of output coefficient (k)

$$k = \frac{Q}{D^2Ln_s} \quad 3.3$$

Where D = Diameter of armature (m) L

= Gross length of armature (m) n_s

= speed of the generator (rps)

For higher output coefficient (k) the product of "D^2Ln_s" is lower. D^2L translate to volume of the generator.

3.2.4 Choice of Specific Loadings

The above output equation shows that the choice of higher value of specific magnetic and electric loading leads to reduced cost and size of the generator.

Specific magnetic loading $(B_{av}) = \frac{p\phi}{\pi DL}$ 3.4

Where p = no of poles; ϕ = flux per pole; D = diameter of armature; L = gross length of armature

Specific electric loading $(q) = \frac{I_a Z_a}{\pi D}$ 3.5

Where I_a= armature current

Z_a= no. of armature conductors

D = diameter of armature

The associated factors for magnetic and electric loading are not discussed in this research, the dimensions that would affect the generator performance were considered, these dimensions are Diameter (D) and Gross length of armature (L) are discussed.

3.2.5 Relationship between D and L

Internal diameter and gross length of the stator can be calculated from the product D^2L, obtained from the output equation, provided a suitable relation is assumed between D and L (Mittle, V. N., Mittle, A.; 2017). A salient-pole synchronous generator uses either round or rectangular pole. The rectangular pole philosophy utilized in the design of the synchronous generator is discussed in the work.

Therefore, the ratio of axial lengths of the core to poles pitch varies from 0.8 to 3 A suitable ratio may be assumed for axial length to pole pitch depending on the design specifications.

$$\frac{\text{Axial length of the core}}{\text{Pole pitch}} = \frac{L}{\tau_p} = 0.8 \text{ to } 3 \qquad 3.6$$

Utilizing equation 3.6 along with output equation, the computation of the internal diameters of the stator and its gross sectional length obtained. The number of poles are many in salient-pole synchronous generator, which indirectly results into larger rotor diameter. The axial length of this generator is smaller than the stator diameter (Upadhyay, K. G 2013). However, once the axial length is obtained; the diameter of the generator must satisfy the limiting value of peripheral speed so that rotor can withstand centrifugal forces produced. The limiting values of peripheral speeds for normal design = 30m/s.

3.3 Factors Affecting Salient-Pole Synchronous Generator Performance

There are many design parameters that affect the synchronous generator performance, some of them relate directly with inductance and physical dimension of the generator. The Two Reaction Theory also has connection magnetically with these parameters. Therefore, the two considered parameters are:

i. Short Circuit Ratio ii.
   Air Gap length

3.3.1 Short Circuit Ratio

One of the useful quantities derived from the Short and Open-Circuit Characteristics is the Short-Circuit Ratio (SCR). Short circuit ratio of a synchronous machine is the ratio of the field current required for the rated voltage on open circuit to the field current required for rated armature current on short circuit (Lipo, T. A., 2012). The speed under which both tests should be is the rated speed of the synchronous machine (Mittle, V. N. et al., 2017).

Short circuit ratio is an extremely important parameter of synchronous machine, because it governs the performance such as stability limit, voltage regulation, short circuit current, synchronizing power, parallel operation, size and cost of the machine (Mittle, V. N. et al., 2017).

The SCR value either small or large has its advantage or disadvantage as regards the parameters mentioned above. In order to optimize the design performance of the machine, a standard and acceptable SCR range of 0.9 to 1.3 is recommended for salient-pole synchronous machine (Mittle, V. N. et al., 2017). For good performance to be achieved for salient-pole synchronous generator design, the SCR must conform to these standard limits.

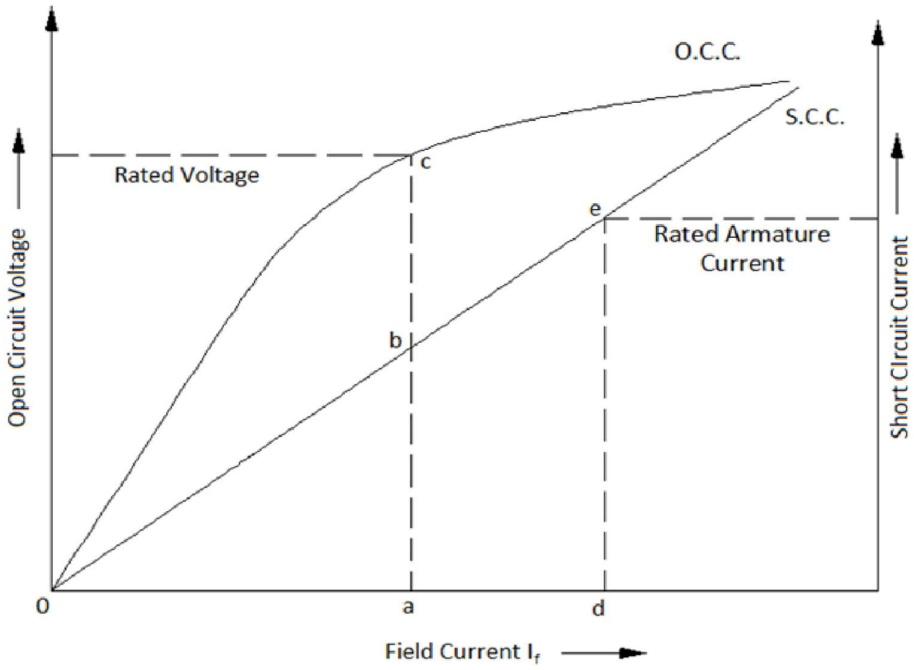

Figure 3.1: Open and short-circuit characteristic of salient-pole synchronous machine A short-circuit characteristic together with an open-circuit characteristic is shown in figure 3.1. From figure 3.1, the short circuit ratio is given by the equation below:

$$SCR = \frac{\text{If for rated O.C voltage}}{\text{If for rated S.C current}} = \frac{Oa}{Od} \quad 3.7$$

Since the triangle Oab and Ode are similar

Therefore $SCR = \frac{Oa}{Od} = \frac{ab}{de}$ 3.8

The direct axis synchronous reactance in ohms is given by

$$X_d = \frac{ac}{ab} \text{ Ohms} \quad 3.9$$

The per-unit value of X_d is given as:

$$X_d pu = \frac{X_d}{\text{Base impedance}} pu \quad 3.10$$

$$\text{Base Impedance} = \frac{\text{Per phase rated voltage}}{\text{Per phase rated armature current}}$$

$$\text{Base Impedance} = \frac{V_{rated}}{I_a rated} = \frac{ac}{de} \text{ Ohms} \quad 3.11$$

$$X_d pu = \frac{ac}{ab} \cdot \frac{de}{ac} = \frac{de}{ab} \quad 3.12$$

Combining equation 3.7 and 3.12 result in equation 3.13

$$SCR = \frac{ab}{de} = \frac{1}{(de/ab)} = \frac{1}{X_d pu} \quad 3.13$$

3.3.2 Air Gap Length

Another useful parameter that is also important in the design of electrical rotating machines is the air gap length. Air gap length contribution to the no load magneto-motive force (MMF) is quite significance. If the synchronous machine is designed with a large air gap, the reluctance offered to the path of the magnetic flux produced by the armature MMF will be larger, thus reducing the effect of armature reaction. Smaller value of direct-axis synchronous reactance and produce higher short circuit ratio. (Mittle, V. N. et al., 2017). Therefore, for salient-pole synchronous machine design, proper choice of the air gap is most essential, due to its effect on the machine performance parameter, example the stability that is directly dependent on SCR.

As a guideline, the approximate value of the air gap length can be expressed in terms of the pole pitch. For salient-pole synchronous generators:

The air gap length (lg) = (0.012 to 0.016) x pole pitch.

3.3.3 Significance of Short Circuit Ratio (SCR) and Air Gap Length to Salient–Pole Synchronous Generator

Short Circuit Ratio, an important performance parameter of the synchronous generator is inversely proportional to per unit value of direct axis synchronous reactance. It affects the operating characteristics, physical size, and cost of the generator. Significance of SCR is better understood when considering two cases:

(i) Low Short Circuit Ratio

The low value of SCR simply means greater value of direct axis reactance. The voltage regulation of the generator is greatly affected by direct axis reactance. The higher the value of direct axis reactance, the poor will be the voltage regulation. This means that, the terminal voltage will vary widely with variation in load. In order to keep the terminal voltage constant, the field current has to be varied over a wide range.

Also low value of SCR affects the stability of synchronous machine. The synchronizing power of synchronous machine is defined as the degree by which the machine has a tendency to be synchronized with the infinite grid system just after experiencing disturbance.

With low value of synchronizing power, the generator will have fewer tendencies to be synchronized again after recovering from disturbance. For the small value of the short circuit ratio (SCR), the synchronizing power is small. As the synchronizing power keeps the generator in synchronism, a lower value of the SCR has a low stability limit. In other words, a generator with a low SCR is less stable when operating in parallel with the other generators.

The only advantage of lower SCR is the lower value of armature current during short circuit.

(ii) High Short Circuit Ratio

A synchronous generator with a high value of SCR had a better voltage regulation, thus the terminal voltage is practically constant during the load variation. It improves steady-state stability limit due to increased value of synchronizing power. High SCR also affects the size, weight and cost of the machine.

The length of the air gap is a very vital parameter as it greatly affects the performance of salientpole synchronous generator. The air gap reluctance or air gap length is directly proportional to the short circuit ratio. If the length of the air gap is increased, the SCR will increase. With the increase in the air gap length, the field MMF is increased for the same value of excitation voltage. Therefore, to increase the value of field MMF either field current or the number of field turns has to be increased. All this requires a greater height of field poles and, as a result, the overall diameter of the machine increases.

Therefore, the choice of air gap length is very critical in case of salient-pole synchronous generator. Here are the following advantages and disadvantages of larger air gap length.

Advantages:

(i) Stability: Higher value of stability limit

(ii) Regulation: Smaller value of inherent regulation

(iii) Synchronizing power: Higher value of synchronizing power

(iv) Cooling: Better cooling

(v) Noise: Reduction in noise

(vi) Magnetic pull: Smaller value of unbalanced magnetic pull

Disadvantage:

(i) Field MMF: Larger value of field MMF is required

(ii) Size: Larger diameter and hence larger size

(iii) Magnetic leakage: Increased magnetic leakage

(iv) Weight of copper: Higher weight of copper in the field winding (v) Cost: Increase overall cost.

Hence, air gap length of the generator must be selected when considering the above effects on the generator performance.

In order to balance the economic benefit with optimum performance, the choice of SCR and air-gap length must be optimally evaluated. These parameters are part of the results comparison and discussion in chapter 4.

3.4 Finite Element Computational Process for Synchronous Generator Modelling

The computational process of obtaining Salient – Pole Synchronous Generator modelling utilizing the two Finite Element software (Finite Element Method Magnetic and ANSYS Maxwell) is illustrated in figure 3.2.

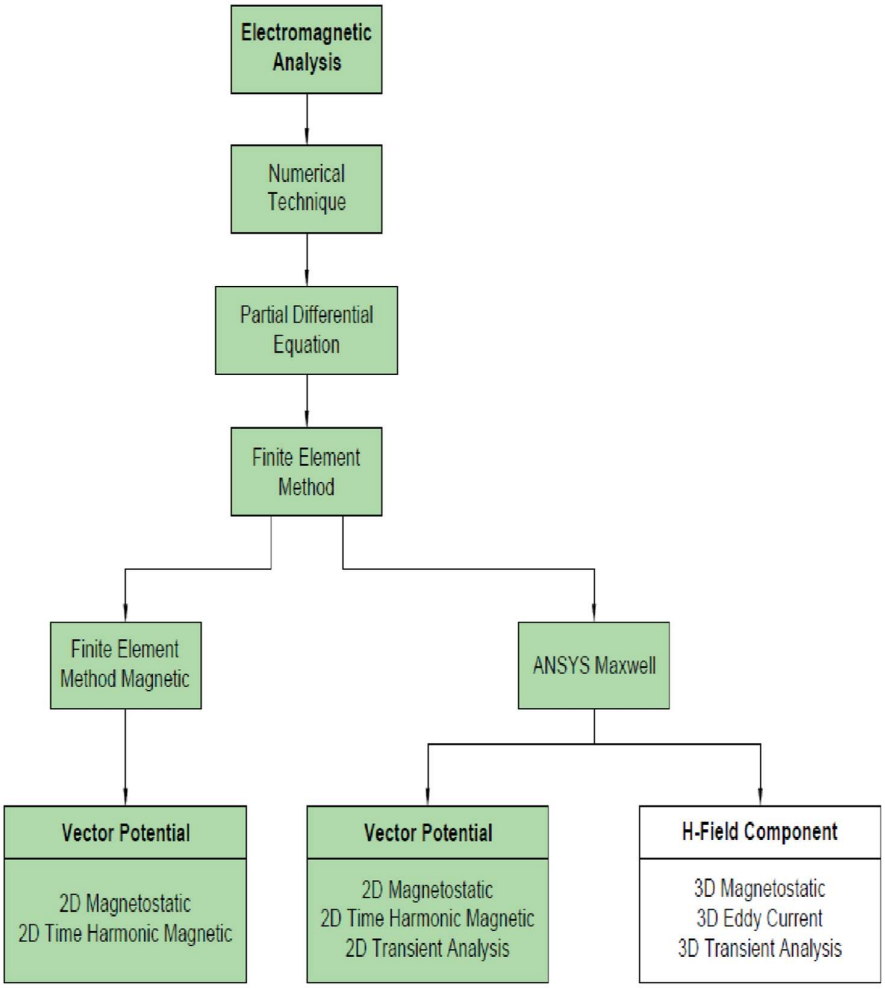

Figure 3.2**:** Finite Element flow process showing utilization model of the numerical algorithm

3.4.1 Application of Finite Element Method Magnetics (FEMM) to Salient-Pole Synchronous Generator

The research uses FEMM 4.0 version to present the magnetic flux density pattern and plots of Salient–Pole and Round Rotor Synchronous Generators at various rotor angles. These field mapping and plots clearly explain better the Two Reaction Theory propounded by Andrew Blondel as a matter of the field mapping and MMF plotting comparison for the Salient-Pole and Cylindrical Synchronous Generators.

Finite Element Method has been widely proven efficient when dealing with

complicated geometries such as the one in this research. The configuration of this generator is considered such that the stator produced MMF rotates at synchronous speed. Since the rotor is also rotating at synchronous speed in the steady state an observer on the rotor experiences a constant field i.e. $\frac{\mathbf{dB}}{\mathrm{dt}} = 0$. Therefore, there are no eddy currents on the rotor. An observer on the stator experiences a time-varying field whose fundamental is at the system frequency

(Salon, S. J 1995). Poisson's Equation and a Magneto-Static Method are adopted for the analysis. By performing static analysis, the following are neglected: -

i. Effects of space harmonics of stator winding on the rotor surface losses.
ii. Effects of tooth permeance losses.
iii. Due to single position analysis, the effect of rotor and stator teeth is neglected.

Table 3.1: Salient-Pole and Cylindrical Synchronous Generator Data

S/N	Parameter	Salient-Pole Synchronous Generator	Cylindrical Synchronous Generator
		Generator Data	
1	Terminal Voltage (Volts)	400	400
2	Frequency (Hertz)	50	50
3	Phase	3	3
4	Number of Poles	4	4
5	Generator Speed (rpm)	1500	1500

Table 3.2: Salient-Pole and Cylindrical Synchronous Generator Characteristics / Properties

S/N	Parameter	Salient-Pole Synchronous Generator	Cylindrical Synchronous Generator
		Stator Characteristics	
1	Number of Slots	36	36
2	Number of Phase	3	3
3	Number of Slot per Pole per Phase	3	3

4	Pole Pitch	9	9
5	Slot Angle (Elect. Degrees)	20	20
6	Coil pitch	8	8

		Stator Properties	
1	Stator Material	Steel_ 1008_2DSF0.950	Steel_ 1008_2DSF0.950
2	Electrical Conductivity	58	58

		Stator Boundary Condition	
1	External Stator Surface	Prescribe A	Prescribe A

		Rotor Properties	
1	Rotor Material	Steel_ 1008_2DSF0.950	Steel_ 1008_2DSF0.950
2	Electrical Conductivity (MS/m)	58	58

		Field Excitation	
1	Property Name	RC	RC
2	Conductor	Copper	Copper
3	Number of Turns	45	5
4	Electrical Conductivity (MS/m)	58	58
5	Relative Permeability	1	1

		Rotor Boundary Conditi on	
1	Rotor Shoe Pole	Mixed (Neumann or Robin)	Mixed (Neumann or Robin)

		Air Gap Boundary Condition	
1	Air Gap	Mixed	Mixed

The procedure for numerical computation of magnetic field distribution problem for synchronous generator using finite element method involves mathematical process that is explained in chapter two of the “solution of the problem” which can be summarized in the three steps below.

3.4.1.1 Pre-Processing

Specification of the different materials in these synchronous generators computation space is shown in fig. 3.3(a) 3.3(b). The Derivation of the finite element model of the two generators under consideration involves defining conduction materials, electromagnetic materials and their properties and boundary conditions and eventually resulted in mesh generation. The generator is made up of two sections, the rotor and stator. The materials properties and boundary conditions will be detailed to rotor and stator as expressed in Table 3.1.

The cross section of computation space for synchronous generators are simply detailed in the computation space shown in fig 3.3(a) and Fig 3.3(b). The properties specified in the rotor, stator and air gap are inputs into various defined region and section of the space. These values are sued for computation within the defined boundary of the region and labelled as a block called “Block Labels”. The air gap is defined by a boundary condition which is a circle separating the rotor/inner section of the generator with the stator slots and the steel structure. The stator is made up of 36 slots, each slot is defined by copper conductor defined as “Cu”, with three phases (a^+, a^-), (b^+, b^-), (c^+, c^-), spanning around the stator in the slots. The characteristics and properties of the two generators are in Table 3.1 and 3.2. The shaft is defined as air or vacuum property. Some of the properties especially conductors are taken from the FEMM library and confirmed from electrical data book.

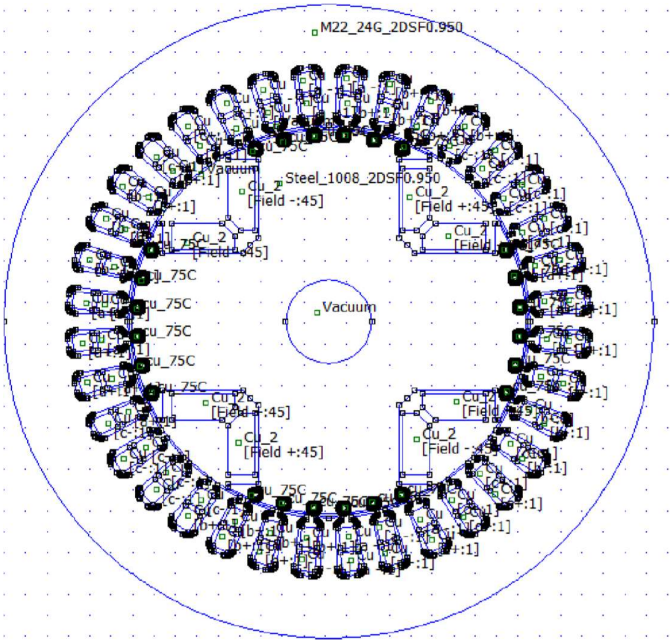

Figure 3.3(a): Section and Computation Space - Salient-Pole Synchronous Generator

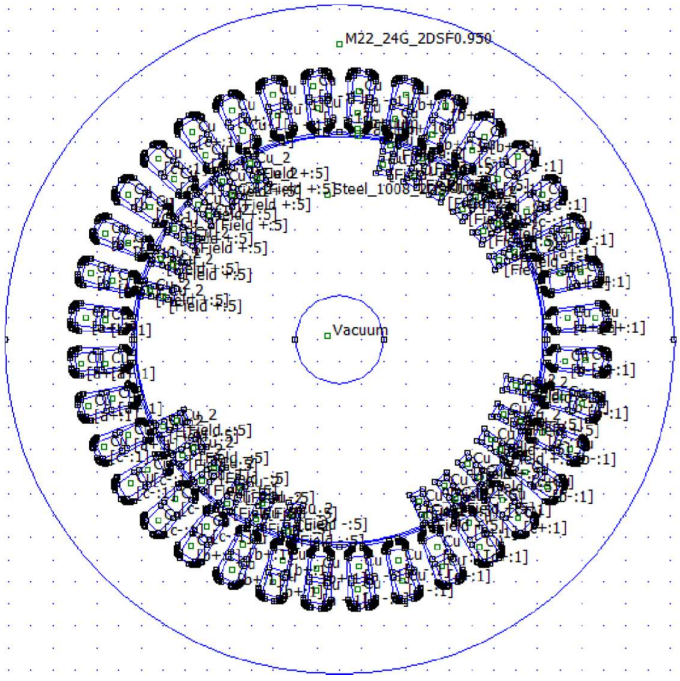

Figure 3.3(b): Section and Computation Space - Cylindrical Synchronous Generator

The figures 3.4(a) and 3.4(b) are part of pre-processing that shows a typical representation of mesh generation in synchronous generator computation space generated by

triangle.exe file of finite element method magnetic of interactive shell. This executable file breaks down the entire synchronous generator solution region defined by materials, circuit properties and boundary conditions into a large number of 672,588 triangular elements and 336,375 nodes for Salient - Pole Synchronous Generator and 540,598 triangular elements and 270,380 nodes for Cylindrical Synchronous Generator before the solver (fker.exe) does the mathematical computation.

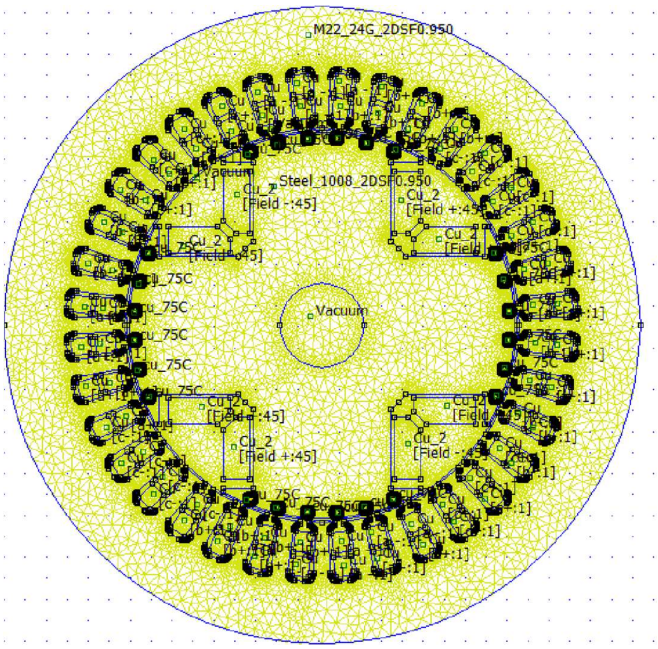

Figure 3.4(a): Generated Mesh in Computational Space - Salient-Pole Synchronous Generator

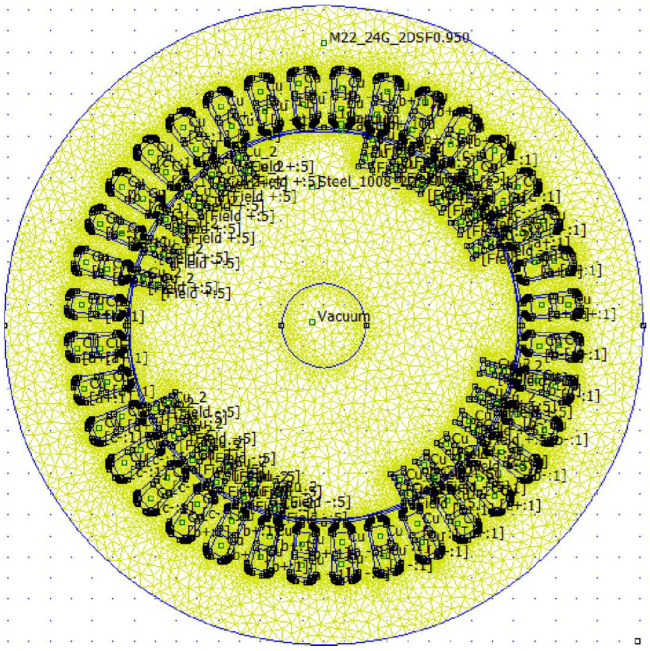

Figure 3.4(b): Generated Mesh in Computational Space - Cylindrical Synchronous Generator

3.4.1.2 Post-Processing

This is the process of calculating and presenting a synchronous generator flux pattern and deducing some results as well as parameters from the analysed model (Zlatko et al 2005). Figures 3.5(a) and 3.5(b) are the flux patterns obtained from the computations. Finite Element Method Magnetic (FEMM 4.0) solver takes a set of data that describe the problem from the region and solves relevant Maxwell's equations to obtain field values, which are translated to field distribution in the analyzed domain for this generator. In order to obtain the desired result Finite Element Method Magnetic will then be run at arbitrary condition with winding excitation and loading condition as shown in chapter 4.

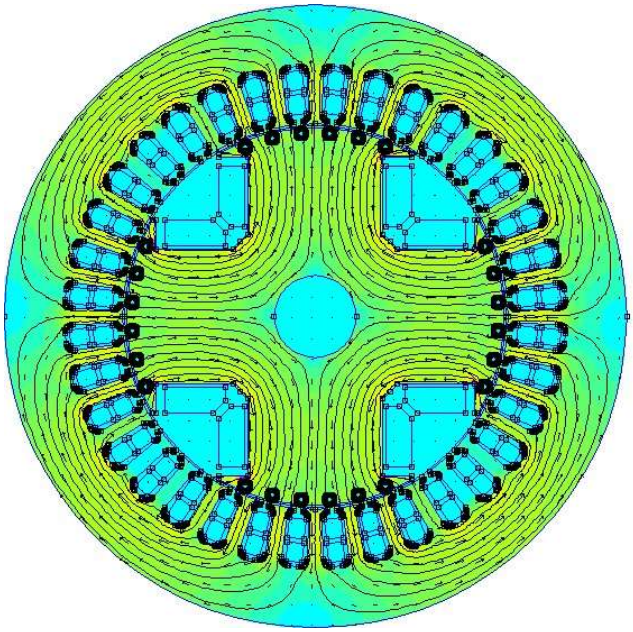

Figure 3.5(a): Magnetic Flux Pattern Obtained by Finite Element Magnetic Method - Salient-Pole Synchronous Generator

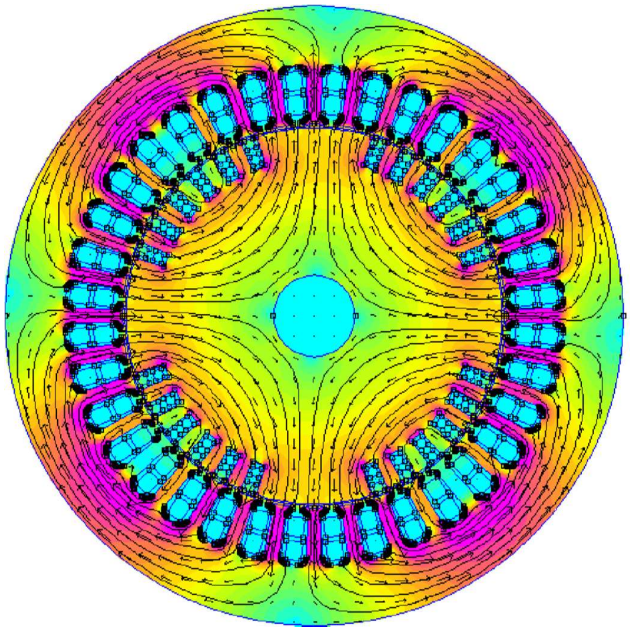

Figure 3.5(b): Magnetic Flux Pattern Obtained by Finite Element Magnetic Method Cylindrical Synchronous Generator

3.4.2 Application of ANSYS Maxwell to Salient-Pole Synchronous Generator

Modelling, simulation and analysis of windings of rotating electrical machines have a long history from the beginning of electric machines some years ago. In general, it is possible to achieve or realize sinusoidal winding distribution along the air gap circumference. Thus, the generated magneto motive force (MMF) of discretely distributed winding and its resultant electromotive force (EMF) are not ideally sinusoidal anymore. To accomplish this, the

application of RMxprt is useful.

RMxprt (Rotating Machine Expert) is a template-based tool for electrical machine design that provide fast analytical calculation and simulation of machine performance. The 2dimensional (2-D), 3-dimensional (3-D) machine geometry can be created for finite element

computation in ANYSYS Maxwell.

ANYSYS Maxwell provide a robust and flexible platform for electromagnetic analysis for rotating machines. The inclusion of RMxprt into ANSYS Maxwell made the design and analysis of Salient Pole Synchronous Generator as applied to this research more convenient, user friendly and rewarding. The RMxprt is particularly useful for designers of electrical machine since it gives the ability to optimize the machine with best performance.

As mentioned in chapter two about the features and the capabilities of RMxprt, a SalientPole Synchronous Generator (SPSG) model shown in figure 3.6 was drawn with AutoCAD and adopted in RMxprt environment. The model was drawn according to a known generator specification. The generator details, dimensions and winding diagram of the SPSG are provided in the Tables 3.3. Using RMxprt and ANSYS Maxwell as a tool, many generator parameters obtained for optimum operational performance. These parameters are:

i. Winding current ii. Magnetizing Inductances iii. Flux linkage iv. Induced voltage

v. Input voltage and current

vi. Damper bar current and voltage vii. Moving Torque

Further plots obtained from RMxprt as follows:

i. Air Gap Permeance (Air Gap Function)

ii. Armature Phase Current iii. Flux Density iv. Induced Voltage

v. Power Angle Curve vi. Generator Speed

vii. Open and Short Circuit characteristics

3.4.3 Generator Design Details

The generator design details are as shown in table 3.3, table 3.4, table 3.5 and table 3.6.

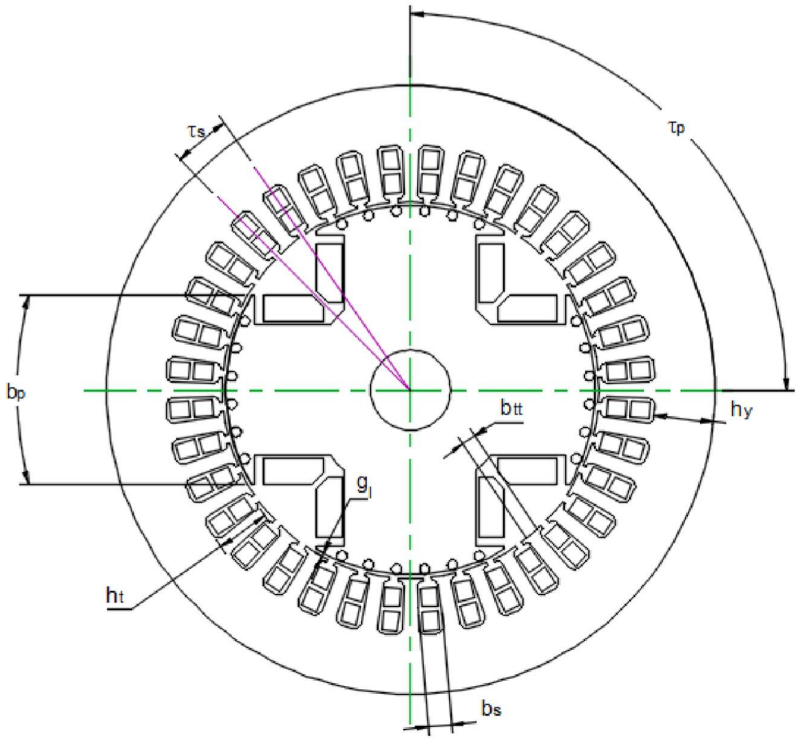

Figure 3.6: Salient-Pole Synchronous Generator Physical Geometrical Diagram **Legend: Generator Geometrical Abbreviations**

Symbol	Description
b_p	Pole arc
τ_p	Pole pitch
g_l	Air gap length
b_{tt}	Minimum width of teeth
b_s	Width of slot
h_t	Height of slot
h_y	Distance from slot to stator circumference
τ_s	Slot pitch

Table 3.3: Generator parameter dimensions

Parameters	Value
Generator Physical Dimensions	
Pole arc (mm)	98.61
Pole pitch (mm)	144.51
Air gap length (mm)	1.78
Minimum width of teeth (mm)	7.01
Width of slot (degree)	7
Height of slot (mm)	26.84
Distance of slot to stator circumference (mm)	29.40
Slot pitch (degree)	10
Rotor shaft diameter (mm)	40
Generator Operating Data	
Rated Apparent Power (kVA)	20
Rated Power Factor	0.85
Rated Voltage (V)	400
Winding connection	Wye
Number of Poles	4
Frequency (Hz)	50
Rated Speed (rpm)	1500
Operating Temperature (℃)	75

Major Stator Data	
Number of Stator Slots	36
Stator Outer Diameter (mm)	304
Stator Inner Diameter (mm)	188
Length of Stator Core (mm)	275
Stator material (Type of Steel)	M22 - 24G
Coil Pitch	8
Number of conductors per slot	10
Stator Winding Factor	0.9452

Table 3.3: Generator parameter dimensions (continued)

Physical Dimension for Winding Function Computation	
Parameter	**Value**
Winding type	Distributed
Coil pitch	9
Number of slots	36
Number of poles	4
Number of winding turn	5
Rotor outer diameter	188.05mm
Generator effective length	275mm
Air gap length	2.025mm
Ratio of pole arc to pole pitch	0.682
Stator outer diameter	304mm

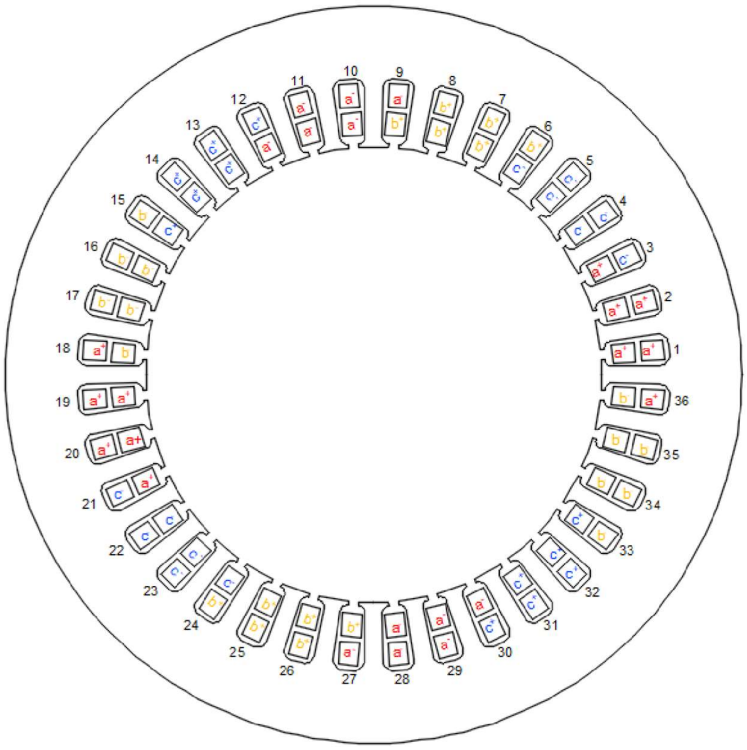

Figure 3.7 (a): Stator diagram from AutoCAD

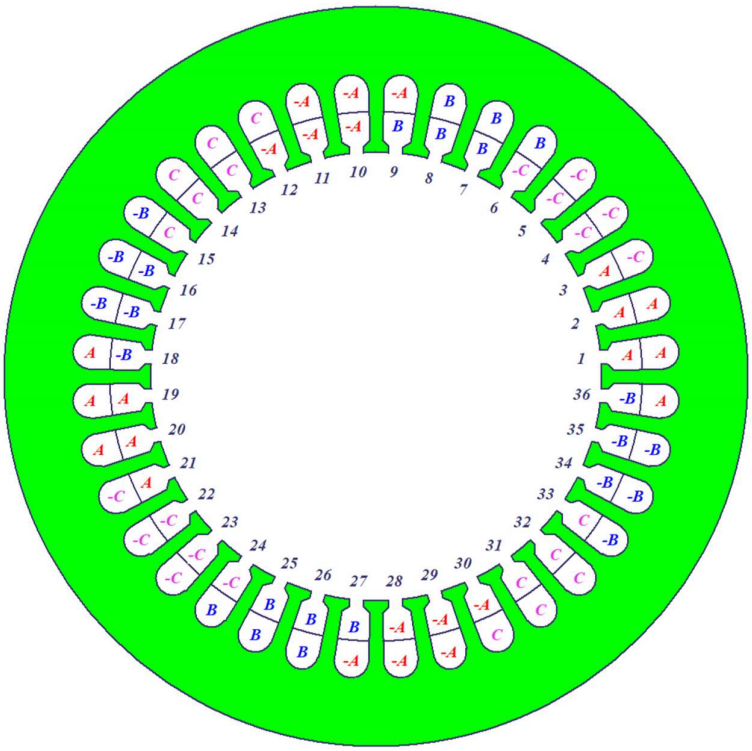

Figure 3.7 (b): Stator diagram from RMxprt

The parameter in Table 3.4 below indicates rotor physical dimensions and materials. Table 3.4: Rotor Data

Parameters		**Value**
Minimum Air Gap (mm)		2.025
Inner Diameter (mm)		40
Rotor Length (mm)		275
Rotor material		
(i)	Type of Yoke Steel	Steel_1008
(ii)	Type of Pole	Steel_1008

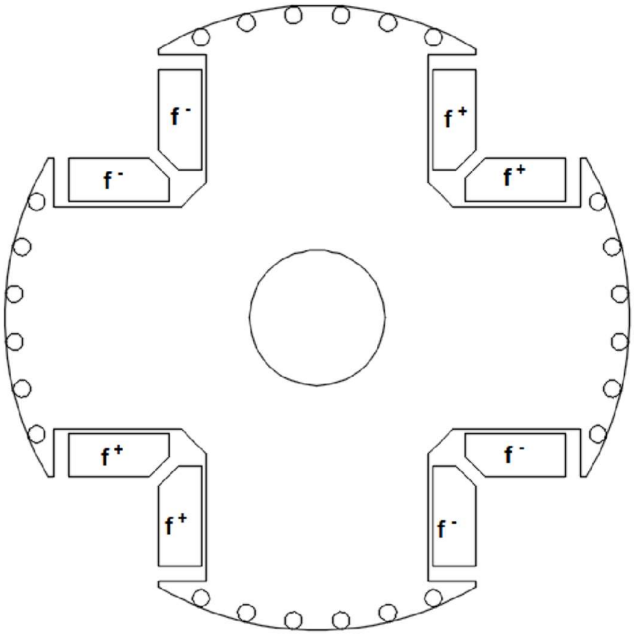

Figure 3.8 (a): Rotor diagram from AutoCAD

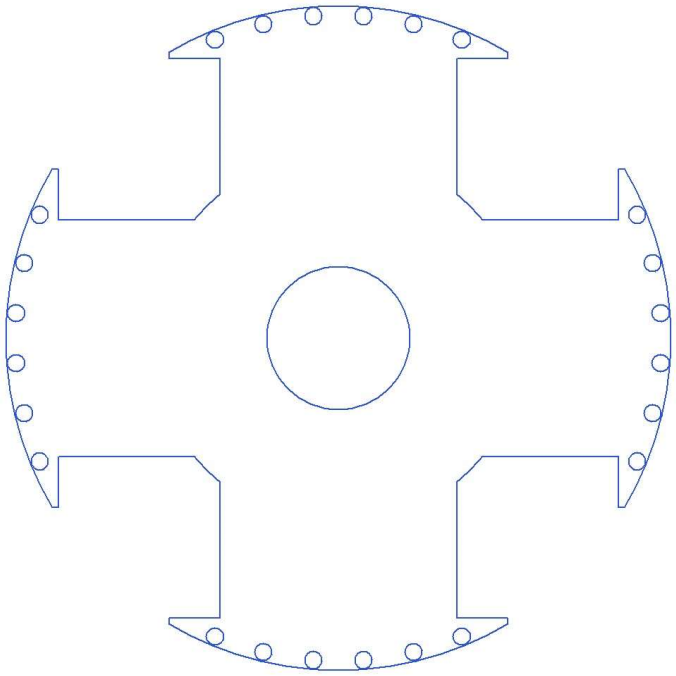

Figure 3.8 (b): Rotor diagram from RMxprt

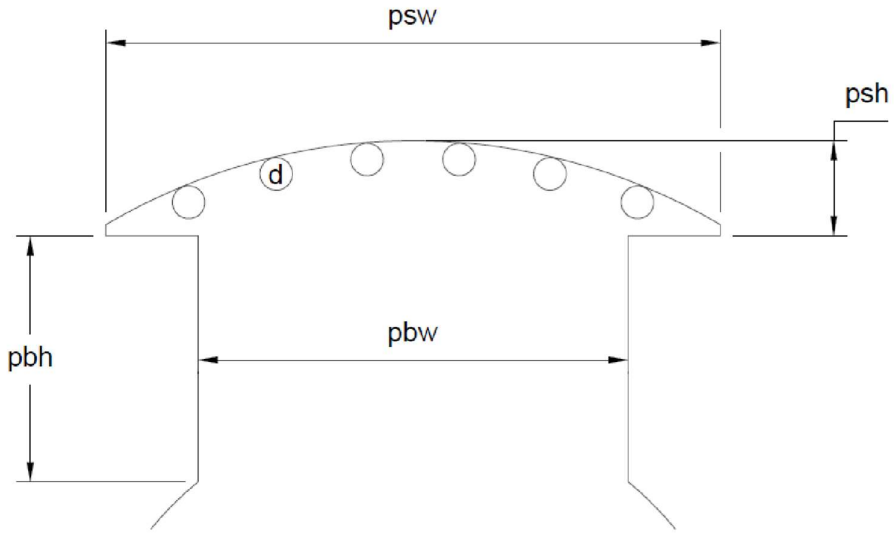

Figure 3.9: Rotor Pole Description

Legend: Damper Bar (End Connection) Abbreviations

Symbol	Description
pbh	Pole body height
pbw	Pole body width
psh	Pole shoe height
psw	Pole shoe width
d	Damper Bar

Table 3.5: Damper Data

Parameters	Value
Number of Damper per pole	6
Slot Pitch (mech degrees)	9

Table 3.6: Stator Slot Data

Parameters	Value
Hs0 (mm)	1.55
Hs1 (mm)	2.88
Hs2 (mm)	19.96
Bs0 (mm)	4.13
Bs1 (mm)	10.19
Bs2 (mm)	12.8
Rs (mm)	4

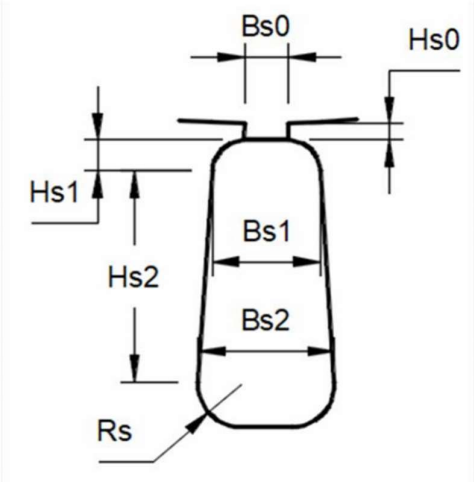

Figure 3.10: Stator Slot Description

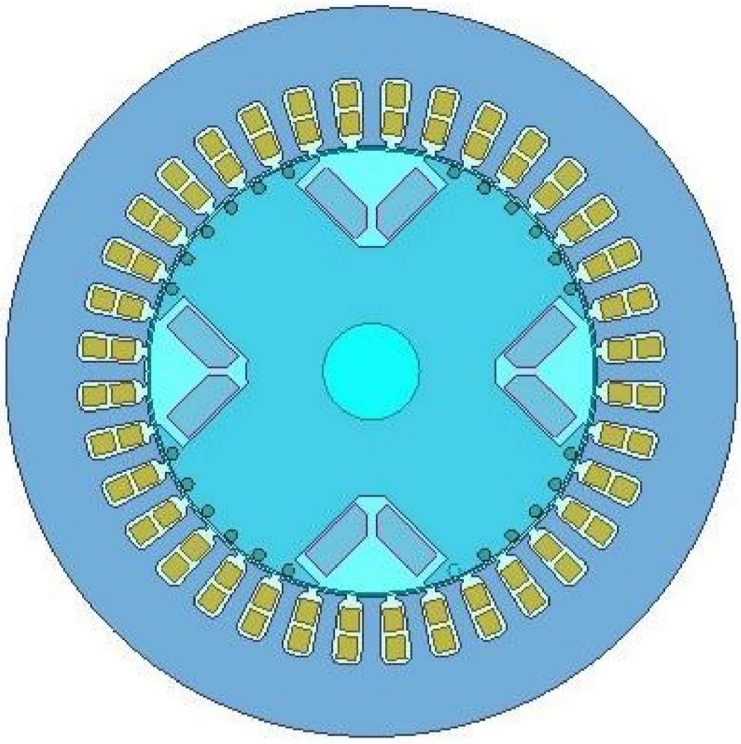

Figure 3.11: ANSYS Maxwell Model of Salient Four Pole Synchronous Generator

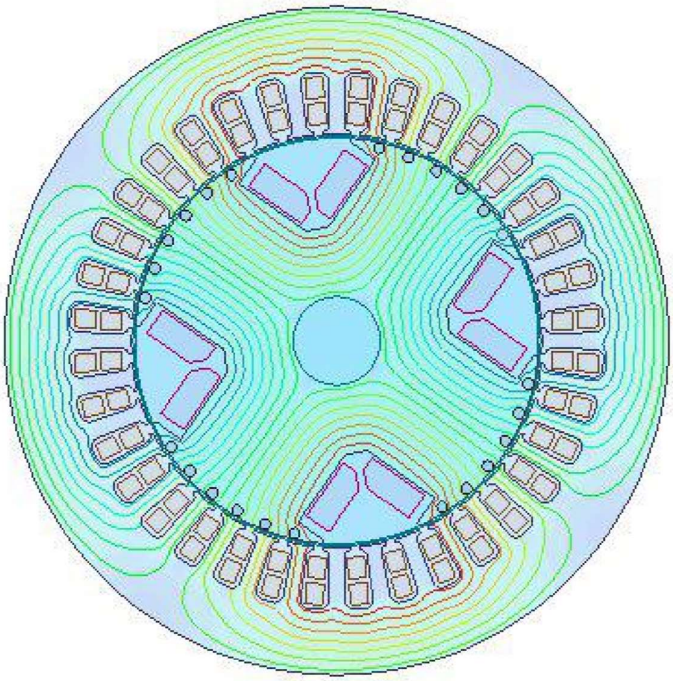

Figure 3.12: Magnetic Field Mapping from ANSYS Maxwell

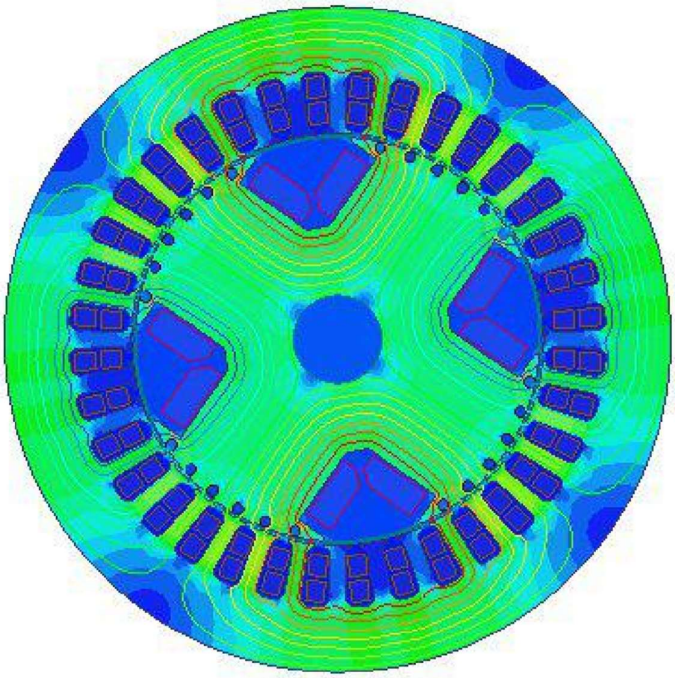

Figure 3.13: Magnetic Flux Density from ANSYS Maxwell

3.5 External Circuit Connected to the Salient Pole Synchronous Generator

The external circuit of the generator is made up of two circuits, the load circuit and the three-phase short circuit which are created using the circuit editor which is part of the ANSYS

Maxwell Program. The two circuit models are linked to two-dimensional Finite Elements Model to simulate these conditions.

3.5.1 Load Circuit

The circuit carries the stator winding parameters: winding resistance (R452, R453 and R454) and the winding inductance (L457, L456 and L455). The value of the parameters are the generated data from ANSYS Maxwell, and are entered in the circuit Editor as indicated in figure 3.14.

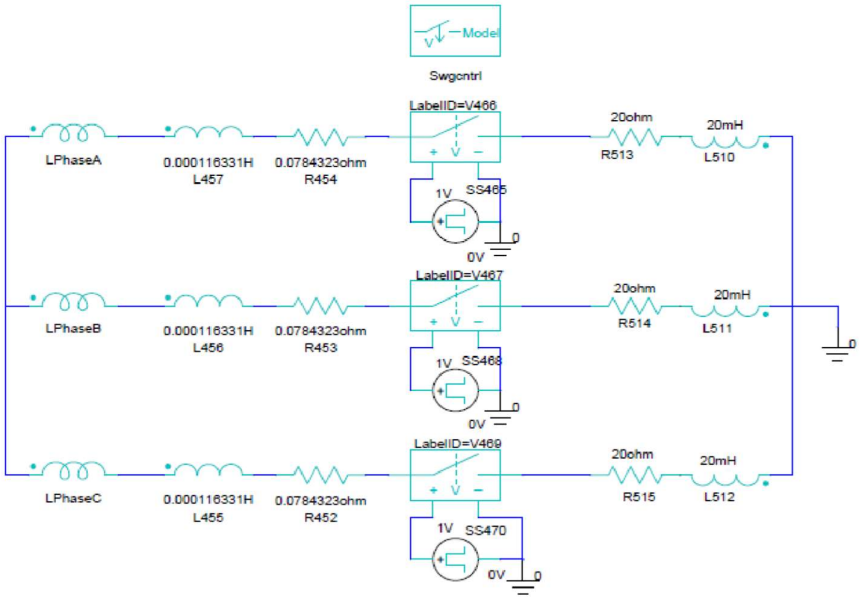

Figure 3.14: External Circuit on Load from ANSYS Maxwell Circuit Editor

The connected loads on three-phases of the generator are made up of resistive-inductive (RL) loads. The values are the same as that of a balance three-phase system.

Their numerical values are:

i) Resistive loads (R513, R514, and R515) = 20 Ohms ii)

Inductive loads (L510, L511 and L512) = 20 milli Henry

The loads linked with the generator when the following switches (SS465, SS468 and SS470) are closed; as the generator is running at constant speed of 1500 RPM. Detail explanation on the behaviour of the salient-pole synchronous generator on switching from no-load to load condition are shown on plots in figure 4.11(a), 4.11(c), 4.11(e), 4.11(g), 4.11(i), 4.11(k) and

4.11(m).

3.5.2 Three Phase Short Circuit

Similarly, the balanced three-phase short circuit is simulated with the circuit in figure 3.15. The stator winding parameters remain the same as in load circuit explained in Section

3.5.1.

In order to simulate the three-phase short circuit the three switches (SS472, SS474 and SS481) were in closed position to link the salient-pole synchronous generator circuit to the ground; shown in figure 3.15 causing three phase ground fault on the generator. The behaviour of the generator's ground faults are indicated on the plots in figure 4.11(b), 4.11(d), 4.11(f), 4.11(h),

4.11(j), 4.11(l) and 4.11(n).

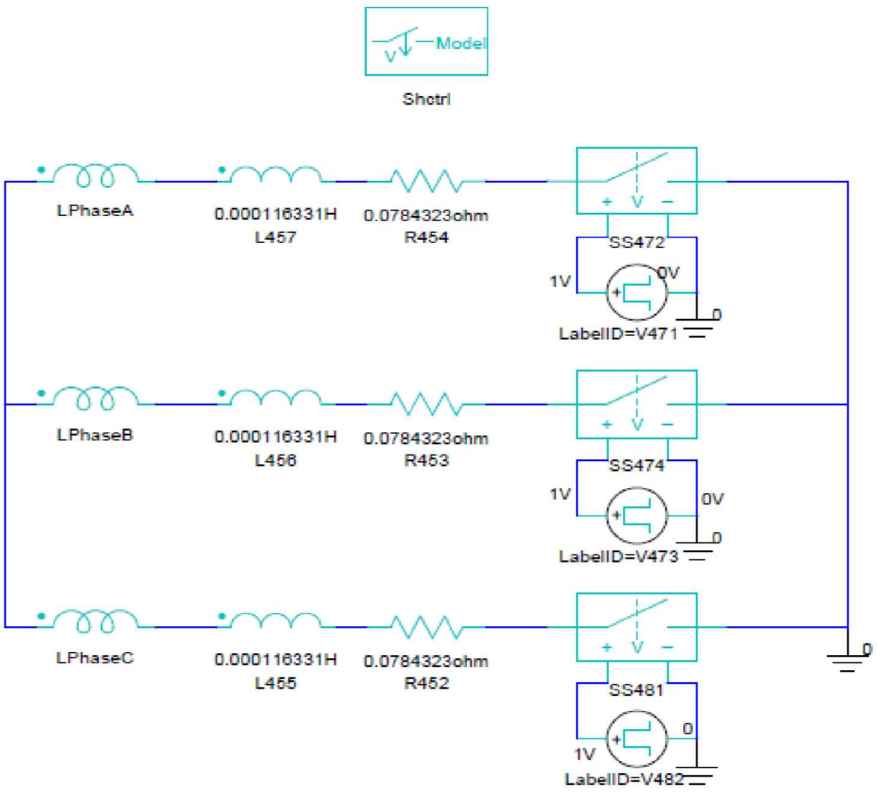

Figure 3.15: Short Circuit from ANSYS Maxwell Circuit Editor

3.6 Three-to-Two Phase Transformation ($abc - \alpha\beta - dq0$ Transformation)

The transformations of three-phase AC machines are described by their voltage equations and inductances. It is known that some of these machine inductances are functions of rotor angles. The coefficients of the differential equations which describe the behaviour of these machine are time-varying except when the rotor is at standstill. However, a change of variables is often used to reduce the complexity of these differential equations.

Utilizing these transformations, many properties of electrical machine can be evaluated without complexities in the voltage equation. It is possible to obtain analytical solutions to the system of differential equations on the assumption that the speed ω is constant. It is equally possible to simplify these equations largely by means of a special technique referred to as

Blondel-Clarke-Park Transformation shown in figure 3.16. The technique involves the introduction of a new set of voltage and current variables or components (Elgend, 1971). These components are: called Direct-Axis (d), Quadrature-Axis (q) and Zero-Sequence (0).

This transformation (Park's Transformation) has many advantages compared with three phase variables as numerated below. It,

i. enable the computation of various machines parameters to be much easier.

ii. allow independent control of the active (d-axis) and reactive (q-axis) components of the current. This also include flux and torque control in electrical machines.

iii. In dq0-frame, the mutual inductance is constant, thus allow for desired output as the inductance is dependent quantities are constant.

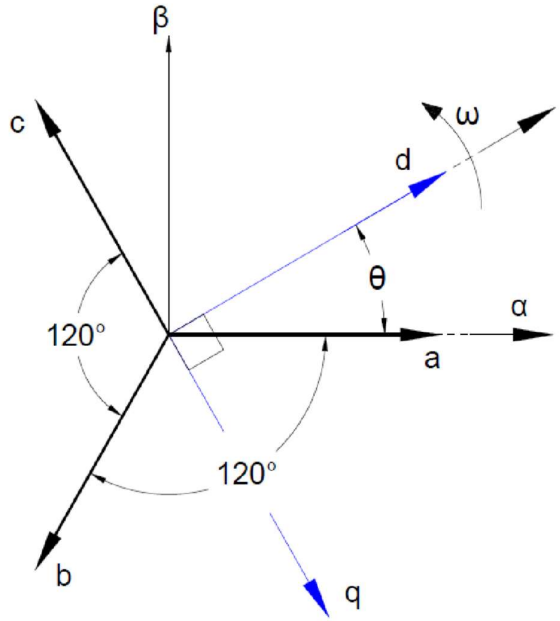

Figure 3.16: Blondel-Clarke-Park Transformation

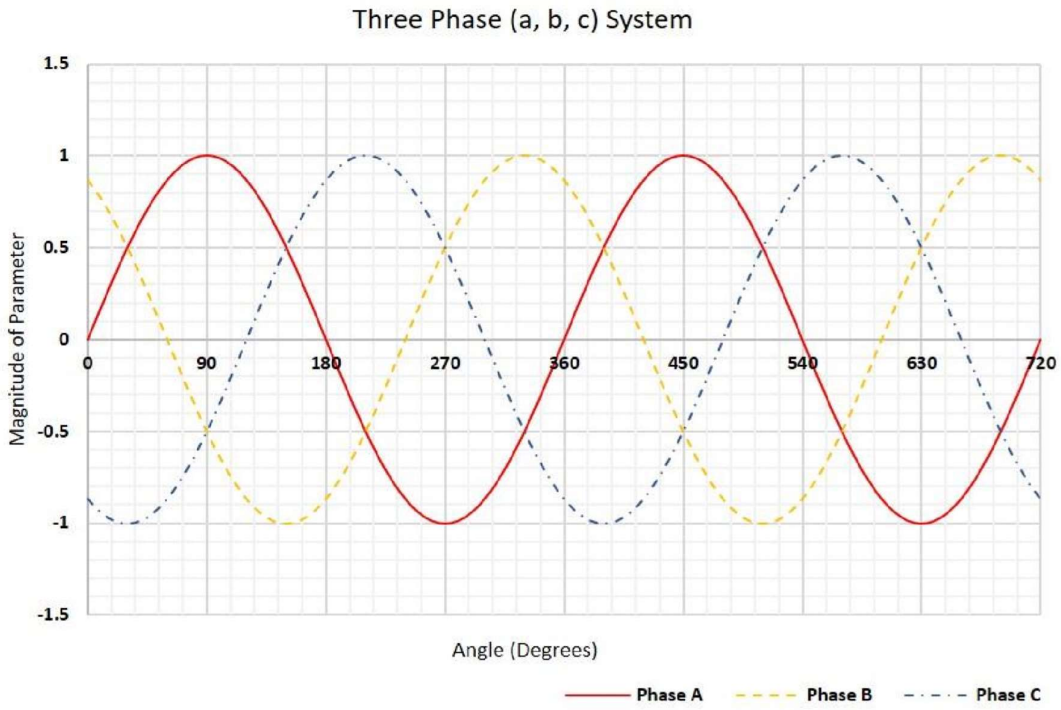

Figure 3.17: (a) Three-Phase System

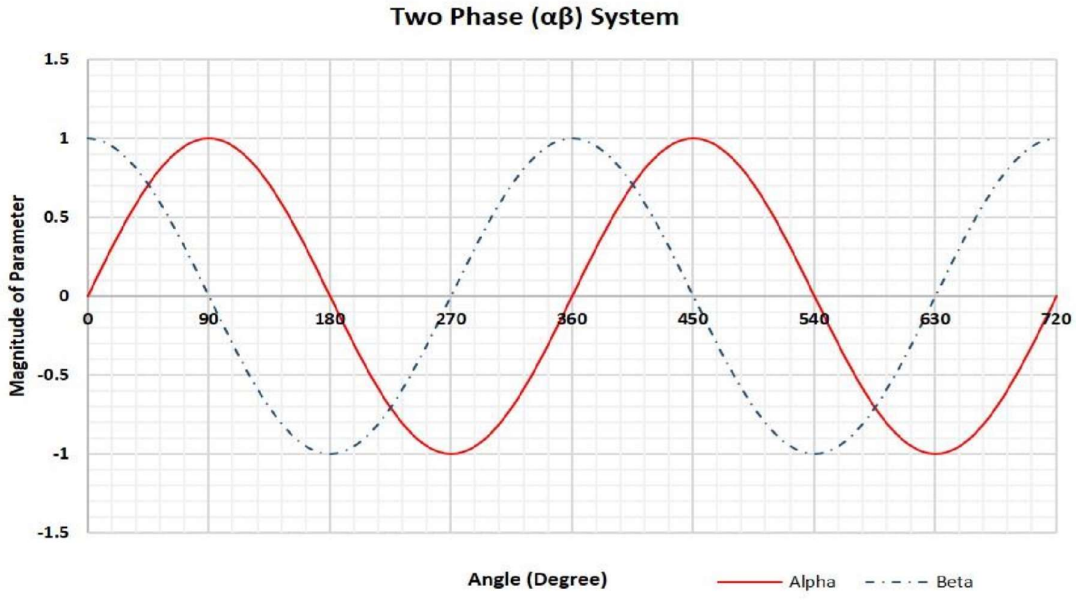

Figure 3.17(b): Two-Phase System

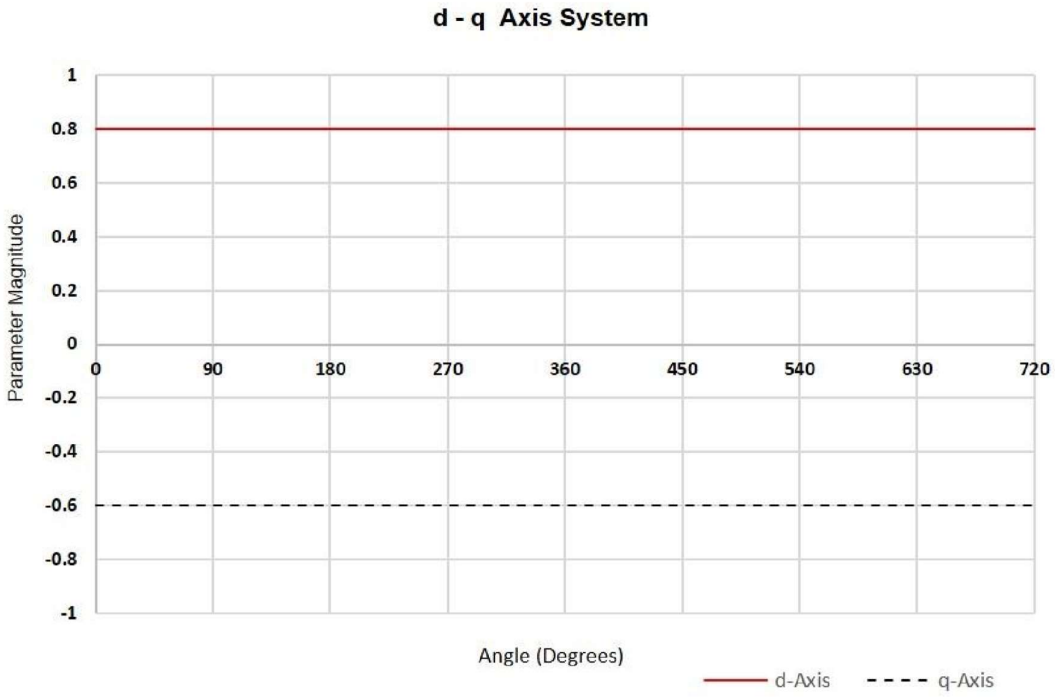

Figure 3.17(c): Direct - Quadrature Axis System

Figure 3.17(a), (b) and (c): Three-to-Two Phase Transformation ($abc - \alpha\beta - dq0$ Transformation)

3.7 Space Vector Representation of a Three Phase System into Direct – Quadrature Axis Frame

In a Salient-Pole Synchronous Machine, the three-phase balance stator current will form a rotating magnetic field in the air gap. This rotating field can be represented by a space vector with magnetic and the angular position as in figure 3.18.

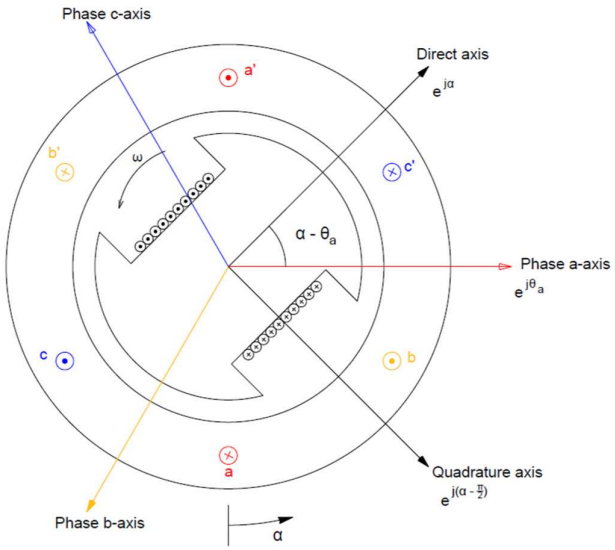

Figure 3.18: Three _ phase current vector decomposition on d. q. frame

The three-phase balanced current form a forward rotating magnetic field using field space vector concept.

Let the magnitude of the induced three-phase current be I_m then phase current can be written in equations 3.14, 3.15 and 3.16.

$$i_a(t) = I_m \cos(\omega t + \theta_a) \qquad 3.14$$

$$i_b(t) = I_m \cos(\omega t + \theta_a - \tfrac{2\pi}{3}) \qquad 3.15$$

$$i_c(t) = I_m \cos(\omega t + \theta_a + \tfrac{2\pi}{3}) \qquad 3.16$$

Where θ_a the 'a' phase position.

From figure 3.18 the direct and quadrature axis components of phase 'a' are expressed in equations 3.17 and 3.18

$$\hat{i}_d = I_m \cos(\alpha - \theta_a) \qquad 3.17$$

$$\hat{i}_q = I_m \sin(\alpha - \theta_a) \qquad 3.18$$

Since the three-phase current is balanced, the current space vector î can be obtained by summation of $i_a(t)$, $i_b(t)$ and $i_c(t)$ as in equation 3.14, 3.15 and 3.16

$$\hat{i} = \frac{2}{3}(i_a(t)e^{j\theta} + i_b(t)e^{j\frac{2\pi}{3}} + i_c(t)e^{-j\frac{2\pi}{3}}) \quad 3.19$$

Considering phase ‚a, current only while phase 'b, and phase 'c' will have similar analytical process. Therefore î can be expressed in terms of $\hat{i}_{(a)}$ and I_m.

$$\hat{i}_{(a)} = I_m e^{j(\theta_a+\omega t)} = I_m e^{j\theta_a} . e^{j\omega t} \quad 3.20$$

$\hat{i}_{(a)}$ can be decomposed by projecting to both d-axis and q-axis as shown in figure 3.18 and expressed in equations 3.21 and 3.22.

The d-q components are:

$$\hat{i}_d = I_m\cos(\alpha - \theta_a)\, e^{j\alpha} \quad 3.21$$

$$\hat{i}_q = I_m\sin(\alpha - \theta_a)\, e^{j(\alpha - \frac{\pi}{2})} \quad 3.22$$

Where α is the angular rotor position

The summation of $\hat{i}_d$ and $\hat{i}_q$ give the current space vector that will be revolving along with the rotor.

$$\hat{i}_{(a)} = \hat{i}_d + \hat{i}_q$$
$$= I_m\cos(\alpha - \theta_a)e^{j\alpha} + I_m\sin(\alpha - \theta_a)\, e^{j(\alpha - \frac{\pi}{2})} \quad 3.23$$

$e^{j\alpha}$ is expressed as $\cos\alpha + j\sin\alpha$ and

$e^{j(\alpha - \frac{\pi}{2})} = \sin\alpha - j\cos\alpha$, it can also be expressed as

$$= -j^2\sin\alpha - j\cos\alpha$$
$$= -j(j\sin\alpha + \cos\alpha) = -j\, e^{j\alpha} \quad 3.24$$

Substituting equation 3.24 into equation 3.23 to obtain equation 3.25.

$$\hat{i}_{(a)} = I_m\cos(\alpha - \theta_a)\, e^{j\alpha} + I_m\sin(\alpha - \theta_a) - j\, e^{j\alpha}$$

$$\hat{i}_{(a)} = I_m\, e^{j\alpha}\,[\cos(\alpha - \theta_a)) - j\sin(\alpha - \theta_a)]$$

$$\hat{i}_{(a)} = I_m\, e^{j\alpha}\,[e^{j(\alpha - \theta_a)}]$$

$= I_m e^{j(\alpha - \alpha + \theta_a)} = I_m e^{j\theta_a}$ 3.25

The current space vector (î) on the rotating frame of the machine rotor is the two coupled projected three-phase components on the direct and quadrature axis of the machine rotor. During the transformation on the rotational axis of the rotor referencing the armature parameters, the resultant of armature variables would be seen as stationary as described by **Einstein General Theory of Relativity.**

3.8 Derivation of Inverse Air-Gap Function Equation with Fourier Analysis Method

The winding function of SPSG is one of the areas of interest in this research work. The winding configuration is subsequently obtained in detail as shown below.

3.8.1 Air Gap Function Analysis

The air gap function of this machine will be considered in terms of direct axis and quadrature axis air gap over an angular displacement of a period of 2π as shown in figure 3.19; as the actual salient-pole synchronous generator air gap function obtained from RMxprt and ANSYS Maxwell as air gap permeance.

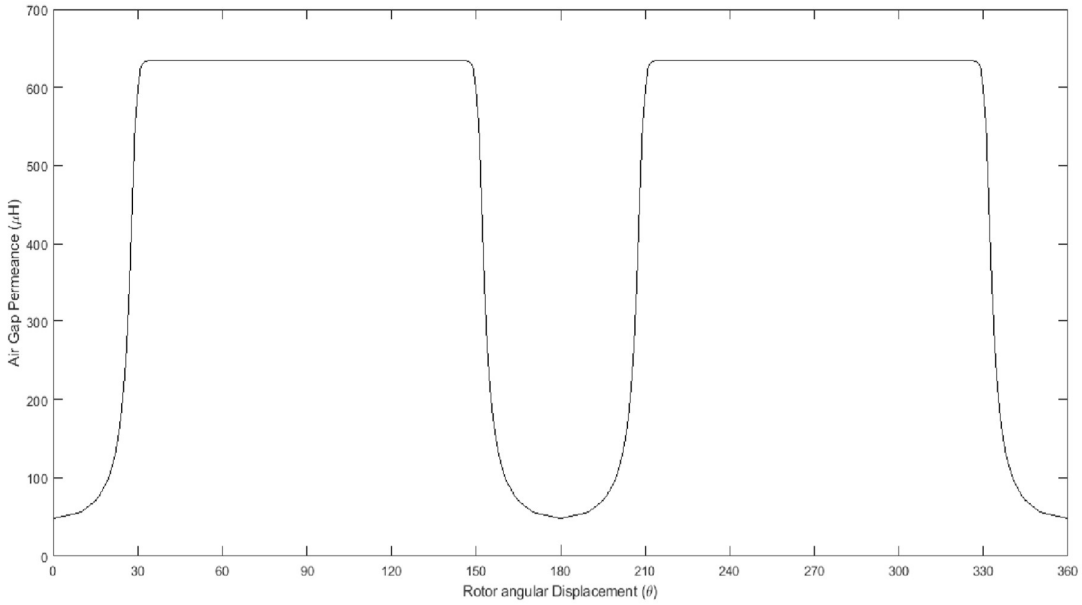

Figure 3.19: Air Gap Permeance from RMxprt

3.8.2 Air Gap Permeance

The air-gap permeance waveform obtained from RMxprt and ANSYS Maxwell is modelled into a known waveform that can be simplified using Fourier series analysis as shown in figure 3.19. In real life situation, the rotor is designed to have an even number of symmetrically shaped poles with equal number of north and south poles. Therefore, the inverse gap function $g^{-1}(\theta)$ consists of a constant term plus even harmonic of the form

$$g^{-1}(\theta) = a_0 + a_n \sum_{n=2}^{\infty} \left(\cos n\,(\theta - \theta_r)\right) \tag{3.26}$$

$$g^{-1}(\theta) = a_0 + a_2 \cos 2(\theta - \theta_r) + a_4 \cos 4(\theta - \theta_r) \tag{3.27}$$

Using Fourier Series analysis, the even function shown in figure 3.21 is expressed with a_0 and a_2 coefficients which will be derived as the coefficient for the inverse gap function. The average values a_0 and a_n coefficients of the series are expressed in equation 3.28

$$\left.\begin{aligned} a_0 &= \frac{1}{\pi}\int_0^{2\pi} g^{-1}(\theta)d(\theta) \\ a_n &= \frac{1}{\pi}\int_0^{2\pi} g_1^{-1}(\theta)cosnd\theta \end{aligned}\right\} \tag{3.28}$$

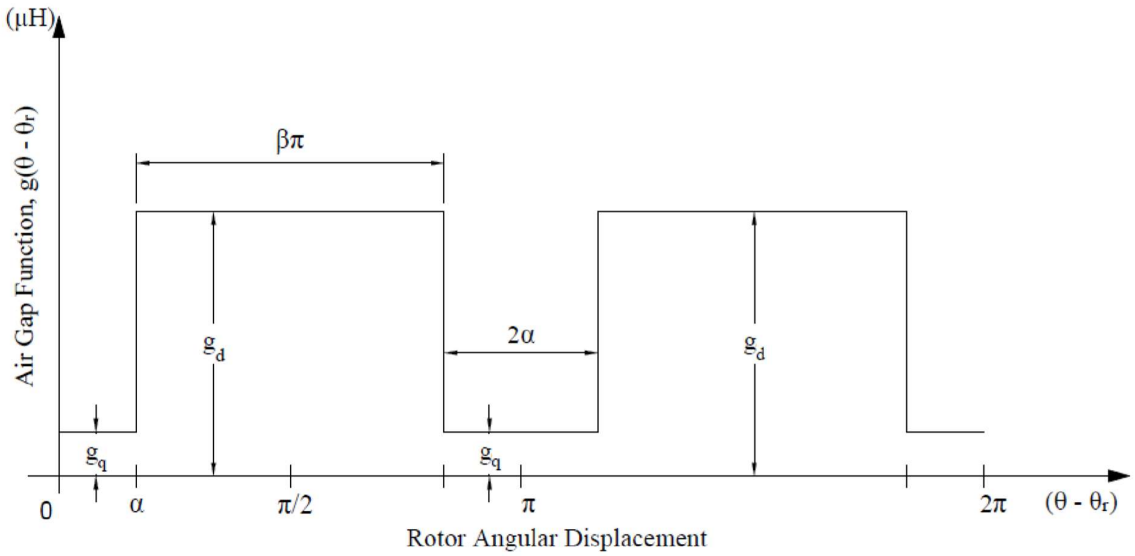

Figure 3.20: Air Gap Function

3.8.3 Air Gap and Inverse Air Gap Function Analysis

The inverse air gap function is expressed as a function of the two air gap (direct and quadrature axis) dimensions as shown in figure 3.19 and figure 3.20 is represented as g_1 and g_2 respectively.

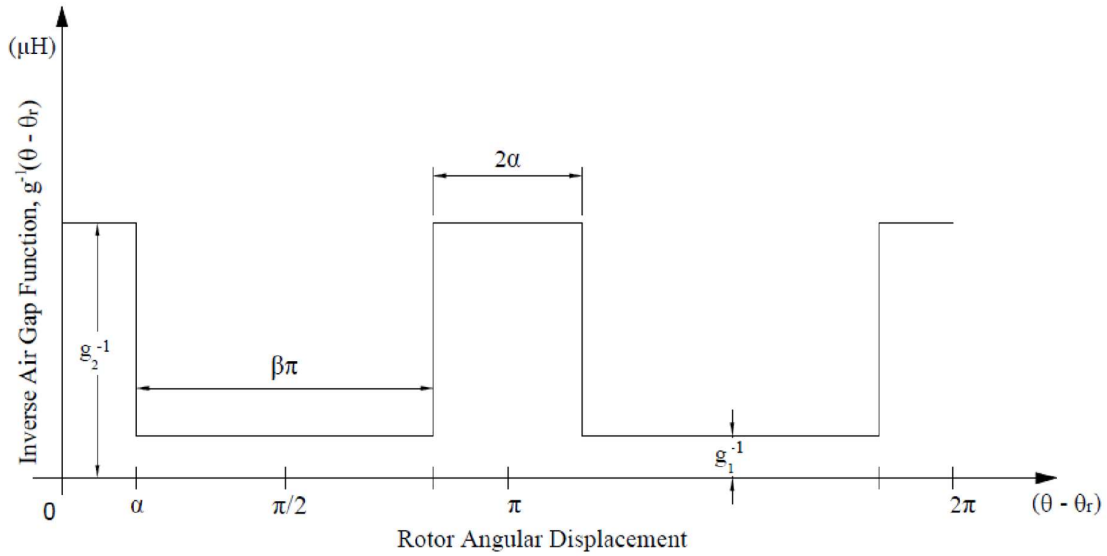

Figure 3.21: Inverse Air Gap Function

The permeance of the direct & quadrature axis air gap is expressed as:

$$p = \frac{A\mu_0\mu_r}{g} \quad 3.29$$

Where: A = Cross sectional area

μ_0 = Vacuum permeability μ_r = Air permeability g = Generator air gap

The ratio of pole arc to pole pitch for salient pole synchronous generator is expressed as:

$$\frac{Pole\ arc}{Pole\ pitch} = \beta \quad 3.30$$

Pole pitch = π; Pole arc = πβ

The general Fourier Series of a function is expressed as:

$$f(x) = \frac{a_0}{2} + a_1 \cos x + a_2 \cos 2x + \ldots b_1 \sin x + b_2 \sin 2x + \ldots a_n \sum_{n=3}^{\infty} \cos nx + b_n \sum_{n=3}^{\infty} \sin nx$$

Magnetizing Inductance Formula from Winding & Air Gap Function of the magnetizing inductance for the phase winding **aa**, **bb** and **cc** are given by:

$$L_{ij} = \mu_0 rl \int_0^{2\pi} \frac{1}{g(\varphi,\theta_r)} n_i(\theta_r) N_j(\theta)\, d\theta \quad 3.31$$

$$\left.\begin{aligned} L_{aa} &= \frac{\mu_0 rl}{g} \int_0^{2\pi} n_A(\theta_r) N_A(\theta)\, d\theta \\ L_{bb} &= \frac{\mu_0 rl}{g} \int_0^{2\pi} n_B(\theta_r) N_B(\theta)\, d\theta \\ L_{cc} &= \frac{\mu_0 rl}{g} \int_0^{2\pi} n_C(\theta_r) N_C(\theta)\, d\theta \end{aligned}\right\} \quad 3.32$$

While mutual magnetizing inductance between the phases will be given by:

$$L_{ab} = \frac{\mu_0 rl}{g} \int_0^{2\pi} n_A(\theta_r) N_B(\theta)\, d\theta \quad 3.33$$

The winding function has already been explained in Section 2.10.2 and the equation 3.32 and 3.33 established.

The magnetizing inductance cannot be computed without the air gap function (g). The air gap that is non-uniform in Salient-Pole Synchronous Generator can be related as a periodic function with a series of trigonometric function expressed in the form of even inverse gap function as:

$$g^{-1}(\phi + \alpha) = g_1^{-1} + g^{-}{}_2{}^1 \cos 2\,(\phi + \alpha) + g_4^{-1} \cos 4\,(\phi + \alpha) \qquad 3.34$$

$$g^{-1} = \begin{cases} g_1^{-1}, & 0 < \theta_r < \alpha \\ g_2^{-1}, & \alpha < \theta_r < \beta\pi + \alpha \\ g_1^{-1}, & \beta\pi + \alpha < \theta_r < \pi \end{cases} \qquad 3.35$$

The a_0 coefficient can be obtained as follows:

$$a_0 = \frac{1}{\pi}\left[\int_0^{\alpha} g_1^{-1} d\theta_r + \int_{\alpha}^{\beta\pi+\alpha} g_2^{-1} d\theta_r + \int_{\beta\pi+\alpha}^{\pi} g_1^{-1} d\theta_r\right] \qquad 3.36$$

Integrate equation 3.36 with limit to obtain equation 3.37

$$a_0 = \frac{1}{\pi}\left[g_1^{-1}[\theta_r]_0^{\alpha} + g_2^{-1}[\theta_r] + g_1[\theta_r]\right] \qquad 3.37$$

$$= \frac{1}{\pi}\left[g_1^{-1}\alpha + g_2^{-1}(\beta\pi + \alpha - \alpha) + g_1^{-1}(\pi - \beta\pi - \alpha)\right]$$

$$= \frac{1}{\pi}\left[g_1^{-1}\alpha + g_2^{-1}\beta\pi + g_1^{-1}(\pi - \beta\pi - \alpha)\right]$$

$$= \frac{1}{\pi}\left[g_1^{-1}\alpha + g_2^{-1}\beta\pi + g_1^{-1}\pi - g_1^{-1}\beta\pi - g_1^{-1}\alpha\right]$$

$$= \frac{1}{\pi}\left[\frac{\beta\pi}{g_2} + \frac{\pi}{g_1} - \frac{\beta\pi}{g_1}\right]$$

$$= \frac{\pi}{\pi}\left[\frac{\beta}{g_2} + \frac{1}{g_1} - \frac{\beta}{g_1}\right]$$

$$= \left[\frac{\beta}{g_2} + \frac{(1-\beta)}{g_1}\right]$$

The average component of the function becomes:

$$a_0 = \frac{\beta}{g_2} + \frac{(1-\beta)}{g_1} \quad 3.38$$

The function is an even function, therefore the b_n components become zero.

In obtaining, a_n the first even coefficient of the function. This is achieved as follows.

$$a_n = \frac{1}{\pi}\left[\int_0^{\alpha} g_1^{-1} cosnd\theta_r + \int_{\alpha}^{\beta\pi+\alpha} g_2^{-1} cosnd\theta_r + \int_{\beta\pi+\alpha}^{\pi} g_1^{-1} cosnd\theta_r\right] \quad 3.39$$

Integrating equation 3.39 with limit gives equation 3.40

$$a_n = \frac{1}{n\pi}\left[\left[g_1^{-1} sinn\theta_r\right]_0^{\alpha} + \left[g_2^{-1} sinn\theta_r\right] \square\square\square\square^{-1} \square + [g_1 sinn\theta_r] \square\square\square\square\right]$$

$$= \frac{1}{\pi n}\left[g_1^{-1} sinn\alpha - g_1^{-1} sinn0° + g_2^{-1} sinn(\beta\pi + \alpha) - g_2^{-1} sinn\alpha + g_1^{-1} sinn\pi - g_1^{-1} sinn(\beta\pi + \alpha)\right] \quad 3.40$$

From figure 3.19 the following identities are established

$2\alpha + \beta\pi = \pi$

$2\alpha = \pi - \beta\pi$

$\alpha = \frac{\pi}{2}(1 - \beta)$ 3.41

Expressing the following trigonometric identity, $\sin\alpha$, $\sin(\alpha + \beta\pi)$ as a function of α.

Equation 3.40 will be simplified to equation 3.41

$$\sin n\,\alpha = sinn\left(\frac{\pi}{2} - \frac{\pi\beta}{2}\right) \quad 3.42$$

$$\sin n(\alpha + \beta\pi) = sinn\left(\frac{\pi}{2} - \frac{\pi\beta}{2} + \pi\beta\right) = sinn\left(\frac{\pi}{2} + \frac{\pi\beta}{2}\right) \quad 3.43$$

$$\sin n\,\alpha = sinn\frac{\pi}{2}cosn\frac{\pi\beta}{2} - cosn\frac{\pi}{2}sinn\frac{\pi\beta}{2}$$

$$\sin n(\alpha + \beta\pi) = sinn\frac{\pi}{2}cosn\frac{\pi\beta}{2} + cosn\frac{\pi}{2}sinn\frac{\pi\beta}{2}$$

Applying harmonic series number n = 1, 2 into equation 3.40. The following first and second conditions result in equations 3.45 and 3.47.

First condition: **n = 1**

The second term of the trigonometry identify of equation 3.43 will be zero as expressed in equation 3.48

Therefore equation 3.42 becomes

$\sin\alpha = sin\frac{\pi}{2}cos\frac{\pi\beta}{2}$, the second term is zero

$= cos\frac{\pi\beta}{2}$ 3.44

Similarly equation 3.43 becomes

$\sin(\alpha + \beta\pi) = sin\frac{\pi}{2}cos\frac{\pi\beta}{2}$, the second term also is zero

$= cos\frac{\pi\beta}{2}$ 3.45

Second condition: **n** = **2**

Implementing similar process for harmonic number n = 2 on equation 3.40 and substituting it with equations 3.46 and 3.47. Equation 3.49 obtained.

$\sin2\alpha = sin\pi.cos\pi\beta - cos\pi.sin\pi\beta$

$= sin\pi\beta$ 3.46

$\sin2(\alpha+\beta\pi) = sin\pi.cos\pi\beta + cos\pi.sin\pi\beta$

$= - sin\pi\beta$ 3.47

$a_1 = \frac{1}{\pi}\left[g_1^{-1}cos\frac{\pi\beta}{2} + g_2^{-1}cos\pi\beta - g_2^{-1}cos\pi\beta - g_1^{-1}cos\frac{\pi\beta}{2}\right] = 0$ 3.48

Similarly, substitute equation 3.46 and 3.47 to obtain equation 3.49

$$a_2 = \frac{1}{2\pi}\left[g_1^{-1}sin\pi\beta - g_2^{-1}sin\pi\beta - g_2^{-1}sin\pi\beta + g_1^{-1}sin\pi\beta\right]$$

$$a_2 = \frac{1}{2\pi}\left[\frac{2}{g_1}sin\pi\beta - \frac{2}{g_2}sin\pi\beta\right]$$

$$= \frac{2}{2\pi}\left[\frac{1}{g_1} sin\pi\beta \; - \; \frac{1}{g_2} sin\pi\beta\right]$$

$$= \frac{1}{\pi}\left[\frac{1}{g_1} \; - \; \frac{1}{g_2}\right] sin\pi\beta \qquad 3.49$$

$g^{-1}(\theta) = a_0 + a_2 \cos 2\theta$ for π cycles

For complete 2π cycles

$g^{-1}(\theta) = 2a_0 + 2a_2 \cos 2\theta$

Relating this equation to the general Fourier series equation gives

$$f(x) = \frac{a_0}{2} + a_2 \cos 2\theta + a_4 \cos 4\theta \ldots. \qquad 3.50$$

$$g^{-1}(\theta - \theta_r) = a_0 + 2a_2 \cos 2(\theta - \theta_r) + 2a_4 \cos 4(\theta - \theta_r) \qquad 3.51$$

$$= \frac{\beta}{g_2} + \frac{(1-\beta)}{g_1} + \frac{2}{\pi}\left[\frac{1}{g_1} \; - \; \frac{1}{g_2}\right] sin\pi\beta \qquad 3.52$$

3.9 Winding and Turn Function Analysis

Figure 3.22 depicts the actual arrangement of the stator winding of the salient-pole synchronous generator described in this research. The arrangement is further spread laterally to show the winding in three-phase groups as shown in figure 3.23(a) – 3.23(f) as Turn Function and Winding Function for phase inductance computation.

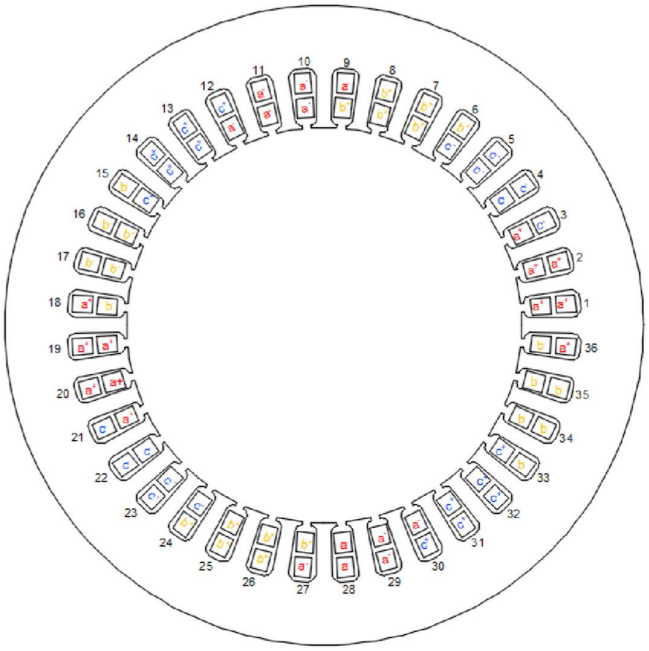

Figure 3.22: Winding Arrangement around Generator Stator

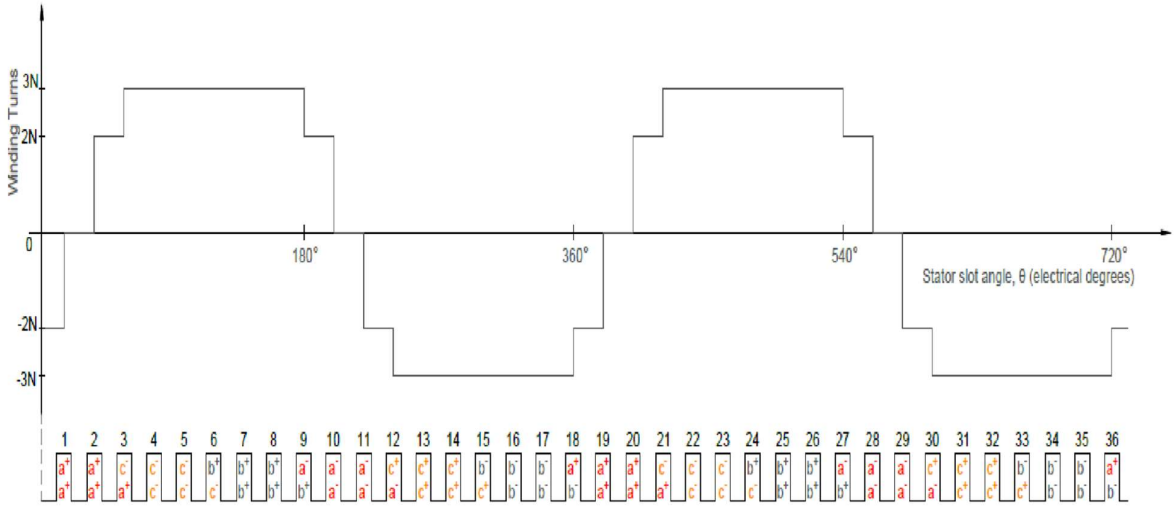

Figure 3.23(a): Phase A Winding Function

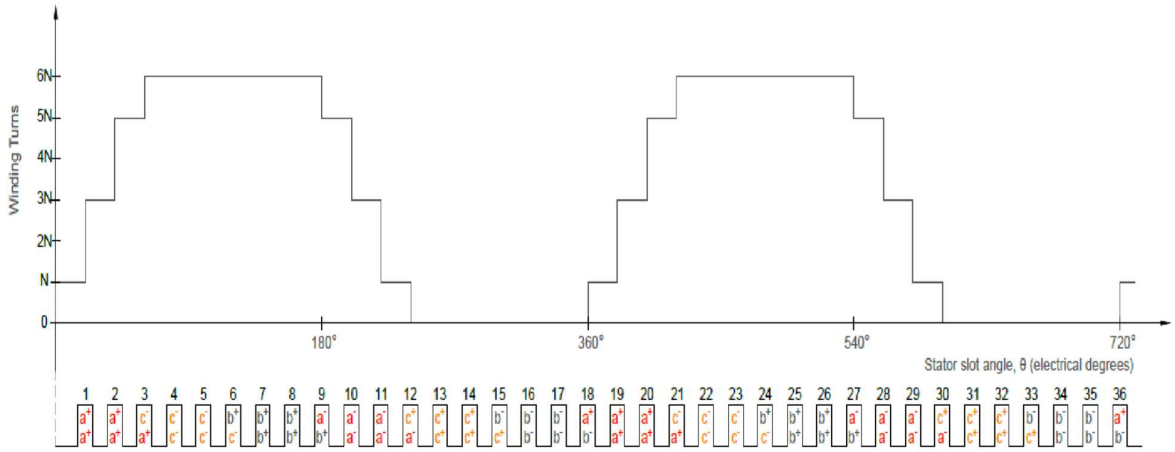

Figure 3.23(b): Phase A Turn Function

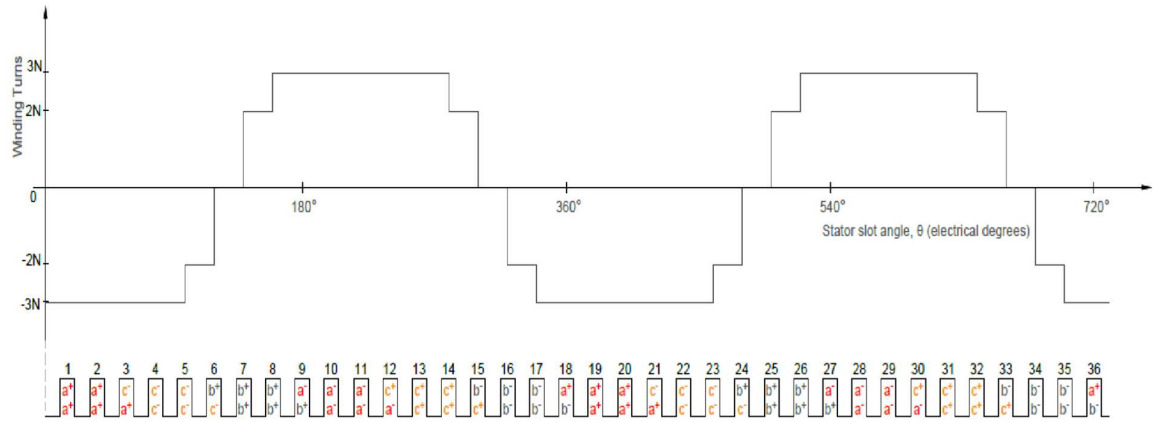

Figure 3.23(c): Phase B Winding Function

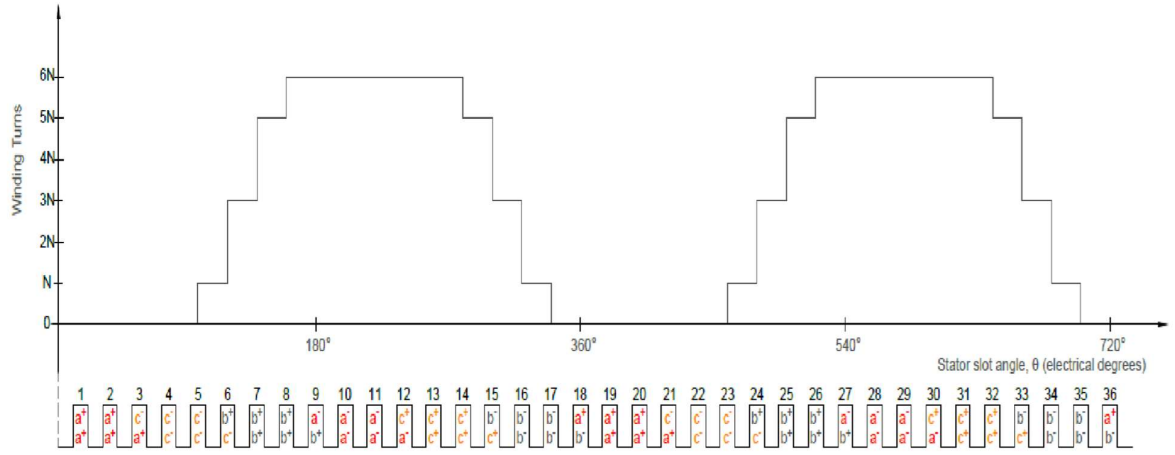

Figure 3.23(d): Phase B Turn Function

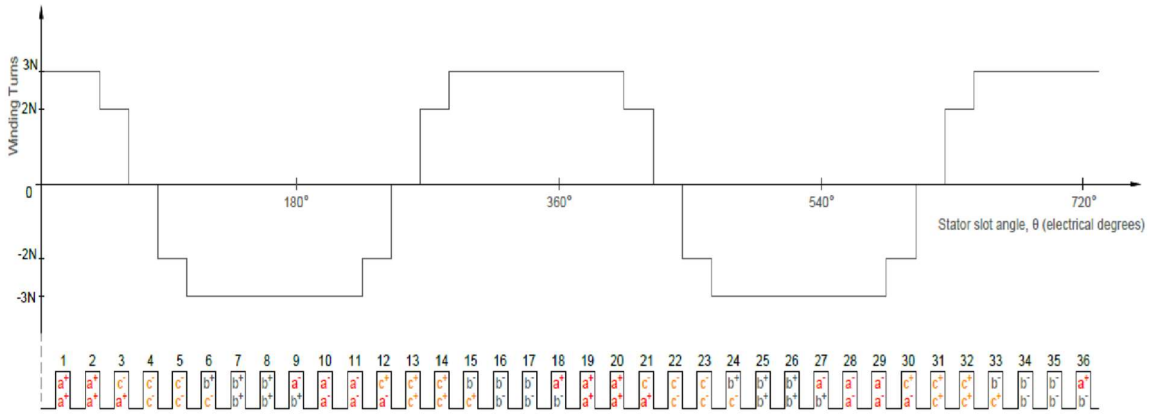

Figure 3.23(e): Phase C Winding Function

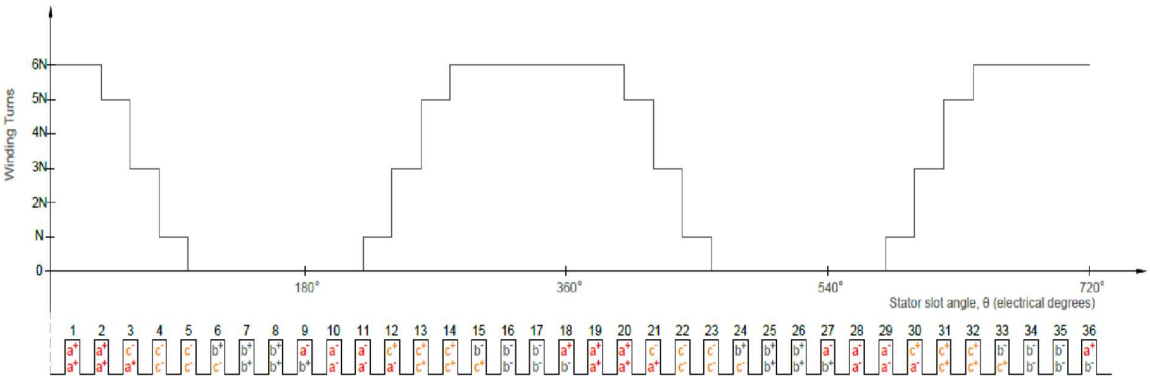

Figure 3.23(f): Phase C Turn Function

Figure 3.23: Turn Function and Winding Function

3.10 Inverse Air-Gap and Winding Function Application in Numerical Computation of Magnetizing Inductance of Salient-Pole Synchronous Generator

The inverse air-gap function equation derived above is applied with Winding Function to compute Salient-Pole Synchronous Generator magnetizing inductance as detailed below.

$$g^{-1}(\phi, \theta_r) = a_0 + a_2 \cos 2(\phi - \theta_r) \qquad 3.53$$

From the derived formula of equation 3.52

$$a_0 = \frac{\beta}{g_2} + \frac{(1-\beta)}{g_1}, \qquad a_2 = \frac{2}{\pi}\left[\frac{1}{g_1} - \frac{1}{g_2}\right] sin\pi\beta \qquad 3.54$$

Where $\beta = \frac{\text{Pole arc}}{\text{Pole pitch}}$ 3.55

The pole arc of the generator = 98.61mm

Pole pitch = $\frac{\pi \text{ x Stator Inner Diameter}}{\text{No.of Pole}}$ 3.56

Stator Inner Diameter = 184mm

Number of Pole = 4

Pole pitch = $\frac{\pi \, x \, 184}{4}$ = 144.5lmm

3.11 Computational Data for Magnetizing Inductance using Winding Function (WF)

Table 3.7: Data for Inductance computation from WF

Generator Data	**Value**
Generator length(mm)	275
Generator stator inner radius (mm)	94
Minimum air gap (g_1) (mm)	2.025
Maximum air gap (g_2) (mm)	42.24
(Pole arc / pole pitch) ratio (β)	0.682

Inserting all the parameters obtained from table 3.7 into equations 3.38 and 3.49 to obtain a_0 and a_2

Coefficient, $a_0 = \frac{(1-\beta)}{g_1} + \frac{\beta}{g_2}$

$$a_0 = \frac{(1-0.682)}{0.002025} + \frac{0.682}{0.04224}$$

$$= \frac{0.32}{0.002025} + 16.15$$

$$= 158.02 + 16.15$$

$$= 174.17$$

Coefficient, $a_2 = \frac{1}{\pi}\left[\frac{1}{g_1} - \frac{1}{g_2}\right]\sin\pi\beta$

$$= \frac{1}{\pi}\left[\frac{1}{0.002025} - \frac{1}{0.04224}\right]\sin\pi\beta$$

$$= \frac{1}{\pi}[493.83 - 23.67]\sin\pi\beta$$

$$= \frac{1}{\pi}[470.16]\sin\pi\beta$$

$$= 149.66\sin(\pi\beta)$$

$$= 149.66\sin(\pi x 0.682)$$

$$= 149.66x\ 0.841$$

$$a_2 = 125.86$$

Since the Fourier analysis was conducted for a complete period the coefficient $\frac{a_0}{2}$ and

a_2 become $a_0 = 174.17$ and $a_2 = 125.86$

From the diagrams of the winding and turn functions in figure 3.21 the following magnetizing inductances will be obtained using Winding Function theory which states that the phase inductances L_{ij} between any two winding i and j is obtained using equation 3.57

$$L_{ij} = \mu_0 rlm \int_0^{2\pi} \frac{1}{g(\varphi,\theta_r)} n_i(\theta_r) N_j(\theta)\, d\theta \qquad 3.57$$

$$m = \frac{2\pi}{360}$$

Where μ_0 is the permeability of free space, r is the effective radius of the generator stator bore, l is the generator stack length, N_i and N_j are the winding functions for winding i and j respectively, g is the air gap function, φ is the stator circumferential position and θ_r is the rotor position.

Simplified form of equation 3.57 in terms of winding and turn functions is expressed in equation 3.58

The machines inductances have different harmonics including DC, second, fourth, sixth and tenth order. Neglecting the harmonics with frequencies higher than two, the general equation for the inductances can be expressed as:

$$\mathbf{L_{ij}} = \mu_0 rlm[a_0 \frac{N^2}{2} + a_2 \frac{N^2}{4} \cos 2(\varphi + \theta_r)] \quad 3.58$$

The inductance with full cycle is $\mathbf{L_{ij}} = \mu_0 rlm[a_0 N^2 + a_2 \frac{N^2}{2} \cos 2(\varphi + \theta_r)]$ 3.59

From equation 3.59, self and mutual inductances are computed as shown in Section 3.11.1 and 3.11.2.

3.11.1 Self Inductance (L_{aa}):

$$L_{aa} = \frac{\mu_0 rl}{g}\, m\left[\int_0^{2.5}(N)(-2N)d\phi + \int_{7.5}^{12.5}(2N)\,(5N)d\phi + \int_{12.5}^{42.5}(3N)(6N)\,d\phi + \right.$$

$$\int_{42.5}^{47.5}(2N)\,(5N)d\phi + \int_{52.5}^{57.5}(-2N)\,(N)d\phi + \int_{87.5}^{92.5}(-2N)\,(N)d\phi + \int_{97.5}^{102.5}(2N)\,(5N)d\phi +$$

$$\left.\int_{102.5}^{132.5}(3N)\,(6N)d\phi + \int_{132.5}^{137.5}(2N)\,(5N)d\phi + \int_{142.5}^{147.5}(-2N)\,(N)d\phi + \int_{177.5}^{180}(N)\,(-2N)d\phi\right]$$

Where,

$$\int_{0}^{2.5} (N)(-2N)d\phi = -2N^2\ x\ 5\ =\ -5N^2$$

$$\int_{7.5}^{12.5} (2N)\,(5N)d\phi = 10N^2\ x\ 5\ =\ 50N^2$$

$$\int_{12.5}^{42.5} (3N)(6N)\,d\phi = 18N^2 x\ 30\ =\ 540N^2$$

$$\int_{42.5}^{47.5} (2N)\,(5N)d\phi = 10N^2\ x\ 5\ =\ 50N^2$$

$$\int_{52.5}^{57.5} (-2N)\,(N)d\phi = -2N^2\ x\ 5\ =\ -10N^2$$

$$\int_{87.5}^{92.5} (-2N)\,(N)d\phi = -2N^2 x\ 5\ =\ -10N^2$$

$$\int_{97.5}^{102.5} (2N)\,(5N)d\phi = 10N^2\ x\ 5\ =\ 50N^2$$

$$\int_{102.5}^{132.5} (3N)\,(6N)d\phi = 18N^2\ x\ 30\ =\ 540N^2$$

$$\int_{132.5}^{137.5} (2N)\,(5N)\quad d\phi\quad x\quad = 10N^2\quad 5\ =\ 50N^2$$

$$\int_{142.5}^{147.5} (-2N)\,(N)d\phi = -2N^2\ x\ 5 = -10N^2$$

$$\int_{177.5}^{180} (N)\,(-2N)d\phi = -2N^2 \times 2.5\ =\ -5N^2$$

$$L_{aa} = -5N^2 + 50N^2 + 540N^2 + 50N^2 - 10N^2 - 10N^2 + 50N^2 + 540N^2 + 50N^2$$

$$- 10N^2 - 5N^2 = 1240N^2$$

N = Number of turns per slot, N = 5 turns

The waveform of the three-phase winding functions was generated using MATLAB scripts as shown in Appendix G. The fundamental and harmonic components of the winding function

obtained from Fourier analysis using MATLAB codes in Appendix H for the three phase windings expressed in equation 3.60 and 3.61.

The waveforms of the three phases plots of the piecewise waveform of the winding function and it curve fittings are displayed in Appendix I, numerical components of fundamental and harmonics is shown in Appendix J.

$$\left.\begin{aligned} N_{as} &= N_s \sin(\phi_s - \delta) \\ N_{bs} &= N_s \sin(\phi_s - \delta - 120°) \\ N_{cs} &= N_s \sin(\phi_s - \delta + 120°) \end{aligned}\right\} \quad 3.60$$

The phase ‚a„, 'b' and 'c' expressed in equation 3.61

$$\left.\begin{aligned} N_{as} &= 1.778 \sin \angle - 2.2784 \\ N_{bs} &= 1.778 \sin \angle - 0.1844 \\ N_{cs} &= 1.778 \sin \angle 1.8096 \end{aligned}\right\} \quad 3.61$$

Therefore, the three-phase stator winding inductances are computed utilizing equation 3.51 after substituting values of a_0 and a_2 to obtain equation 3.52.

The fundamental component of 1.778 multiply with the number of turns per slot to obtain the actual number of turns considering the periodic arrangement of the stator winding within the

slots.

$L_{aa} = \mu_0 r l m N_x n_x g^{-1}(\phi, \theta_r)$ 3.62

Where N_x is equal to the magnitude of N_{as}, N_{bs} and N_{cs} as expressed in equation 3.61 m = $\frac{2\pi}{360}$

$$L_{aa} = 4\pi x 10^{-7} x\ 0.094 \text{ x } 0.275 \text{ x } \frac{2\pi}{360} \text{ x } 1240 \text{ x } 79 \text{ x } g^{-1}(\phi, \theta_r)$$

$= 5.554 \text{ x } 10^{-5} g^{-1}(\phi, \theta_r)$

$= 5.554 \text{ x } 10^{-5}[(174.17 + 125.86)\cos 2(\phi - \theta_r)]$

$= [(9.67 \text{ x } 10^{-3} + 3.50 \text{ x } 10^{-3})\cos 2(\phi - \theta_r)]H$

$= 9.67 + 3.50\cos2(\phi - \theta_r)\text{mH}$

3.11.2 Mutual Inductance Computation (L_{ab}):

$$L_{ab} = \frac{\mu_0 rlm}{g}\int_0^{2\pi} N_A(\phi)n_B(\phi)d\phi \qquad 3.63$$

$$L_{ab} = \frac{\mu_0 rlm}{g}\Big[\int_{27.5}^{32.5} 3N \times Nd\phi + \int_{32.5}^{37.5} 3N \times 3Nd\phi + \int_{37.5}^{42.5} 3N \times 5Nd\phi$$

$$+ \int_{42.5}^{47.5} 2N \times 6Nd\phi + \int_{47.5}^{52.5} 0 \times 6Nd\phi + \int_{52.5}^{57.5} -2N \times 6Nd\phi$$

$$+ \int_{57.5}^{62.5} -3N \times 6Nd\phi + \int_{62.5}^{67.5} -3N \times 6Nd\phi + \int_{67.5}^{72.5} -3N \times 6Nd\phi$$

$$+ \int_{72.5}^{77.5} -3N \times 5Nd\phi + \int_{77.5}^{82.5} -3N \times 3Nd\phi + \int_{82.5}^{87.5} -3N \times Nd\phi$$

$$+ \int_{87.5}^{92.5} -2N \times 0d\phi + \int_{92.5}^{97.5} 0 \times 0d\phi + \int_{97.5}^{102.5} 2N \times 0d\phi + \int_{102.5}^{107.5} 3N \times 0d\phi$$

$$+ \int_{107.5}^{112.5} 3N \times 0d\phi + \int_{112.5}^{117.5} 3N \times 0d\phi + \int_{117.5}^{122.5} 3N \times Nd\phi$$

$$+ \int_{122.5}^{127.5} 3N \times 3Nd\phi + \int_{127.5}^{132.5} 3N \times 5Nd\phi + \int_{132.5}^{137.5} 2N \times 6Nd\phi$$

$$+ \int_{137.5}^{142.5} 0 \times 6Nd\phi + \int_{142.5}^{147.5} -2N \times 6Nd\phi + \int_{147.5}^{152.5} -3N \times 6Nd\phi$$

$$+ \int_{152.5}^{157.5} -3N \times 6Nd\phi + \int_{157.5}^{162.5} -3N \times 6Nd\phi + \int_{162.5}^{167.5} -3N \times 5Nd\phi$$

$$+ \int_{167.5}^{172.5} -3N \times 3Nd\phi + \int_{172.5}^{177.5} -3N \times Nd\phi + \int_{177.5}^{180} -2N \times 0d\phi\Big]$$

$$\int_0^{2\pi} N_A(\phi)\, n_B(\phi)d\phi = 15N^2 + 45N^2 + 75N^2 + 60N^2 - 60N^2 - 90N^2 - 90N^2 -$$

$$90N^2 - 75N^2 - 45N^2 - 15N^2 + 15N^2 + 45N^2 + 75N^2 + 60N^2 - 60N^2 - 90N^2 -$$

$$90N^2 - 90N^2 - 75N^2 - 45N^2 - 15N^2 = -540N^2 \text{ x } \frac{2\pi}{360}$$

$$\int_0^{\pi} \text{N}_\text{A}(\phi)\, \text{n}_\text{B}(\phi)\text{d}\phi = -3\pi\text{N}^2 \qquad 3.64$$

$$L_{ab} = \frac{\mu_0 rl}{g}[-3\pi N^2]$$

$$L_{ab} = -4\pi \text{ x}10^{-7} \text{ x } 0.094 \text{ x } 0.275 \text{ x } \frac{2\pi}{360} \text{ x } 540N^2$$

$L_{ab} = -4\pi \text{ x}10^{-7} \text{ x } 0.094 \text{ x } 0.275 \text{ x } 3\pi \text{ x } 79g^{-1}(\phi, \theta_r)$

$L_{ab} = -2.42 \text{ x } 10^{-6}[174.17 + 125.86] \cos 2(\phi - \theta_r)$

$L_{ab} = -4.212 \times 10^{-3} - 1.513\text{x}10^{-3} \cos 2(\phi - \theta_r)$

From the above winding function computation of self and mutual inductance, the generator stator inductances (L_{ss}) of stator winding a, b, c varies periodically with position and ϕ as illustrated below.

$$L_{ss} = \frac{\mu_0 rl}{g}\pi N_{abc}^2 \begin{bmatrix} \frac{62}{9} & -3 & -3 \\ -3 & \frac{62}{9} & -3 \\ -3 & -3 & \frac{62}{9} \end{bmatrix} \quad 3.65$$

Therefore L_{ss} can be expressed in the general form as in equation 3.40

$$\left.\begin{aligned} L_{aa} &= 9.67 + 3.50 \cos 2\phi \text{mH} \\ L_{bb} &= 9.67 + 3.50 \cos 2(\phi - 120°) \text{ mH} \\ L_{cc} &= 9.67 + 3.50 \cos 2(\phi + 120°) \text{ mH} \end{aligned}\right\} \quad 3.66$$

Similarly, the mutual inductances are obtained as:

$$\left.\begin{aligned} L_{ab} &= -4.21 - 1.51 \cos(2\phi - 120°) \text{ mH} \\ L_{bc} &= -4.491 - 1.51 \cos 2\phi \text{mH} \\ L_{ac} &= -4.491 - 1.51 \cos(2\phi + 120°) \text{ mH} \end{aligned}\right\} \quad 3.67$$

The generator stator inductances matrix L_{ss} is expressed as:

$$L_{ss} = \begin{bmatrix} L_{aa} & L_{ab} & L_{ac} \\ L_{ba} & L_{bb} & L_{bc} \\ L_{ca} & L_{cb} & L_{cc} \end{bmatrix}$$

$$L_{ss} = \frac{\mu_0 rl}{g} \pi N_{abc}^2 \begin{bmatrix} \frac{62}{9} & -3 & -3 \\ -3 & \frac{62}{9} & -3 \\ -3 & -3 & \frac{62}{9} \end{bmatrix}$$

Where

$L_{ab} = L_{ba}$; $L_{bc} = L_{cb}$; $L_{ca} = L_{ac}$

CHAPTER FOUR

RESULTS AND DISCUSSION

4.1 Salient-Pole Synchronous Generator Simulation

The generator model shown in figure 3.11 is used for the simulation of Salient-Pole Synchronous Generator. The generator has to rotate at a constant speed (synchronous speed) with the help of a prime mover. To accomplish this condition, the motion setup of the ANSYS

FE model, the mechanical transients are removed and constant speed is setup for the model. Therefore, the model is made to rotate at a required constant speed of 1500rpm.

The results of the generator simulation are shown in figure 4.11(a) to figure 4.13.

4.2 Results and Comparison

4.2.1 Magnetic Field Mapping: Two Reaction (Andrew Blondel) Theory

The generator model shown in figure 4.1(a) and figure 4.1(b) are simulated as SalientPole Synchronous Generator (SPSG) and Round Rotor Synchronous Generator (RRSG) using Finite Element Magnetic Method (FEMM). Magnetic field mapping and magnetic flux density plotting are shown in figure 4.1(a) through 4.8(b). These geometrical presentations are comparatively illustrated to show magnetic flux density pattern for the two generators at various rotor angles in appendix as displayed in the figures. Magnetic flux density displayed in figure 4.1(a), 4.3(a), 4.5(a) and 4.7(a) for Salient-Pole Synchronous Generator shows disparity in magnetic flux density plots at 0° ° ° °, 30 , 60 , 90 while figure 4.2(a), 4.4(a), 4.6(a), and 4.8(a) of Cylindrical Synchronous Generator show no significant change in the magnetic field density plots at these angles. The dissimilarity shown in magnetic flux density plot from Salient-Pole Synchronous Generator at these various rotor angles indicate the reason for the innovation of the Two-Reaction Theory propounded by Andrew Blondel to resolve the analysis of this Generator without deploying conventional Cylindrical Rotor Generator method to approximate the analysis.

The computational plot presented in this chapter in figures 4.9(a) through 4.9(f) affirm the variation of the fundamental components of armature magneto-motive force which is the summation of direct and quadrature axis components, as the rotor moves around the generator air gap. The result of the magnetic field mapping and magnetic flux density plots obtained from Finite Element Method Magnetic (FEMM) were excited with phase - 'a', stator winding with 1 ampere without field (rotor) excitation. The generated codes from MATLAB were used to rotate the synchronous generator rotor at various angular positions in FEMM as displayed in Appendices E and F.

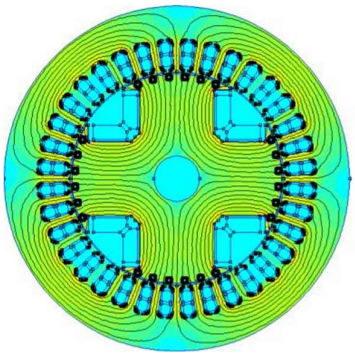

Figure 4.1a Salient-Pole Rotor Synchronous Generator Magnetic Field Plot at 0° Rotor Angle

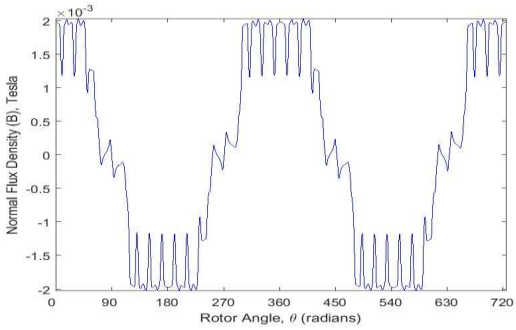

Figure 4.1b Salient-Pole Synchronous Generator Magnetic Flux Density at 0° Rotor Angle

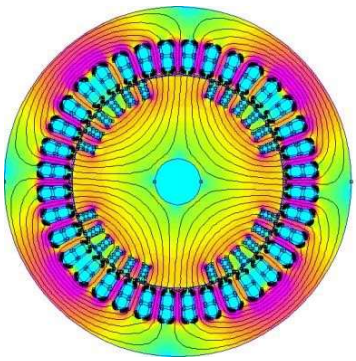

Figure 4.2a Round Rotor Synchronous Generator Magnetic Field Plot at 0° Rotor Angle

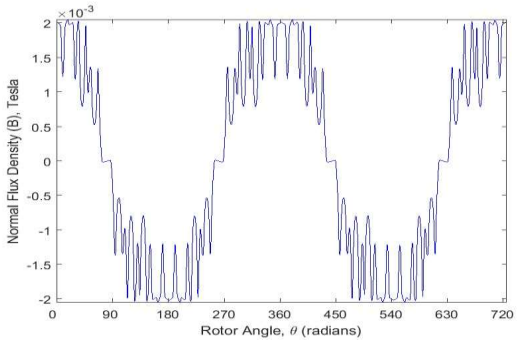

Figure 4.2b Round Rotor Synchronous Generator Magnetic Flux Density at 0° Rotor Angle

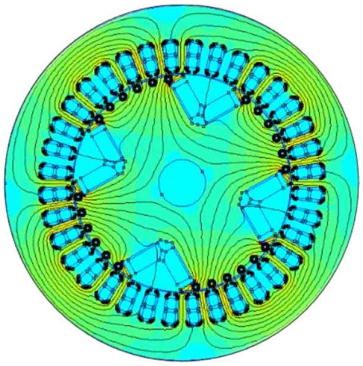

Figure 4.3a Salient-Pole Rotor Synchronous Generator Magnetic Field Plot at 30° Rotor Angle

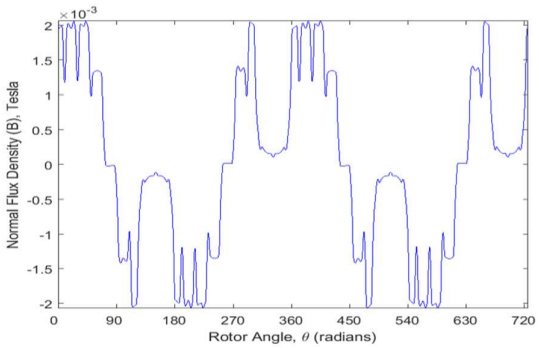

Figure 4.3b Salient-Pole Synchronous Generator Magnetic Flux Density at 30° Rotor Angle

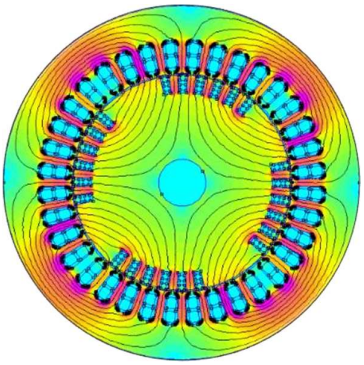

Figure 4.4a Round Rotor Synchronous Generator Magnetic Field Plot at 30° Rotor Angle

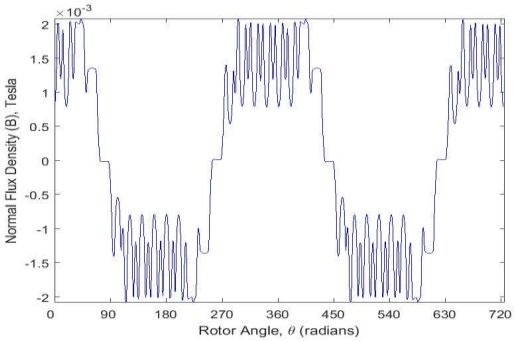

Figure 4.4b Round Rotor Synchronous Generator Magnetic Flux Density at 30° Rotor Angle

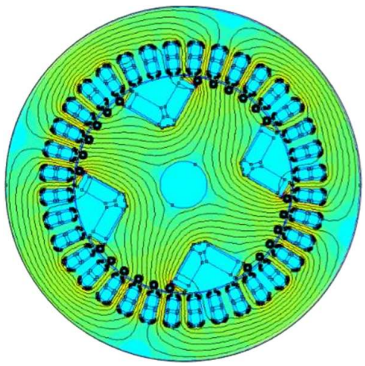

Figure 4.5a Salient-Pole Synchronous Generator Magnetic Field Density at 60° Rotor Angle

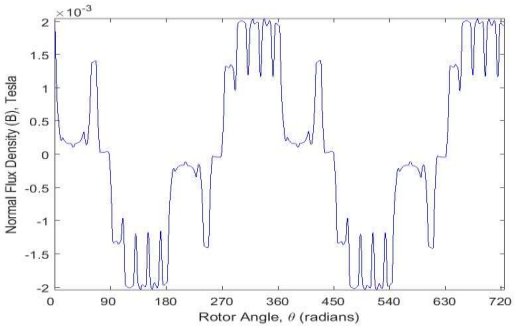

Figure 4.5b Salient-Pole Synchronous Generator Magnetic Flux Density at 60° Rotor Angle

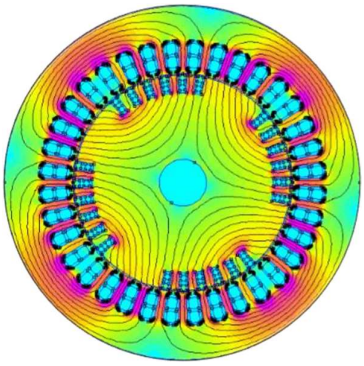

Figure 4.6a Round Rotor Synchronous Generator Generator Magnetic Field Density at 60° Rotor Angle

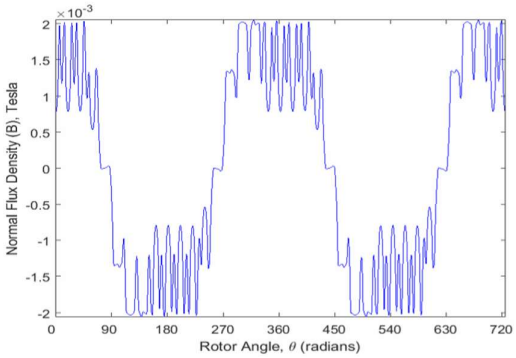

Figure 4.6b Round Rotor Synchronous Magnetic Flux Density at 60° Rotor Angle

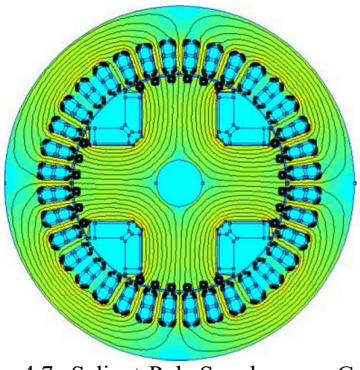

Figure 4.7a Salient-Pole Synchronous Generator Field Density at 90° Rotor Angle

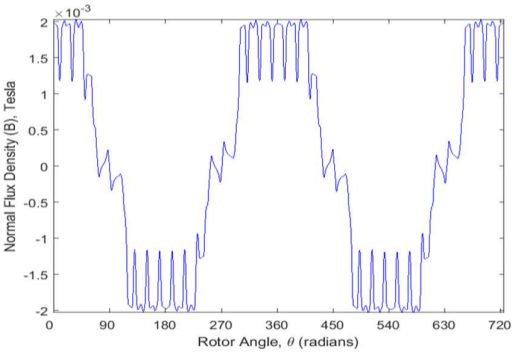

Figure. 4.7b Salient-Pole Synchronous Generator Magnetic Flux Density at 90° Rotor Angle

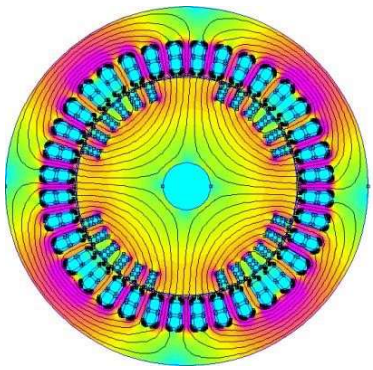

Figure 4.8a Round Rotor Synchronous Generator Magnetic Field Density at 90° Rotor Angle

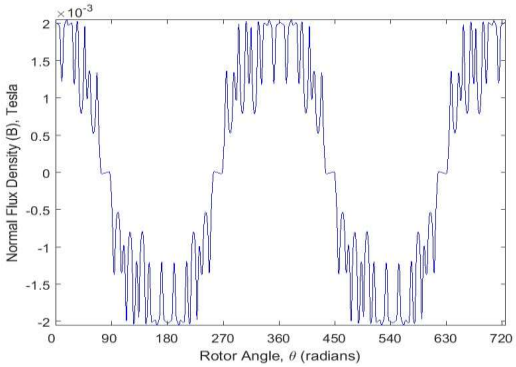

Figure 4.8b Round Rotor Synchronous Generator Magnetic Flux Density at 90° Rotor Angle

4.2.2 Magneto-motive force (MMF) Illustration of Two Reaction Theory

Figure 4.9(a) to Figure 4.9(f) show the variation of the MMF components of the armature along direct and quadrature axis at various rotor angles; and phase 'a' fundamental armature mmf as space vectoral summation of the two projected armature MMF components on the (**d** and **q**) axis.

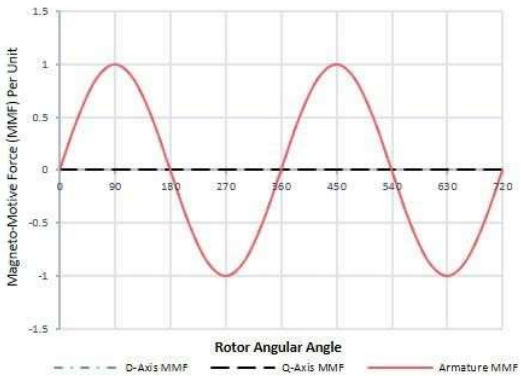

Figure 4.9 (a). Rotor angle θ_r at 0°

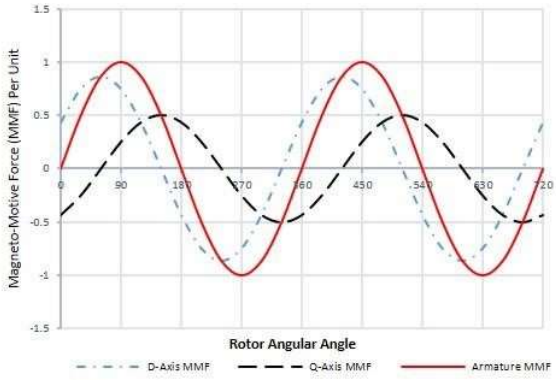

Figure 4.9 (b). Rotor angle θ_r at 30°

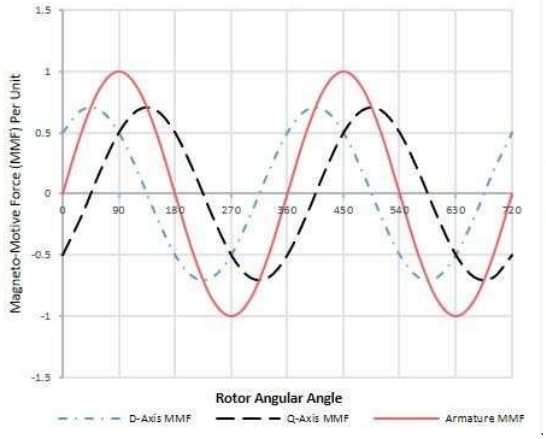

Figure 4.9 (c). Rotor angle θ_r at 45°

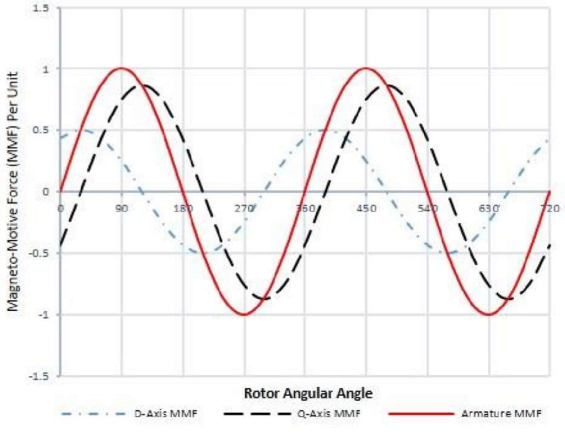

Figure 4.9 (d). Rotor angle θ_r at 60°

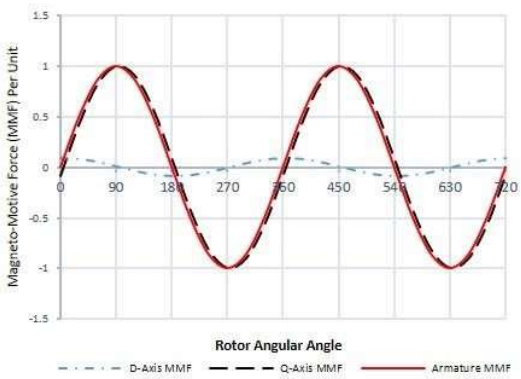

Figure 4.9 (e). Rotor angle θ_r at 85

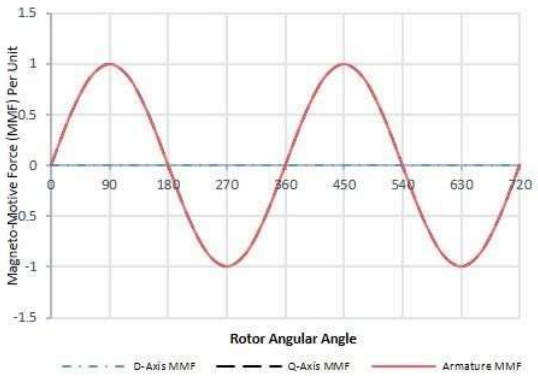

Figure 4.9 (f). Rotor angle θ_r at 90 ∘ ∘

Figure 4.9: Variation of MMF component at different Rotor Angles

The simulated parameters from ANSYS Maxwell (RMxprt) are presented in Table 4.1.

Table 4.1: Simulated Parameters from Rotating Machinery Expat (RMxprt)

Parameters	Actual Value	Per Unit Value
Unsaturated Steady State Parameter		
Armature Resistance R1 (Ohm)	0.0810638	0.010133
Armature Leakage Reactance X_l (Ohm)	0.365723	0.0457154
D-Axis Reactive Reactance Xad (Ohm)	6.92656	0.865821
Q-Axis Reactive Reactance Xaq (Ohm)	3.7479	0.468488
D-Axis Reactance X_1+Xad (Ohm)	7.29229	0.911536
Q-Axis Reactance X_1+Xaq (Ohm)	4.11363	0.514203
Field Winding Resistance Rf (Ohm)	0.18713	0.00394709
No-Load Magnetic Data		
Air-Gap Flux Density (Tesla)	0.605116	
No-Load Exciting Current (A)	25.994	
Full-Load Data		
Exciting Current at Short-Circuit Current (A)	21.7247	
Power Factor Angle (degree)	32.1387	
Power Angle (degree)	18.5412	
Output Power (kW)	16.9353	

Short Circuit Ratio	1.1965

Table 4.1: Simulated Parameters from RMxprt (Continued)

Transient Parameter & Time Constants	Actual Value	Per Unit Value
D-axis Transient Reactance (Ohm)	0.949278	0.11866
Field Leakage Reactance Xf (Ohm)	0.637242	0.0796552
Negative-Sequence Reactance (Ohm)	0.556438	0.0695548
Zero-Sequence Reactance (Ohm)	0.365723	0.0457154
D-axis Transient Time Constant (s)	0.0992552	
Armature Time Constant (s)	0.0218494	
Field Winding Time constant with open circuit armature (s)	0.762471	

Transient FEA Input Data	
Bar Resistance (ohm)	0.000393044
End Ring Resistance (ohm)	5.03173e-005
End Ring Inductance (H)	3.2545e-008

4.3 Salient-Pole Synchronous Generator on No-Load and Three-Phase Short Circuit

The Salient-Pole Synchronous Generator modeled in this research is subjected to the following practical realizable conditions:

i. No-Load Condition. ii.

Load Condition.

iii. Three Phase Short Circuit.

These three conditions are presented in the plots shown in figure 4.11 (a) to figure 4.11 (n). The plots are:

1. Generator Moving Torque.
2. Generator Winding Current.

3. Generator Phase Current.
4. Generator Phase Inductance.
5. Generator Field Inductance.
6. Generator Magnetic Flux Linkage.
7. Generator Induced Voltage.
8. Generator Damper Bar Current and Voltage
9. Generator Power Angle Curve
10. Generator Synchronous Speed

4.3.1 Generator Moving Torque

The figures 4.10 (a) and (b) indicate the generator moving torque on No-load, Load and Three phase short circuit conditions. The switching timing for these conditions as clearly shown on the plots as 50msecs for no-load and switching to three-phase ground fault at 100msecs. These plots indicate initial condition of the generator torque and the prime-mover operating at synchronism where the electromagnetic torque (Te) and the mechanical torque (Tm) are equal, i.e. Tm = Te. This condition is observed between zero sec to 50msecs for figure 4.10 (a) on no-load and between zero to 100msecs for figure 4.10(b) for ground fault. After these timing the generator responds to negative torque (-60Nm) as usual indicating negative acceleration to normalize the operating condition at steady state for load situation and swing to (-1.15kNm) and progresses to steady-state after fault is removed or shutdown if the fault persists. The peak-to-peak value of Te is 35Nm as indicated on the two plots.

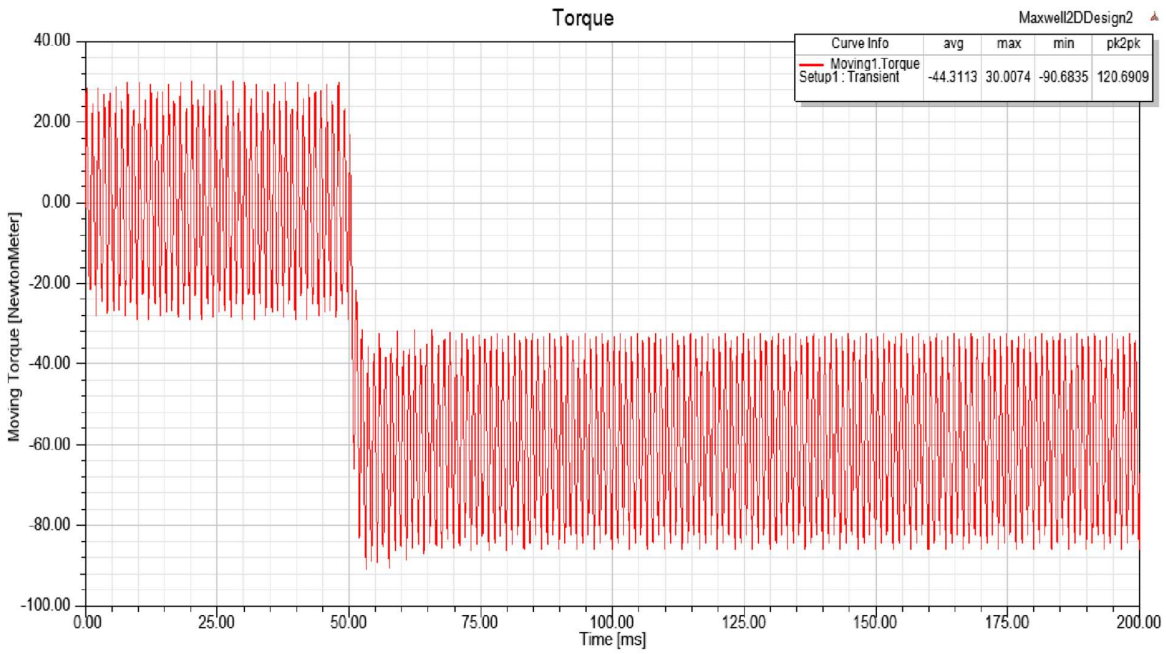

Fig. 4.10 (a) Moving Torque at No Load and Load Condition at 0.05secs

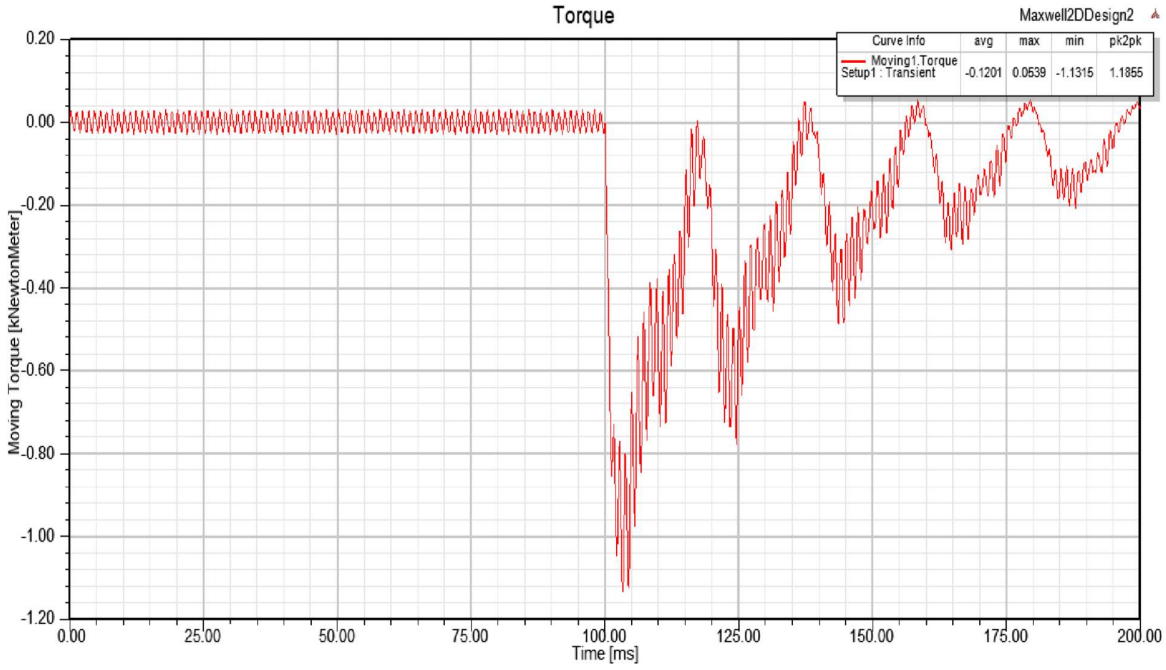

Fig. 4.10 (b) Moving Torque at Three phase circuit at 0.1secs

4.3.2 Generator Winding and Phase Current

The plots in figure 4.10(c) to 4.10(f) explain what happens when generator is subjected to no-load, load and three phase short circuits. Comparing the three conditions, it is observed that from zero to 50milisecs and 100milisecs, the winding and phase currents were zero ampere indicating the generator is not delivering any power within the period. From 50milisecs and 100milisecs up, it is shown how the generator winding and phase current went up 17Amps and stays throughout the period while on three phase fault the winding and phase current went to above 340Amp and decay with time. These conditions are normal behaviour of generator on no-load, load and three phase short circuit conditions.

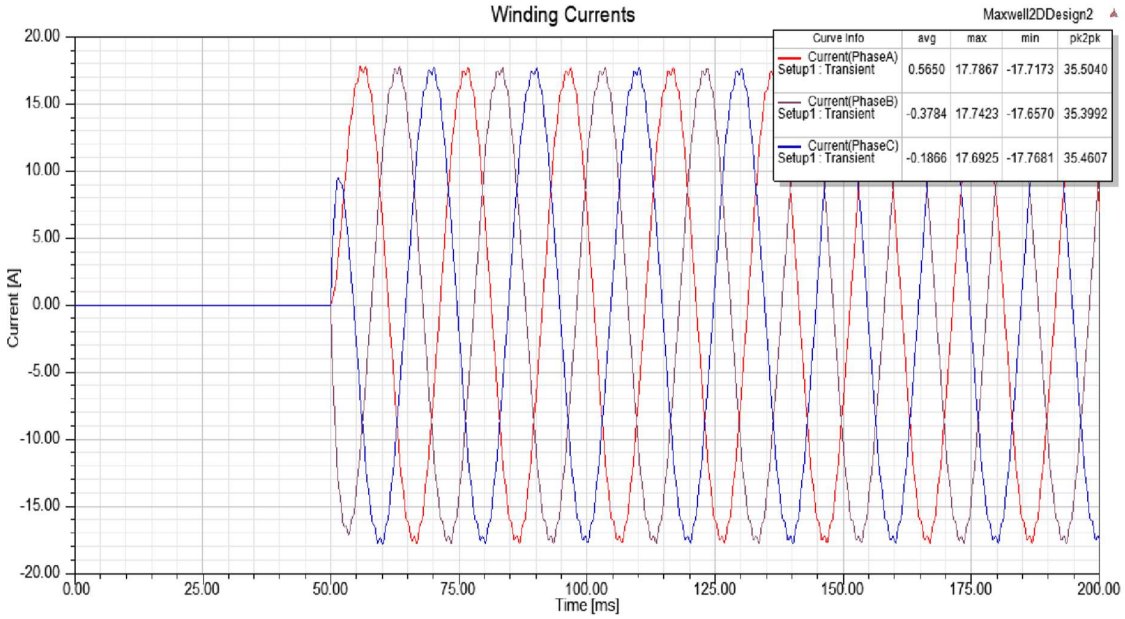

Figure 4.10 (c) Winding Current of the Generator on No-Load and Load condition

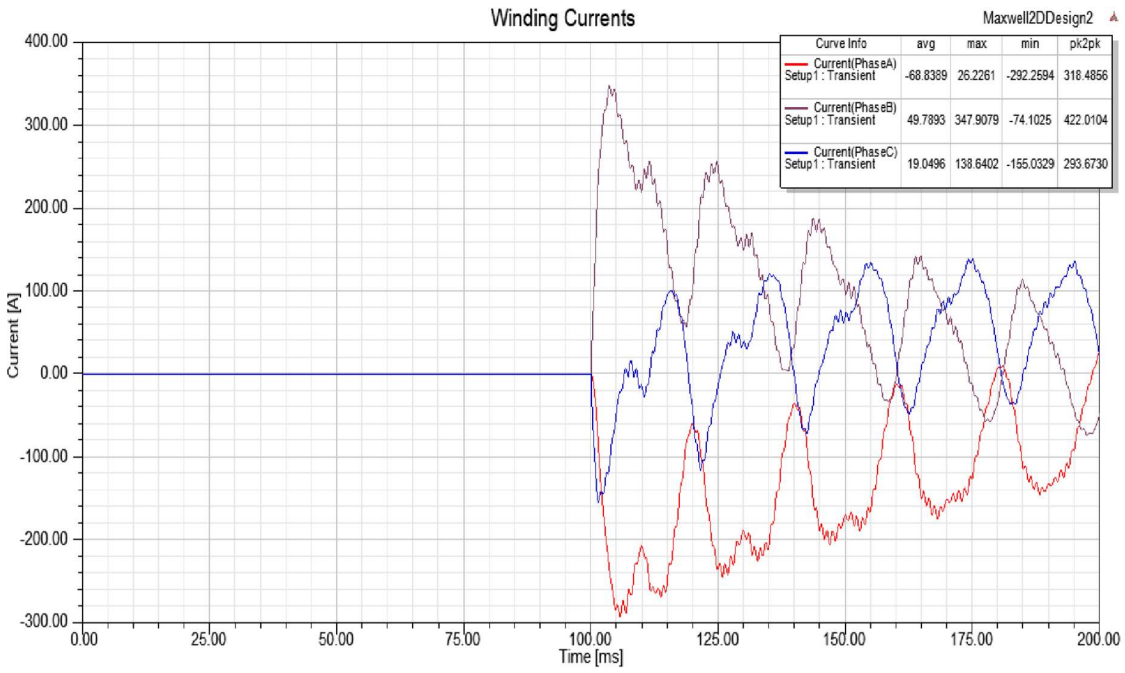

Figure 4.10 (d) Generator Winding on Three Phase fault Condition

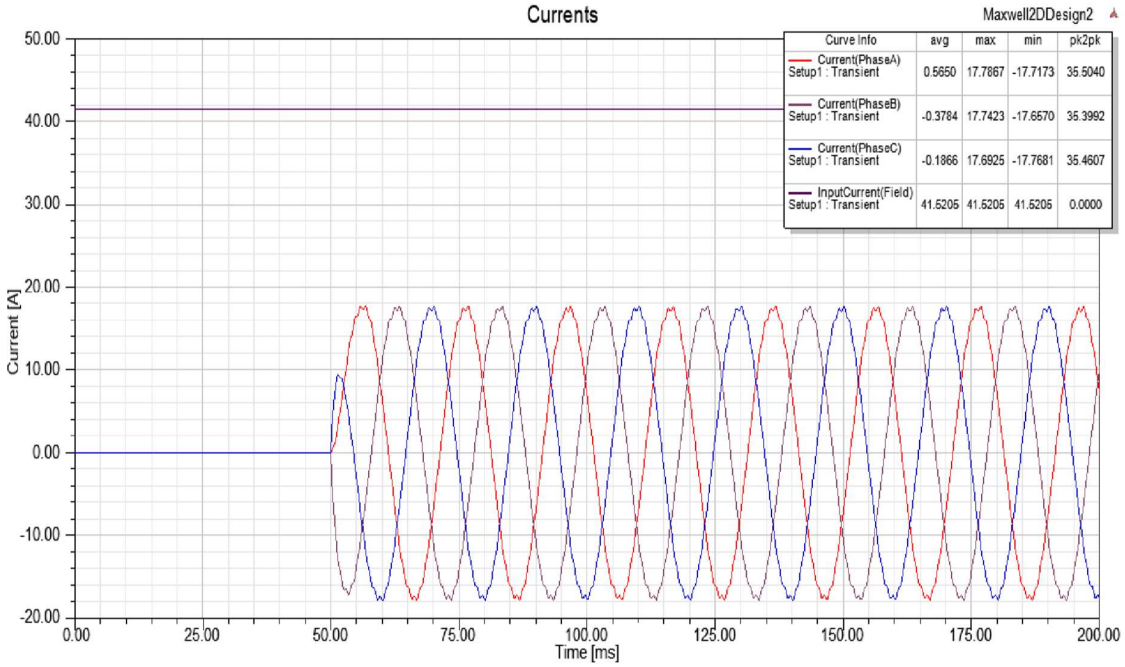

Figure 4.10 (e) Generator Phase Current on No-Load and Load Condition

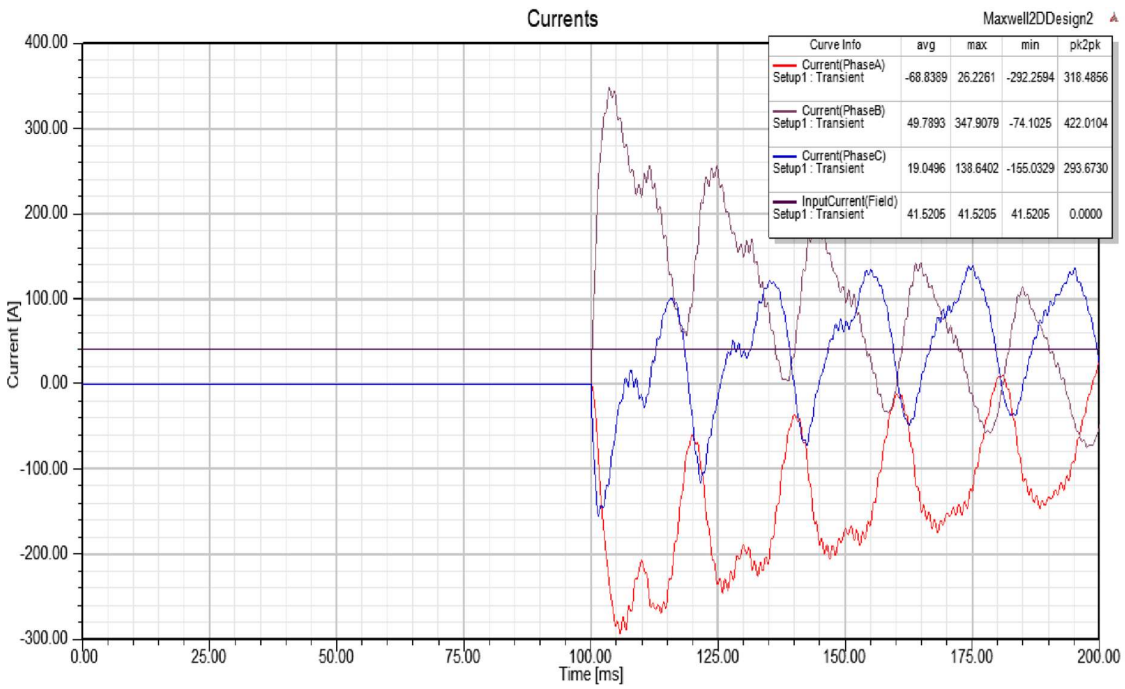

Figure 4.10 (f) Generator Phase Current on No-Load and Three-Phase fault Condition

4.3.3 Generator Phase and Field Inductance

The generator phase and field inductances shown in figures 4.10(g) and 4.10(h) indicate slight increase in generator phase and field inductances for no-load and load condition. While there is significant increase in generator, phase and field inductances during the three-phase fault at

100milisecs. This explains the importance of inductance in generator performance analysis.

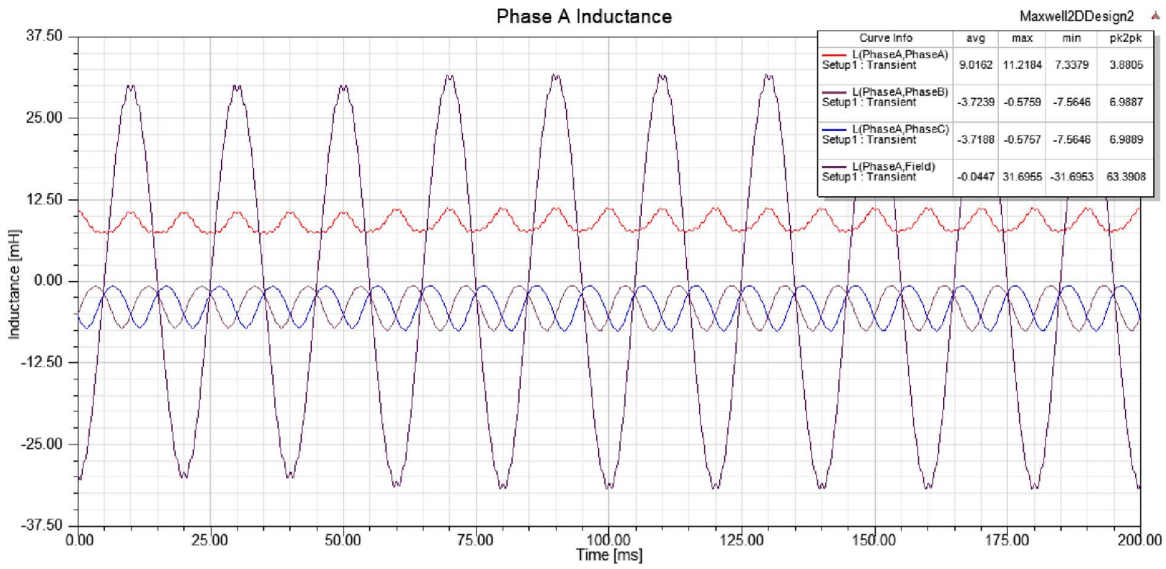

Figure 4.10 (g) Generator Phase Inductance on No-Load and Load Condition

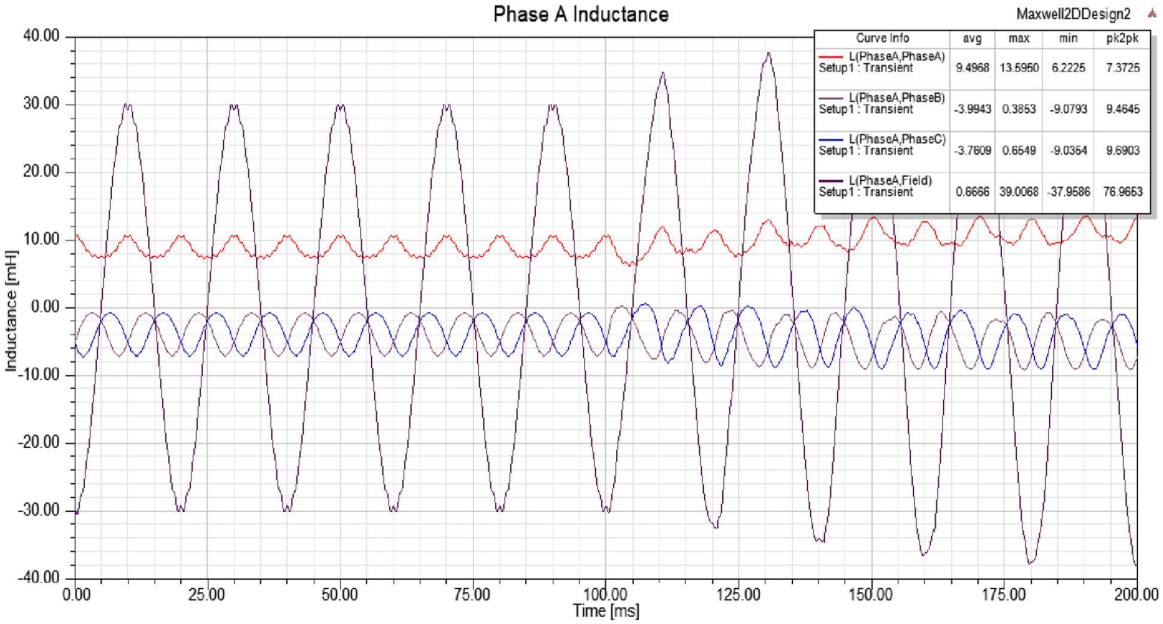

Figure 4.10 (h) Generator Phase Inductance at Three - Phase Fault Condition

4.3.4 Generator Induced Voltage

The generator induced voltage shown in figures 4.10(i) and 4.10(j) explain the generator behaviour on no-load, load and three phase fault conditions. The No-load situation maintain almost a constant line voltage of 400V and field voltage, except at 50milisecs where there is a slight increase in field voltage and decrease in line voltage due to load switching on the generator. During the three-phase fault, the line voltage dropped significantly to a very low voltage while the induced field voltage went as high as 850Volts and eventually decay with time to recover from the fault if the fault condition is removed, otherwise tripped the generator if it persists.

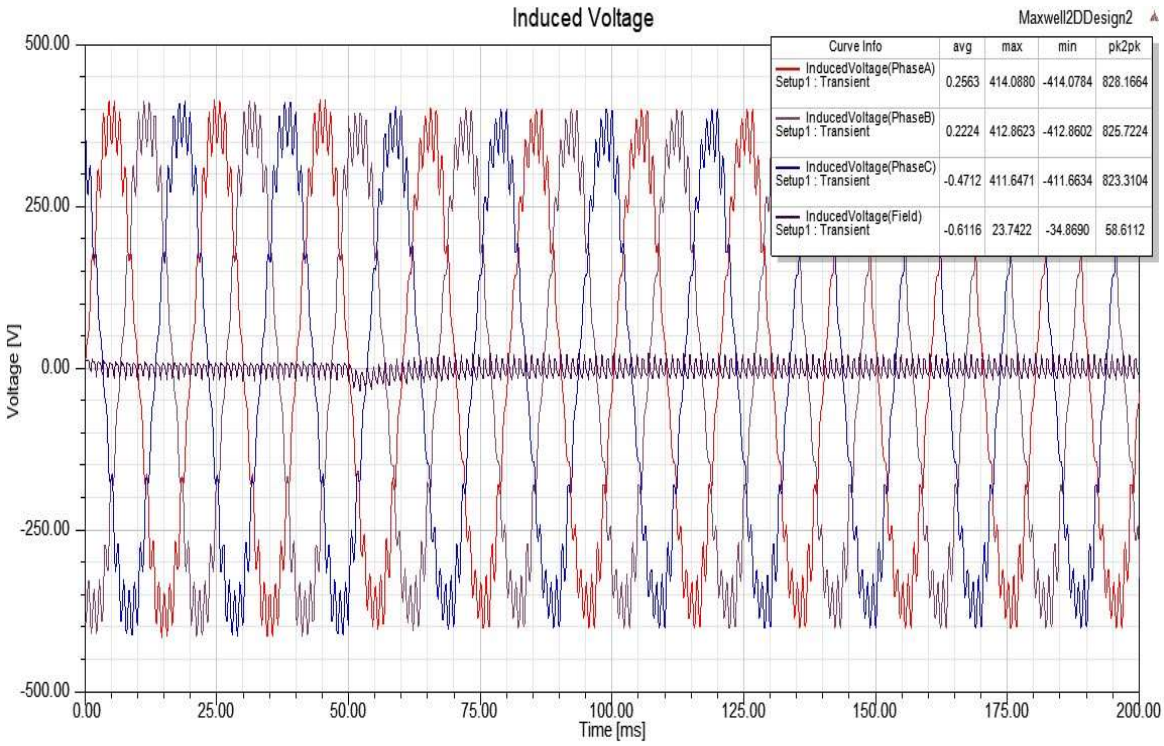

Figure 4.10 (i) Generator Induced Voltage on No-Load and Load Condition

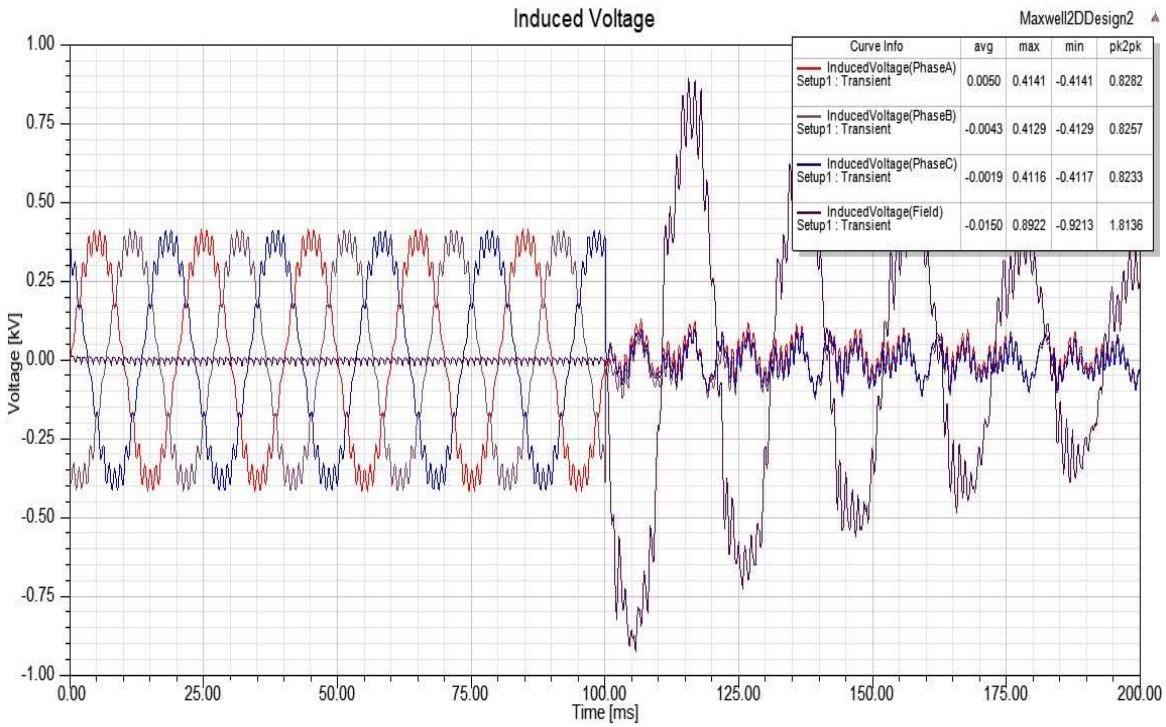

Figure 4.10 (j) Generator Induced Voltage on Fault Condition

4.3.5 Generator Magnetic Flux Linkage

Magnetic flux linkage is essential in establishing generator inductances. The generator phase magnetic flux linkages remain constant from no-load to load condition as shown in figures 4.10(k) while the generator rotor magnetic field flux linkage also remained constant till load was applied before a gradual drop is noticed as shown in figure 4.10(k). In figure 4.10(l) the generator phase magnetic flux linkage also remained constant up to 100milisecs before the phase and field magnetic flux linkage collapsed and decayed with time as shown in the plot.

This indicate how fault condition destroys magnetic field build-up in generators.

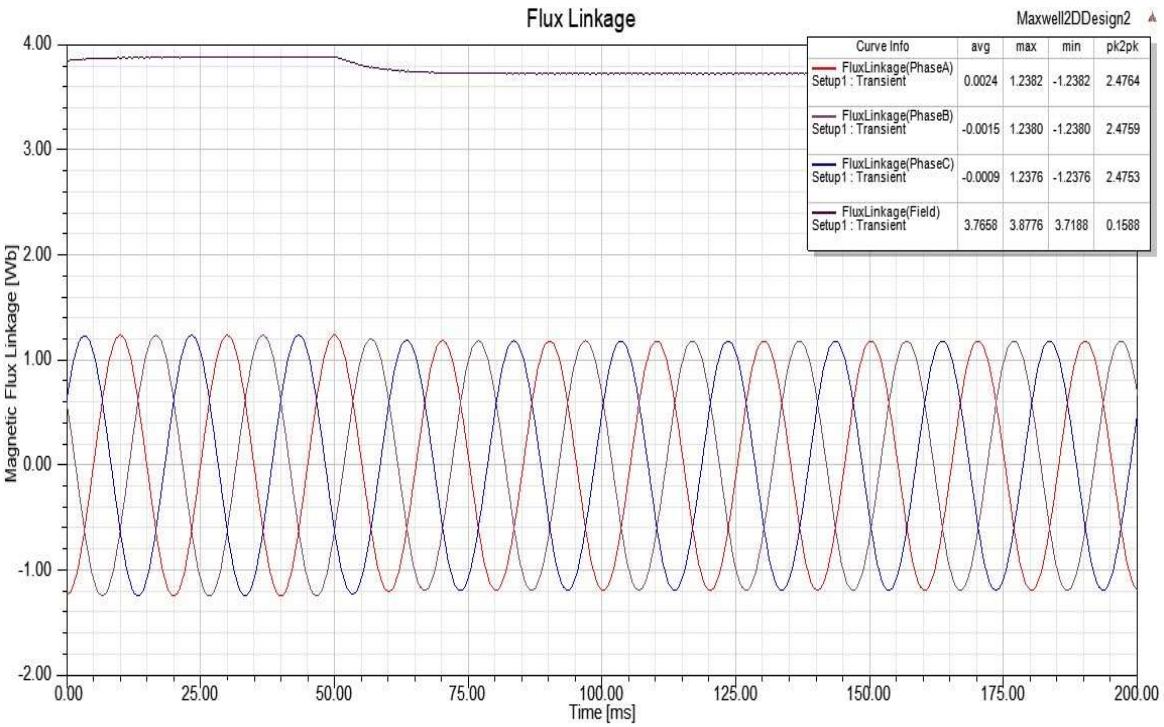

Figure 4.10 (k) Generator Magnetic Flux Linkage on No-Load and Load Condition

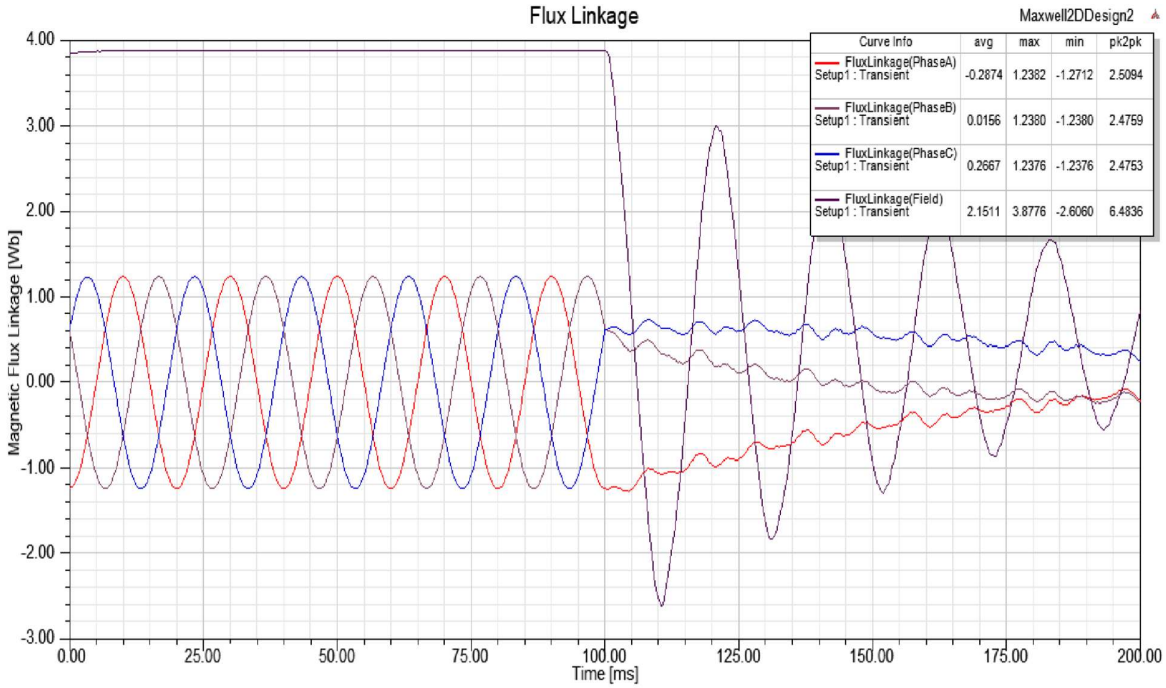

Figure 4.10 (l) Generator Magnetic Flux Linkage on Three-Phase Fault Condition

4.3.6 Generator Damper Bars (End Connection)

Comparative analysis of the plot shown in figure 4.10(m) and figure 4.10(n) from initial timing of zero to 50millisecs and 100millisecs indicate the same pattern showing the generator on noload. While different operating situations were observed for load and three-phase short circuit condition as illustrated in the plots in figure 4.10(m) and figure (n). At no-load condition, the damper bar current is 50 amperes, suddenly jumped to 125 amperes within 5milisecs, and maintain at the steady-state value while the damper bars voltage maintain 75milivolts; indicating that the damper bars will remain non-operational during no-load and load conditions. For the three-phase short circuit, the damper bars operated by suddenly inducing high current and low voltage of 2.8kA, and 2 volts respectively. This occurs to bring back the generator condition to the steady-state or shutdown if the faulty condition persist.

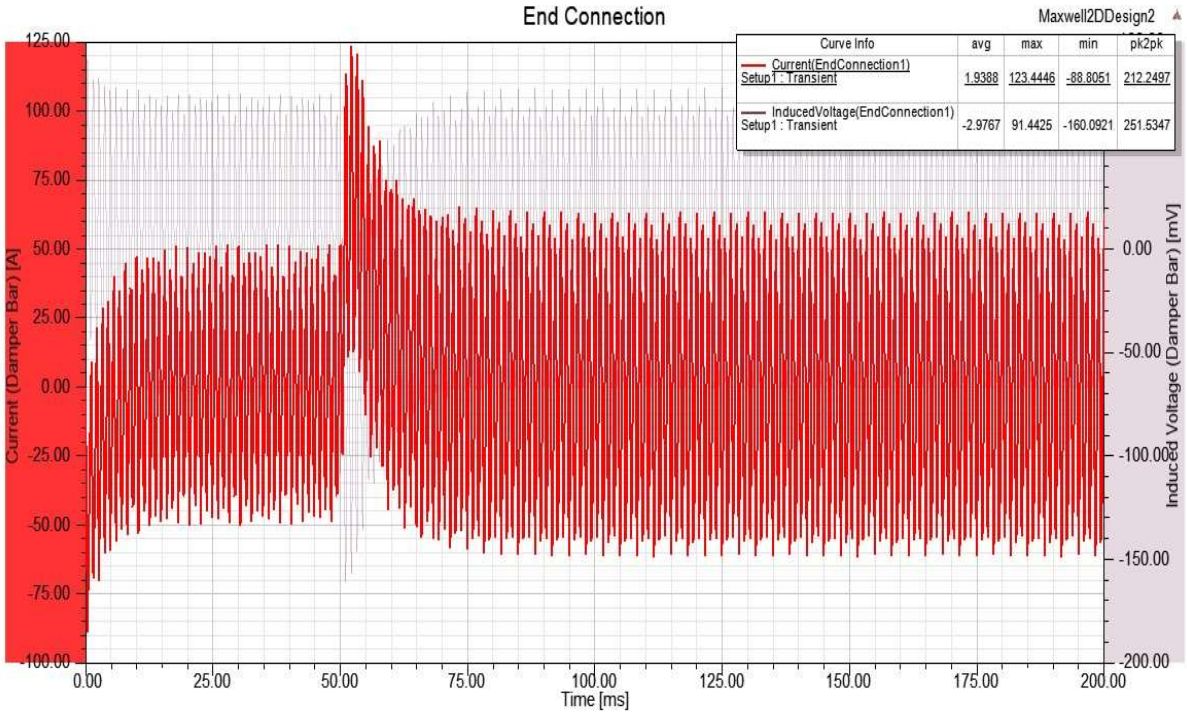

Figure 4.10 (m) Generator Damper Bar on No-Load and Load Condition

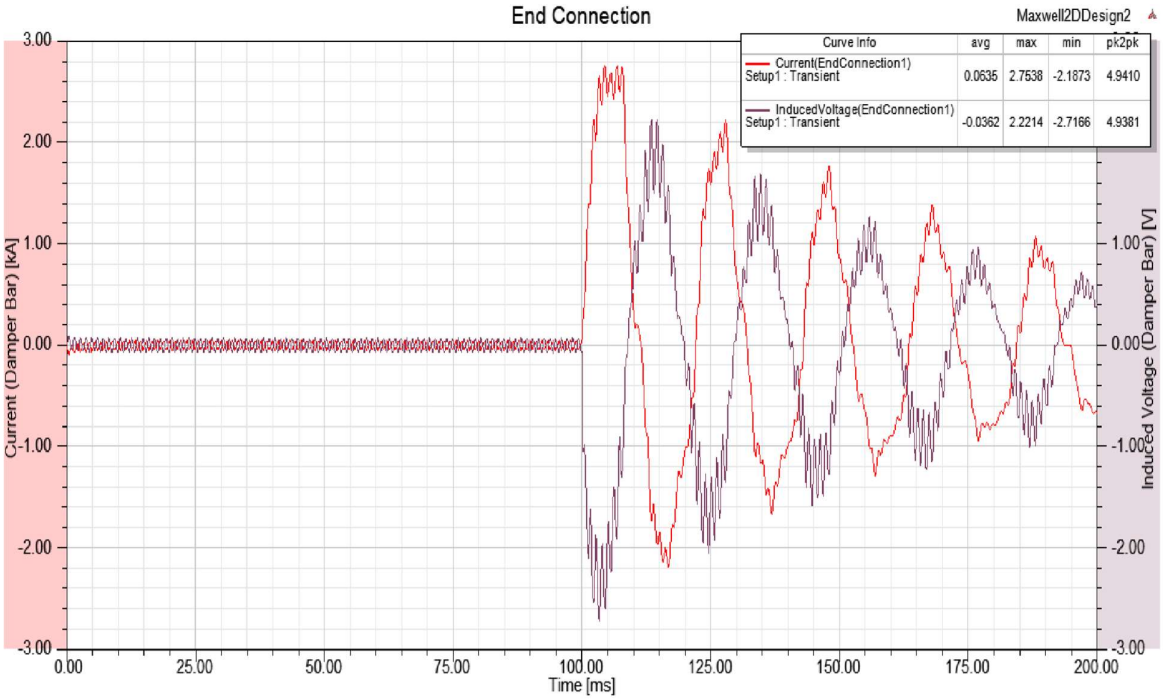

Figure 4.10 (n) Generator Damper Bar on No-Load and Three-Phase Fault Condition

4.3.7 Salient-Pole Synchronous Generator Power Angle Curve

The results obtained for performance evaluation and analysis is displayed in figure 4.11(a) to figure 4.12. These include power angle curves non-saliency and saliency synchronous generators and the generator moving speed.

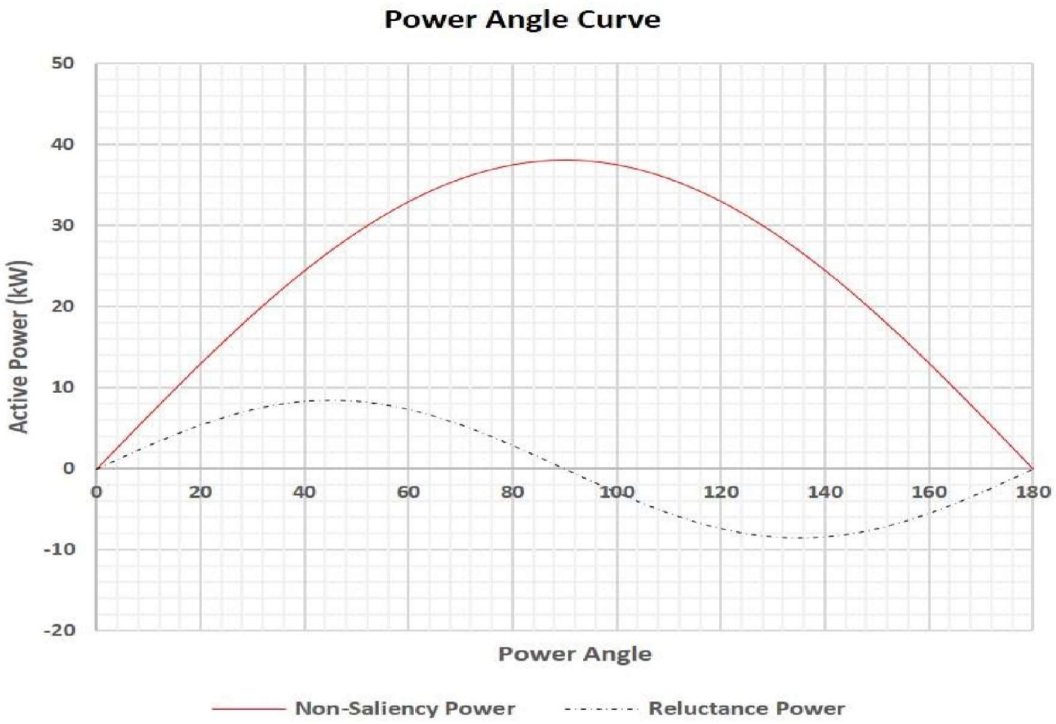

Figure 4.11 (a) Power Angle Curve with Non-Saliency and Reluctance Power

Figure 4.11 (b): Power Angle Curve with Saliency

4.3.8 Generator Moving Speed

The generator rotates at constant speed of 1500rpm as shown in figure 4.12 with the help of a prime mover

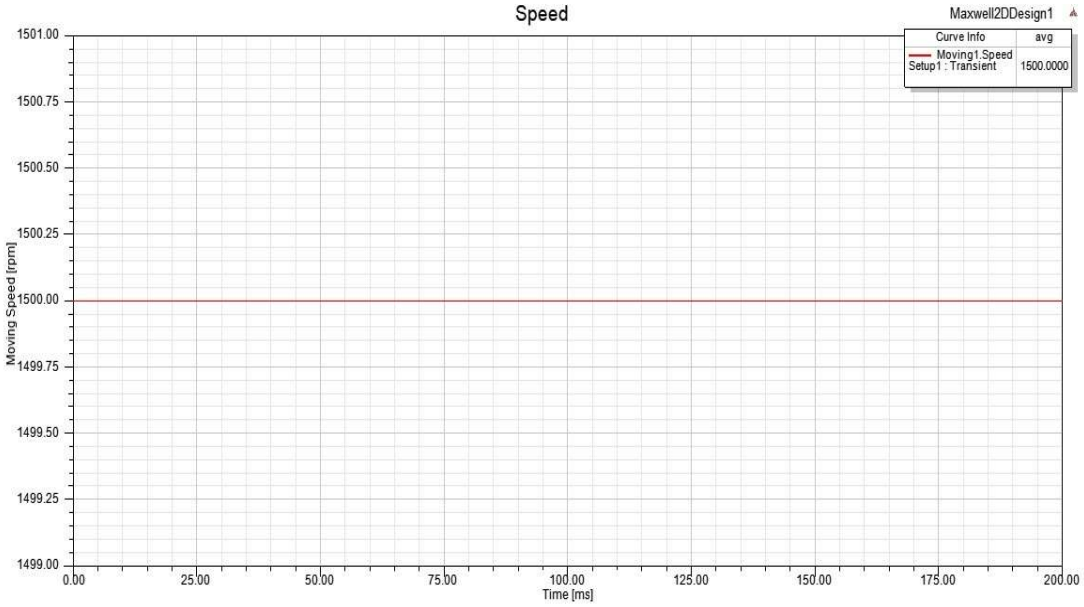

Figure 4.12: Generator Speed

4.4 Result Validation:

4.4.1 ANSYS Maxwell and Winding Function Reactance Comparison

Direct and Quadrature – axis synchronous reactance together with armature leakage reactance though relatively very small, as compared to d-q reactance form part of the major parameters in generator modelling, simulation and analyses. The numerical value of the reactances of any electrical machines explain how stiff the machine is electrically on a bus system (Ames, R. L 1990).

Table 4.2: Result Data from ANSYS Maxwell and Winding Function Method

Reactance	ANSYS Maxwell	Winding Function Method
Direct–axis reactance (X_{ad})	6.93 Ohms	6.21 Ohms
Quadrature–axis inductance (X_{aq})	3.75 Ohms	2.91 Ohms

One of the focus area in this research was to analyse, compute and simulate the salient-pole synchronous generator to obtain generator reactances. Comparative analysis of the direct and quadrature–axis reactances of the generator's results from ANSYS Maxwell and Modified Winding Function Method is presented in table 4.2. The reactances computed from modified winding function method are from physical winding arrangement, inverse air-gap and others parameters of the generator. The two results from ANSYS Maxwell and Modified Winding Function are very close to each other despite the computational approach and some geometrical factors such as rotor pole-shoe, stator slots and MMF drop in the iron region, which might have influenced the results.

Although the numerical values of the two results are close, the finite element method (ANSYS Maxwell) offer better advantage compared with the Winding Function Method because of the effect of magnetic flux scattering, leakages and the actual generator air gap geometry that are not necessarily considered in the Winding Function Method.

4.4.2 Optimum Performance Criteria Parameters Evaluation

In Chapter 3, two parameters that are essential in generator performance evaluation were presented, the air gap length (l_g) and the short circuit ratio (SCR).

These parameters obtained from the result of ANSYS Maxwell simulation of the salient-pole synchronous generator with the following generator rotor lengths; (250mm, 255mm, 260mm,

265mm, 270mm, 275mm and 280mm) are presented in Table 4.3 to Table 4.9.
The choice for the parameters were based on optimum operational performance and economical consideration such as material cost and generator size. Table 4.3 to table 4.9 indicate various rotor lengths with corresponding air-gap lengths, SCRs and reactances. Table 4.10 populate acceptable parameters to achieve the expected optimum operational performance.

The relationship between the short circuit ratio (SCR), air-gap length and generator direct and quadrature reactance are presented in figure 4.15 to figure 4.17.

Figure 4.15 shows a direct proportionality of the SCR and air-gap length of the generator, while figure 4.16 and figure 4.17 relate the air-gap length and SCR with the reactance of the generator. Section 3.3.3 explains the significance of these two parameters to the operating performance of salient-pole synchronous generator as regards generator cost, size and stability. Therefore, the comparative analysis of the salient-pole synchronous generator standard specification with the simulated data obtained from ANSYS Maxwell shown in table 4.10 agree with acceptable value of air gap length of **2.025mm**, SCR of **1.196** and core axial length to pole pitch ratio of **1.903** for optimum performance with **275mm** rotor length for SPSG, modelled for this research.

-

Table 4.3: Salient Pole Synchronous Generator: 250mm Rotor Length

Rotor Length	Air Gap Length(mm)	Short Circuit Ratio (SCR)	D -Axis Reactance(Ohms)	Q -Axis Reactance(Ohms)
250mm	3.025	1.87399	4.38988	2.58189
250mm	2.525	1.63845	5.16874	2.92151
250mm	2.275	1.51754	5.67845	3.14194
250mm	2.025	1.39427	6.30602	3.41213
250mm	1.775	1.26866	7.09779	3.74963
250mm	1.525	1.1406	8.13072	4.18729
250mm	1.275	1.00944	9.53905	4.78179
250mm	1.025	0.875178	11.582	5.6418
250mm	0.775	0.736393	14.8364	7.00136
250mm	0.525	0.590871	20.9458	9.54885

Table 4.4: Salient-Pole Synchronous Generator: 255mm Rotor Length

Rotor Length	Air Gap Length(mm)	Short Circuit Ratio (SCR)	D-Axis Reactance(Ohms)	Q-Axis Reactance(Ohms)
255mm	3.025	1.81875	4.4756	2.63231
255mm	2.775	1.70397	4.83904	2.79135
255mm	2.525	1.58718	5.27007	2.97878
255mm	2.275	1.46831	5.78999	3.20366
255mm	2.025	1.34739	6.43013	3.47928
255mm	1.775	1.22418	7.23776	3.82357
255mm	1.525	1.09832	8.29137	4.27002
255mm	1.275	0.969332	9.7279	4.87646
255mm	1.025	0.837313	11.8117	5.75372
255mm	0.775	0.700972	15.1313	7.14053

255mm	0.525	0.558017	21.3629	9.73903

Table 4.5: Salient Pole Synchronous Generator: 260mm Rotor Length

Rotor Length	Air Gap Length(mm)	Short Circuit Ratio (SCR)	D-Axis Reactance(Ohms)	Q-Axis Reactance(Ohms)
260mm	3.025	1.7654	4.56133	2.68273
260mm	2.775	1.65258	4.9319	2.84492
260mm	2.525	1.53788	5.37139	3.03605
260mm	2.275	1.42147	5.90153	3.26537
260mm	2.025	1.30329	6.55423	3.54644
260mm	1.775	1.1837	7.37773	3.89751
260mm	1.525	1.05979	8.45202	4.35276
260mm	1.275	0.933634	9.91676	4.97113
260mm	1.025	0.804039	12.0415	5.86564
260mm	0.775	0.670067	15.4262	7.27969
260mm	0.525	0.529815	21.7801	9.92921

Table 4.6: Salient-Pole Synchronous Generator: 265mm Rotor Length

Rotor Length	Air Gap Length(mm)	Short Circuit Ratio (SCR)	D-Axis Reactance(Ohms)	Q-Axis Reactance(Ohms)
265mm	3.025	1.71859	4.64705	2.73314
265mm	2.775	1.60759	5.02476	2.89849
265mm	2.525	1.49475	5.47272	3.09333
265mm	2.275	1.37987	6.01307	3.32709
265mm	2.025	1.26274	6.67834	3.61359
265mm	1.775	1.14426	7.5177	3.97145

265mm	1.525	1.02342	8.61268	4.4355
265mm	1.275	0.89951	10.1056	5.0658
265mm	1.025	0.772374	12.2712	5.97755
265mm	0.775	0.641128	15.7211	7.41886
265mm	0.525	0.50367	22.1973	10.1194

Table 4.7: Salient Pole Synchronous Generator: 270mm Rotor Length

Rotor Length	Air Gap Length(mm)	Short Circuit Ratio (SCR)	D-Axis Reactance(Ohms)	Q-Axis Reactance(Ohms)
270mm	3.025	1.67685	4.73277	2.78356
270mm	2.775	1.56782	5.11762	2.95205
270mm	2.525	1.4569	5.57405	3.1506
270mm	2.275	1.344	6.12461	3.38881
270mm	2.025	1.22891	6.80245	3.68075
270mm	1.775	1.11158	7.65766	4.0454
270mm	1.525	0.991833	8.77333	4.51823
270mm	1.275	0.869032	10.2945	5.16047
270mm	1.025	0.74294	12.501	6.08947
270mm	0.775	0.613493	16.016	7.55802
270mm	0.525	0.478469	22.6144	10.3096

Table 4.8: Salient-Pole Synchronous Generator: 275mm Rotor Length

Rotor Length	Air Gap Length(mm)	Short Circuit Ratio (SCR)	D-Axis Reactance(Ohms)	Q-Axis Reactance(Ohms)
275mm	3.025	1.63662	4.8185	2.83398
275mm	2.775	1.52943	5.21048	3.00562
275mm	2.525	1.42039	5.67538	3.20787

275mm	2.275	1.30949	6.23615	3.45052
275mm	**2.025**	**1.19652**	**6.92656**	**3.7479**
275mm	1.775	1.08133	7.79763	4.11934
275mm	1.525	0.963653	8.93399	4.60097
275mm	1.275	0.843207	10.4833	5.25514
275mm	1.025	0.719364	12.7307	6.20139
275mm	0.775	0.591251	16.3109	7.69719
275mm	0.525	0.456932	23.0316	10.4997

Table 4.9: Salient Pole Synchronous Generator: 280mm Rotor Length

Rotor Length	Air Gap Length(mm)	Short Circuit Ratio (SCR)	D-Axis Reactance(Ohms)	Q-Axis Reactance(Ohms)
280mm	3.025	1.59963	4.90422	2.8944
280mm	2.775	1.494	5.30335	3.05919
280mm	2.525	1.38653	5.77671	3.26515
280mm	2.275	1.27712	6.34769	3.51224
280mm	2.025	1.16558	7.05067	3.81506
280mm	1.775	1.05219	7.9376	4.19328
280mm	1.525	0.936722	9.09464	4.68371
280mm	1.275	0.818396	10.6722	5.34981
280mm	1.025	0.696677	12.9605	6.31331
280mm	0.775	0.570725	16.6058	7.83635
280mm	0.525	0.438622	23.4488	10.6899

-

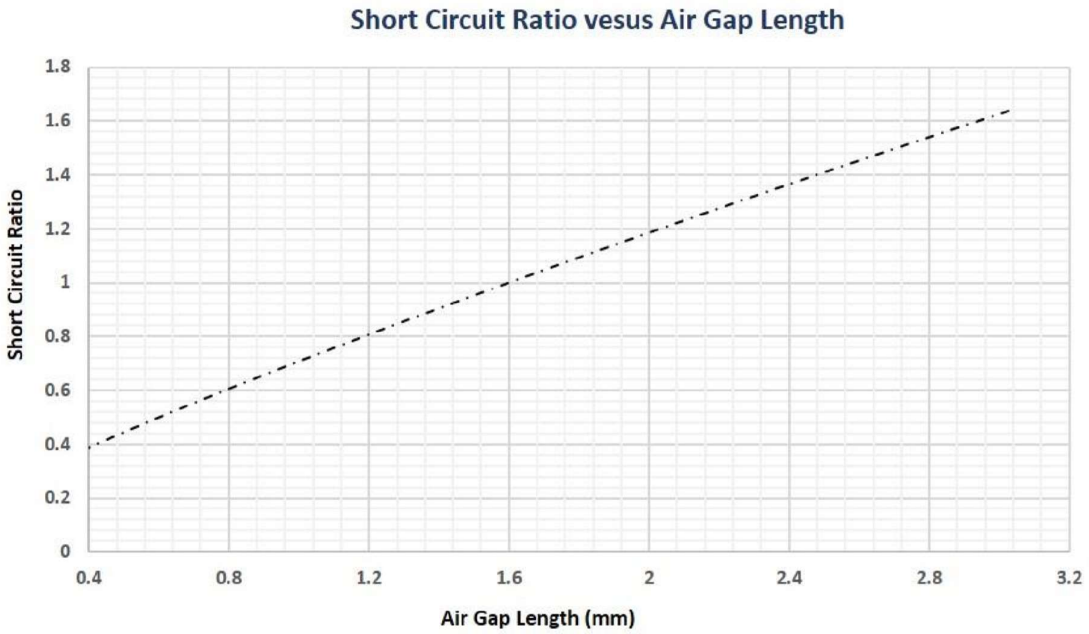

Figure 4.13: Short Circuit Ratio and Air Gap Length of Salient-Pole Synchronous Generator

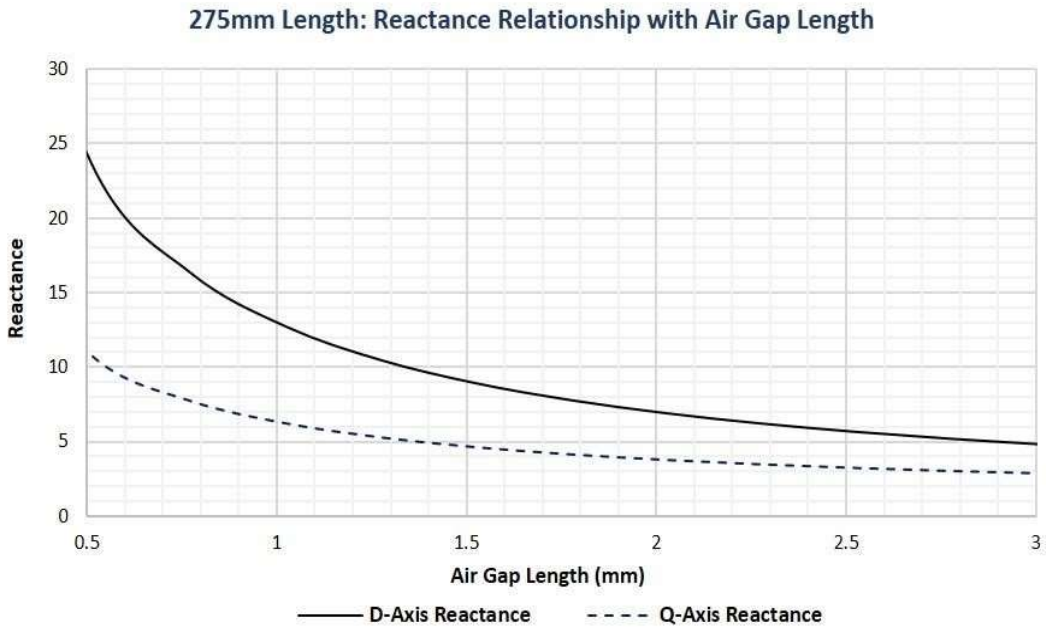

Figure 4.14: Reactance and Air Gap Length of Salient-Pole Synchronous Generator

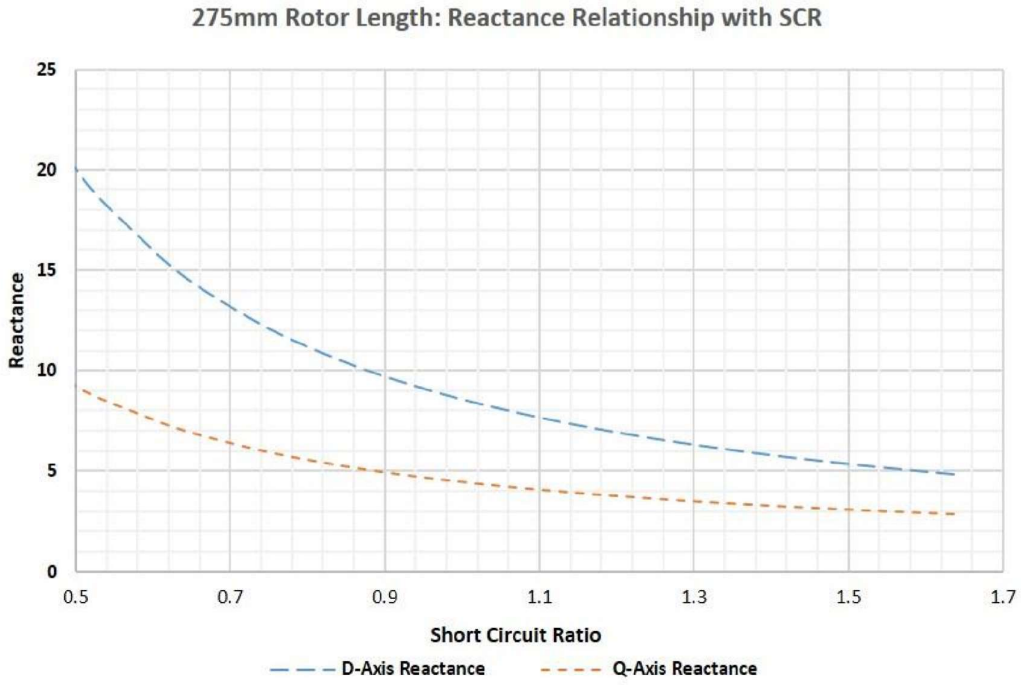

Figure 4.15: Reactance and Short Circuit Ratio of Salient-Pole Synchronous Generator **Table 4.10: Optimum Performance Criteria Comparison: Salient Four Pole Synchronous Generator**

S/N	Recommended Design Specification (Mittle and Mittal, 2017)	RMxprts / Simulated Results
(i)	Generator Air-Gap Length (l_g): (**0.012** – **0.016**) x Pole Pitch: (**1.739** – **2.3186**) mm	**2.025** mm
(ii)	Short Circuit Ratio – (**0.9** – **1.3**)	**1.1965**
(iii)	$\frac{\text{Axial Lengths of the Core}}{\text{Pole pitch}}$ = (**0.8** to **3**)	**1.903**
(iv)	Generator Stator Length should be less than Stator Diameter	Generator Stator Length: **275** mm Stator Diameter: **304** mm

CHAPTER FIVE

CONCLUSION AND RECOMMENDATIONS

5.1 Conclusion

The mathematical expression and geometrical presentation of the Two-Reaction Theory propounded by Andrew Blondel has been proven to completely eliminate the complementary approach of implementing the approximate method of using the Cylindrical Synchronous Generator analysis for Salient-Pole Synchronous Generator. The intended magnetic field mapping of the computational section of the generators and plotting of magnetic flux density, physically illustrate this, by comparing magnetic flux density of salient-pole and cylindrical rotor synchronous generators at various rotor angles. Therefore, this research will assist undergraduate, graduate students and power system engineers with a better understanding and appreciation of Blondel's theory; and its application to electrical machine modelling and analysis. The concept further conveys the usefulness of Clarke's - Park's transformation from rotating three-phase to invariant two-phase variables that is generally applied to electrical machine performance analysis and evaluation.

The two known methods used to evaluate generator inductance (the finite element method and winding function method) were discussed. The generator three-phase inductances obtained from Modified Winding Function were transformed into d-q reactance as displayed in Table 4.2 of the result data. The relative advantage of each of these methods depend on the computational burden and input data collection for the evaluation. Winding function method involve direct computation and is a preferred method to finite element method due to its simplicity and taking into account details such as the actual distribution of generator windings while finite element method requires all the geometrical dimensions, quantities and defined boundary conditions at major generator parts.

The simulation and analysis of this generator clearly demonstrate the usefulness of computational space of the modelled generator geometry by using ANSYS Maxwell and RMxprt software. This was achieved through a careful choice of generator's physical dimensions to obtain generator's parameters, which conform to global standard and specification for a typical salient-pole synchronous generator like the one adopted for this research, in order to enhance generator's performance.

Table 4.10 data explains the result obtained from the simulation and their values compared with expected design specification of salient-pole synchronous generator for this model and physical geometry, in order to achieve optimum performance including cost, size and weight.

5.2. Recommendations

This research work has demonstrated capacity to utilize the two Finite Element software (FEMM and ANSYS Maxwell) together with mathematical proof of Two Reaction Theory to obtain Salient-Pole Synchronous Generator parameters that further determine the optimum operating performance of the generator. Nigeria needs stable energy supply; however, there is need for detailed application of the method for design and analysis of new and existing synchronous generators. This approach will further compliment more effort to acquire knowledge and skill for rotating machine design using the method.

This research used FEMM 4.0, ANSYS Maxwell and enhanced by AutoCAD to obtain the results from the initial geometrical configuration to execution stage of the work. Other coded software could be incorporated for more robust implementation of the methods.

The following are suggested areas of work which will enable users of the methods to fully utilize the potential of the software.

i. A realistic practical synchronous generator whose dimensions and other specifications available in power system engineering laboratory should be acquired for further research.

ii. Acquisition of knowledge and skill in electrical machine design will be needed to solve energy crisis in Nigeria.

iii. Computer software with coding can be implemented with finite element method to enhance wider range of electromagnetic devices design and complex machine dynamics executions.

iv. Other areas of synchronous machine dynamics and stability can also be explored based on this research work.

v. Finite element analysis alongside with Poisson equation has application in other field of engineering (Heat transfer, structures and bridge trusses, hydraulic penetration in porous aquifers). This research will greatly contribute to these areas of interdisciplinary research.

Application of high speed computer system with finite element methods will help reform the computational process needed to utilize the process more efficiently.

5.3 Contribution to knowledge

This research work has illustrated cases in many areas of interest, which in turn contributes to better understanding and application of Finite Element Method; and in fusion with Two Reaction Theory and electrical rotating machines design and modelling, especially

Salient-Pole Synchronous Generator considered in this research.

Major areas of importance to consider are:

i. Electromagnetic field mapping of electrical machine gives new area of numerical approach to machine design and modelling.

ii. Mathematical proof and illustration of Two-Reaction Theory expressed in the form of direct-axis and quadrature-axis magneto motive force (MMF) for Salient-Pole Synchronous Generator.

iii. Finite Element Method Magnetics and ANSYS Maxwell (RMxprt) application to electrical machine design, modelling and analysis. iv. The modified winding and inverse air gap function utilization give a simpler and direct computation of electrical machine inductances.

v. The application of Maxwell's equations demonstrates the usefulness of Ampere's, Gauss' and Faraday's law of electromagnetism in conjunction with second order partial differential equation for the analysis of magnetic behaviour of electrical machines and other electromagnetic devices. vi. The Salient-Pole Synchronous Generator physical geometry variation is essential for optimum performance evaluation.

REFERENCES

Adkins, B. and Harley R. G. (1975). *The General Theory of Alternating Current Machines, Application to Practical Problem*. London: Chapman and Hall.

Ahmed-Zaid, S., Mohammadi, D. and Oteafy, M. A. A. (2015). New Equivalent Circuit of a Salient-Pole Synchronous Machine and its Phasor Interpretation.

Ames, R. L. (1990). *A.C. Generators: Design and Application*. Great Britain: John Willy and Sons Inc.

Andreas, S., Johann, K. and Rudolf, K. (2014). Fractional Slot Winding versus Distributed Winding using Winding Function Method, *IEEE*,

Andri, S. and Agus, P. (2017). Damper Winding Analysis on Synchronous Generator 10625 kVA in Short Circuit Condition, *IEEE*.

Arrillaga, J. and Arnold, C. P. (1990). *Computer System Analysis of Power Systems*. Great Britain: John Wiley and Sons

Asogwa, J. C. and Obe, E. S. (2019). Steady State and Comparative Analysis of Single Phase AC Synchronous Motors. *The NIEEE Technical Transactions.* 1(1): 105 - 119

Bajpai, A. C., Mustoe, L. R. and Walker, D. (1979). *Advanced Engineering Mathematics*. Chichester: John Wiley & Sons

Bassi, C., Giulivo, D. and Tessarolo, A. (2010). Transient Finite-Element Analysis and Testing of a Salient-Pole Synchronous Generator with Different Damper Winding Design

Solution, *IEEE*

Bastos J. P. A. and Sadowski, N. (2003). *Electromagnetic Modeling by Finite Element Method*. New York: Marcel Dekker

Bhattacharayya, M. (2016). *Electrical Machines Modelling and Analysis*. India: PHI Learning Private Limited

Bianchi, N. (2005). *Electrical Machines Analysis Using Finite Elements*. Boca Raton Florida: Taylor & Francis Group

Blondel, A. (1913). Synchronous Motor and Converters – Part III. Translation by C. O. Mailloux, McGraw-Hill

Boldea, I. and Nasar, S.A. (1986). *Electric Machine Dynamics*. New York: Macmillan Publishing Company

Boldea, I. and Tutelea, L. (2010). Electric Machines Steady State, Transients, and Design with MATLAB. U.S.A.: CRC Press

Borisenko, A. I. and Tarapov, I. E. (1968). *Vector and Tensor Analysis with Applications*. U.S.A.: Dover Publication Inc.

Brauer, J. R. (1993). *What Every Engineers Should Know About Finite Element Analysis*, Second Edition, New York: Marcel Dekker, Inc.

Chalmers, B. and Williamson, A. (1991). *A.C. Machines, Electromagnetics and Design*. England: Research Studies Press Ltd

Chari, M. V. K. (1980). Finite Element Analysis of Electrical Machinery and Devices (Invited), *IEEE Transaction on Magnetics*, MAG-16, 1(5): 1014-1018

Cirstea, M. N., Dinu, A., Khor, J. G., and McCormick, M. (2002). *Neural and Fuzzy Logic Control of Drives and Power Systems*. Great Britain: Newnes

Claycom, J. R. (2009). *Applied Electromagnetics using QuickField and MATLAB*. U.S.A.: Jones and Bartlett Publishers

Deng F. and Demerdash, N. A. O. (1996). A Coupled Finite-Element State-Space Approach for Synchronous Generators. Part I: Model Development. *IEEE Transactions on Aerospace and Electronic Systems*. 32(2)

Deng F., Demerdash N. A. O, Vaidya, J. G. and Shah, M. J. (1996). A Coupled Finite-Element State-Space Approach for Synchronous Generators. Part II: Application. *IEEE Transactions on Aerospace and Electronic Systems*

Doherty, R. E. and Nickle, C. A. (1926). Abridgement of Synchronous Machines, Presented at the Annual Convention of the *A. I. E. E.*,

Domnisoru, C. and Musavi, M. (1999). Alternatives in Simulating Electrical Machine Dynamics, *Proceedings of the IEEE Canadian Conference on Electrical and Computer Engineering Shaw Conference Center*,

Doncker, R. D., Pulle, D. W. J. and Veltman, A. (2011*). Advanced Electrical Drives-Analysis, Modeling Control*. U.S.A.: Springer

Emile, M., Slim, T. and Gerard, C. (2008). Synchronous generator modelling and parameters estimation using least squares method, Simulation Modelling Practice and Theory 16,

Erdelyi, E. A., Ahamed, S. V. and Hopkins, R. E. (1965). Nonlinear Theory of Synchronous Machines On-Load, *IEEE Summer Power Meeting*, Detroit, Mich

Escarela-Perez, R., Campero-Littlewood, E., Arijona-Lopez, M. A. and Laureano-Cruces, A. (2005). Comparison of two techniques for two-dimensional finite-element inductance computation of electrical machines, *IEE Proc. Electr. Power Appl*,

Farlow, S. J. (1982). *Partial Differential Equations for Scientists and Engineers*. New York: Dover Publication Inc.

Ferrari, R., and Sylvester, P. (1996). *Finite Element for Electrical Engineers*, Third Edition, New York: Cambridge University Press

Filizadeh, S. (2013). *Electric Machine and Drives – Principle, Control, Modeling and Simulation*. U.S.A.: CRC Press Taylor & Francis Group

Fitzgerald A. E.., Kingsley C. and Umans, S. D. (1990). *Electric Machinery*, Fifth Edition, London: McGraw-Hill Book Company

Fleisch, D. (2008). *A Student's Guide to Maxwell's Equations*. U.S.A.: Cambridge University Press

Fleisch, D. (2012). *A Student's Guide to Vectors and Tensors*. U.S.A.: Cambridge University Press

Fleish, D. and Kinnaman, L. (2015). *A Student's Guide to Waves*. U.S.A.: Cambridge University Press

Gangadhar, K. A. and Ramanathan, P. M. (2015). *Electromagnetic Field Theory*. India: Khanna Publishers

Gao, J., Zhang, L. and Wang, X. (2009). *AC Machine Systems-Mathematical Model and Parameters, Analysis and System Performance*. Germany: Springer

Gerling, D. (2015). *Electrical Machines-Mathematical Fundamentals of Machine Topologies*.

China: Springer

Ghanim, Daw. (2012). Experimental Determination of Equivalent Circuit Parameters for a Laboratory Salient-Pole Synchronous Generator. A. Master Thesis. St. John's, Newfoundland, Canada.

Grainger, J. J., Steveson, W. D. (1994). *Power System Analysis*. Singapore: McGraw-Hill, Inc

Gray A. (1913). *Electrical Machines Design – The Design and Specification of Direct and Alternating Current Machinery*. First Edition, New York: McGraw Hill

Gupta, B. D. (1980). *Mathematical Physics*. India: Vikas Publishing House

Hameyer, K., and Belmans, R. (1999) *Numerical Modeling and Design of Electrical Machines and Devices.* Boston: WIT Press Southampton

Hancock, N. N. (1974). *Matrix Analysis of Electrical Machinery*, 2nd Edition. New York: Pergamon Press

Helmer, R., Duck, P., and Ponick, B. (2010). Determination of Transient Reactances of Salient Pole Synchronous Machines with Analytical and Numerical Methods.

International Symposium on Power Electronics, Electrical Drives, Automation and Motion. IEEE

James, M. L., Smith, G. M. and Wolford J. C. (1977). *Applied Numerical Methods for Digital Computation with Fortran and CSMP*, Second Edition, Harper & Row

Kamaker, H.C. (2000). Practical Design Applications of Time-Stepping Finite Element Analysis to Salient Pole Synchronous Machines, *IEEE*

Khalf, M. Amine, W. R. and Aguglia, D. (2012). Finite Approach for Performances Prediction of a Small Synchronous Generator Using ANSYS Software, *IEEE Canadian Conference on Electrical and Computer Engineering*

Kolondzovski (2004). Evaluation Methods for Calculating Synchronous Generator Reactances. *PhD Seminar Computation of Electromagnetic Fields.*

Kraus, J. D. and Fleisch, D. A. (1999). *Electromagnetics with Applications*, Fifth Edition. U.S.A.: MacGraw-Hill

Krause, P. C., Wasynczuk Oleg, O'Connell, Timothy C., Hasan Maher (2017). Tesla's Contribution to Electric Machine Analysis, *IEEE Transactions on Energy Conversion*

Krause, Paul C. (1985). The Method of Symmetrical Components Derived by Reference Frame Theory, *IEEE Transactions on Power Apparatus and System*,

Krawczyk, A. and Tegopoulos, J. A. (2004). *Numerical Modelling of Eddy Currents*. U.S.A.: Oxford University Press

Lawrenson, K. J. Binns and Trowbridge, C. W. (1994). The Analytical and Numerical Solution of Electric and Magnetic Fields, England: John Wiley and Sons

Lebsir, A., Larake, M., Djeghload, H. and Bentounsi, A. (2014). Modeling and Analysis of a Salient Poles Synchronous Machines Using Finite-Elements Method, IEEE

Li, J., Zhang, Z., Lu, J., and Chen, C. (2018). Analysis and Design of Damper Winding of Salient-Pole Synchronous Generator for Negative-Sequence Reactance Reduction. *21st International Conference on Electrical Machines and Systems (ICEMS).* Jeju, Korea

Lin, D, Zhou, P., He, B. and Lambert, N. (2012). Steady-State and Transient Parameters Computation for Wound Field Synchronous Machine, *IEEE*

Lipo, T. A. (2012). Analysis of Synchronous Machines, Second Edition, U.S.A.: CRC Press

Lipo, T. A. (2017). Introduction to AC Machine Design. U.S.A.: *IEEE* Press Wiley

Lonngren, K. E., Savov, S. V. and Jost, R. J. (2007). *Fundamentals of Electromagnetic with MATLAB*, Second Edition, Canada: Scitech Publishing Inc

Lublin, T., Tahar, H. Hubert, R. and Abderrezak, R. (2007). Comparison Between FiniteElement Analysis and Winding Function Theory for Inductances and Torque

Calculation of a Synchronous Reluctance Machine, *IEEE Transactions on Magnetics*

Manassah, J. T. (2007). *Elementary Mathematical and Computational Tools for Electrical and Computer Engineers using MATLAB*, Second Edition. U.S.A: Taylor and Francis

Manning, C. D. and Abdel-Halim, M. A. (1990). Direct Phase modelling of synchronous generators, *IEEE Proceedings*,

Matsuki, T. Okada and C. and Uenosono, J. (1992). Loss of Synchronous Process of A Synchronous Generator Described By Its Internal Flux and Force Distributions, *IEEE*

Transaction on Energy, Kyoto,Japan Conversion. 7(1): 177-182

McPherson, George. (1981). *An Introduction To Electrical Machines and Transformers*. New York: John Willey and Sons

Meeker, D. (2004). Finite Element Method Magnetics Version 4.0 User's Manual

Mesnajevs, A. and Zviedris, A. (2011). Mathematical Simulation of The Magnetic Field Occurred By Armature Reaction of The Synchronous Machine, *Proceedings 24th European Conference on Modeling and Simulation IEEE*

Mittle, V. N. and Mittal, A. (2017). *Design of Electrical Machines*. Delhi: Standard Publishers Distributors.

Mohammad, J. Tole, S., Nik, I. N. R. and Abdul, A. M. J. (2015). Modeling of Balanced and Unbalanced Three-Phase Induction Motor under Balanced an Unbalanced Supply Based on winding function method, *International Journal of Electrical and Computer*

Engineering,

Mohan, N. (2001). *Advanced Electrical Drives*. U.S.A.: MNPERE,

Mohan, N. (2012). *Electric Machines and Drives*. U.S.A.: John Wiley and Sons Inc

Momoh, J. A. (2009). *Electric Power System Applications of Optimization*, Second Edition. U.S.A: CRC Press

Momoh, J. A. and El-Hawary, M. E. (2000). *Electric Systems, Dynamics, and Stability with Artificial Intelligence Applications*. U.S.A.: Marcel Dekker Inc.

Nabeta, S. I. (1995). A Non-Linear Time-Stepped Finite Element Simulation of Symmetrical Short-Circuit in a Synchronous Machine, *IEEE*

Nabeta, S. I., Dietrich A. B., and Rocco, A. (1999). Harmonic Analysis of a Synchronous Machine Feeding a Non-Linear Load vy a Time-Stepping Finite Element Simulation, *IEEE*

Nagrath, I. J. and Gopal, M. (1982). *Control Systems Engineering*, Second Edition. India: Wiley Eastern Limited

Nagrath, I. J. and Kothari, D. P. (1990). *Modern Power System Analysis*, Second Edition, India: Tata McGraw-Hill Publishing Company Limited

Needham, T. (1998). *Visual Complex Analysis.* United Kingdom: Oxford University Press

Nonaka, S., Kesamaru, K., and Horita, K. (1994). Analysis of Brushless Four-Pole Three-Phase Synchronous Generator Without Exciter by the Finite Element Method, *IEEE*

Transaction on Industry Application. 30(3): 615-620

Novotny, D. W. and Lipo, T. A. (1996). *Vector Control and Dynamics of AC Drives*. London: Oxford University Press

Okon, P. E. (2008). Two Dimensional Electromagnetic Field Mapping of a Salient Four Pole

Synchronous Machine, MEng. Thesis. Federal University of Technology, Owerri

Okon, P. E., Okoro, C. C., and Okafor, E. N. C. (2009). Magnetic Field Mapping of a Direct Current Electrical Machine Using Finite Element Method. *Proceedings of the 3rd International Conference on Power Systems and Telecommunications,*

Okoro, O. I. and Chikuni, E. (2010). The Essential Matlab and Simulink for Engineers and Scientists, U.S.A: Juta and Company ltd

Onah, C. O. and Reuben, J. (2016). Dynamic Modelling and Simulation of Salient Pole Synchronous Motor Using Embedded MATLAB. *American Journal of Engineering Research (AJER).* 5(12): 318 - 325

Ong, C. (1998). Dynamic Simulation of Electric Machinery using MATLAB/SIMULINK. U.S.A.: Prentice Hall Inc.

Onur, M., Raziee, S. M, and Bernd, P. (2016). Determination of the Inductances of Salient Pole Synchronous Machines Based on Voltage Equation of a Single Coil in the Stator Winding, *IEEE Transaction on Industry Application*

Onwuka, I. K. and Uma, U. U. (2015). Determination of the winding inductances of a Twophase Machine, *International Organization of Scientific Research Journal of Engineering*

Onwuka, I. K., Uma, U. U. and Diyoke, G. C. (2015). Analysis of A 2-Phase Stator Winding by Winding Function Methodology, *International Organization of Scientific Research Journal of Engineering*

Pao, Y. C. (1999). *Engineering Analysis – Interactive Methods and Programs with FORTRAN, QuickBasic, MATLAB and Mathematica*. U.S.A.: CRC Press LLC

Park, R. H. (1929). Two-Reaction Theory of Synchronous Machine – Generalized Method of

Analysis – Part 1. *AIEE Transactions.* 48 (3): 716 - 727

Perry, M. P. (1985). *Low Frequency Electromagnetic Design*. U.S.A: Marcel Dekker Inc.

Prasad, R. (2015). *Electrical Machines*. India: PHI Learning Private Limited

Prentice, B. R. (1937). Synchronous Machine Reactance. *AIEE Transaction*

Ratnajeevan, S. and Hoole, H. (1989). Computer Aided Analysis and Design of Electromagnetic devices, New York: *Elsevier*

Reece, A. B. J., and Preston, T. W. (2000). *Finite Element Methods in Electrical Power Engineering*. London: Oxford University Press

Rene, W., Innocent, K. and Mama, C. (2003). Line-to-Line Short-Circuit-Based Finite-Element Performance and ParameterPredictions of Large Hydrogenerators, *IEEE Transaction on Energy Conversion,*

Rui, L. Dengjun, Y. and Wei, L. (2007) Computational Technology of Finite Formulation Method on Electromagnetic Field in Electrical Machines, *Proceeding of International Conference on Electrical Machines and Systems*

Saadat, H. (2004). *Power System Analysis*. Second Edition. Singapore: McGraw Hill

Sadiku, M. N. O. (1989). A simple Introduction to Finite Element Analysis of Electromagnetic Problems, page 85, *IEEE Transaction on Education*, 32 (2)

Sadiku, M. N. O. (2009). *Monte Carlo Methods for Electromagnetics*. U.S.A.: CRC Press

Salon S. J. and Chari (2000). *Numerical Methods in Electromagnetism*, Academic Press, San Diego

Salon, S. J. (1995). *Finite Element Analysis of Electrical Machines*. U.S.A.: Kluwer Academic Publishers

Schey, H. M. (2005). *Div Grad Curl and all That*. Fourth Edition, U.S.A.: W. W. Norton & Company

Schwartz, M. (1972). *Principles of Electrodynamics*. U.S.A.: Dover Publications Inc.

Shaheena, K. Ratnakar, K. L, Ramesh, K. N. and Ravi, R. (2014). Evaluation of Reactances and Time Constants of Synchronous Generator, *International Journal of Research in Engineering and Technology,*

Sheng, C. L. (1948). The Two-Reaction Theory of Salient-Pole. Synchronous Machines, *Ph.D. Thesis*, University of Edinburgh

Silvester, P. P. and Pelosi, G. (1994). Finite Elements for Wave Electromagnetics-Methods and Techniques, U.S.A.: IEEE Press

Skilling, H. H. (1948). *Fundamentals of Electric Waves*, Second Edition, New York: John Wiley

Smith, J. R. (1990). *Response Analysis of A.C. Electrical Machines: Computer Models and Simulations*. Great Britain: John Wiley and Sons Inc.

Spiegel, M. R. (1974). *Theory and Problems of Vector Analysis*. Singapore: McGraw-Hill Book Company

Stevenson, W. D. (1982). *Element of Power System Analysis*, Fourth Edition. Singapore: McGraw-Hill International Edition

Subhasis, N. and Thirumarai, I. C. (2013). Identification of Spectral Components in the line current of eccentric salient pole machines using a binomial series-based inverse air-gap function, *IET Electr. Power Appl*.,

Subramaniam, P., Malik, O. P. (1971) Digital simulation of a synchronous generator in directphase quantities, *Proc. IEE*

Subramanian, J. (2012). Estimating the Magnetic Characteristics of a Salient Pole Synchronous Machine Using Ampere Turns Distribution Method. *A Master Thesis*. University of Victoria

Tandon, S. C., Richter, E. and Chari, M. V. K. (1980). Finite Elements and Electrical Machine Design, *IEEE Transaction on Magnetics*, 1020-1022

Tang, K. Y. (1956). Two-Axis Method of Analyzing Electric Machines. *AIEE Rotating Machinery.*

Tessarolo, A., Bassi, C., and Giulivo (2011). Time-Stepping Finite-Element Analysis of a 14MVA Salient-Pole Shipboard Alternator for Different Damper Winding Design

Solutions, *IEEE Transaction on Industrial Electronics*

Tolstov, G. P., (2015). *Fourier Series*. New York: Dover Publication, INC.

Ulaby, F. T. (2003). *Fundamentals of Applied Electromagnetics*. Prentice Hall,

Upadhyay, K. G. (2013). *Design of Electrical Machines. India*: New Age International Publishers

Vince, J. (2005). *Geometry for Computer Graphics, Formulae, Examples and Proofs*. United Kingdom: Springer

Vince, J. (2007). *Vector Analysis for Computer Graphics*. United Kingdom: Spinger

Vukosavic, S. N. (2013). *Electrical Machines*. U.S.A.: Springer

Wait, J. R. (1985). *Electromagnetic Wave Theory*. Harper and Row Publishers

Wang, R and Demerdash, N. A. (1991). A combined Vector Potential-Scalar Potential Method for FE Computation of 3D Magnetic Fields in Electrical Devices with Iron Cores, *IEEE Transaction on Magnetic*, New York. 27 (5): 3971-3977

Williamson, S., and Voschenk, A. F. (1995). Time-Stepping Finite Element Analysis for a Synchronous Generator Feeding a Rectifier Load, *IEE Proceeding Electrical Power Application*

Wood, A. J. and Wollenberg, B. F. (1996). *Power Operation Generation Operation and*

Control, Second Edition. U.S.A.: John Willey and Sons Inc.

Yamamura, S. (1992). *Spiral Vector Theory of AC Circuit and Machines*. Great Britain: Oxford University Press

Yang, X., Libing, Z., Jin, W. and Rui, Y. (2017). Finite Element Computation of Transient Parameters of a Salient-Pole Synchronous Machine. *Energies,* 10, 1015

Zhe, L. Deliang, L. and Shaofeng, J. (2018). Inductance Calculation for the Symmetrical Nonalient Dual Three-phase PMSM Based on Windong Function Approach, *21st International Conference on Electrical Machines and Systems*

Zlatko, K., Z. and Petkovska, L. (2005). Determination of a Synchronous Generator Characteristics via Finite Element Analysis, *Serbian Journal of Electrical Engineering* 2(2): 157 – 162

Appendix A: Mathematical Proof: Two-Reaction Theory of Salient – Pole Salient Synchronous Generator

---

The mathematical proof illustrated using figure A1 is to clarify Andrew Blondel concept of Two-Reaction Theory of armature magneto-motive force with the components of direct and quadrature axis impinged on the rotor. The proof is concluded with graphical illustrations in figure 4.9 (a) to figure 4.9 (f). Assume phase 'A' of the armature is excited in figure A1 (a) and figure A2 (b) showing the actual four poles used for this work, while for this mathematical proof, the two-pole generator is used for simplicity. The air gap along direct axis is referred to as (d-axis) and 90° electrical degree from direct axis is referred to as quadrature axis. The total magnetic flux density along the air gap will be the summation of the magnetic flux of the direct and quadrature axis. This can be illustrated analytically and presented by equations described below:

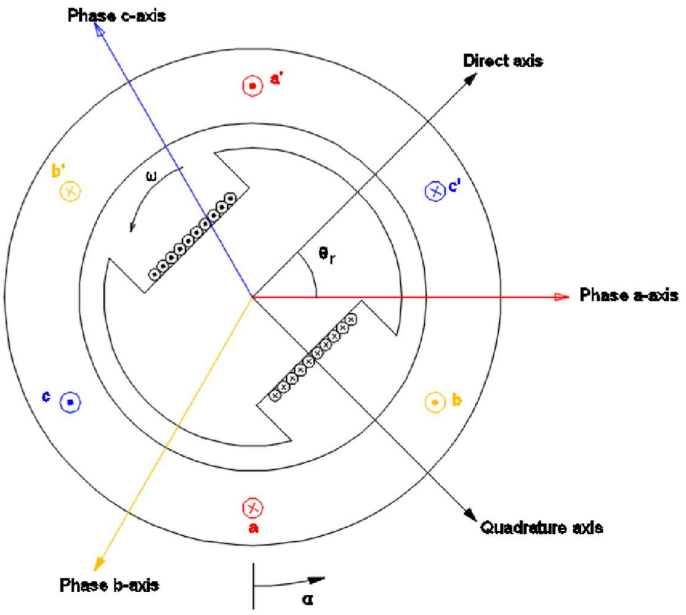

Figure A1: Two-Pole Salient Type Synchronous Generator with Phase Current, d-axis and q-axis

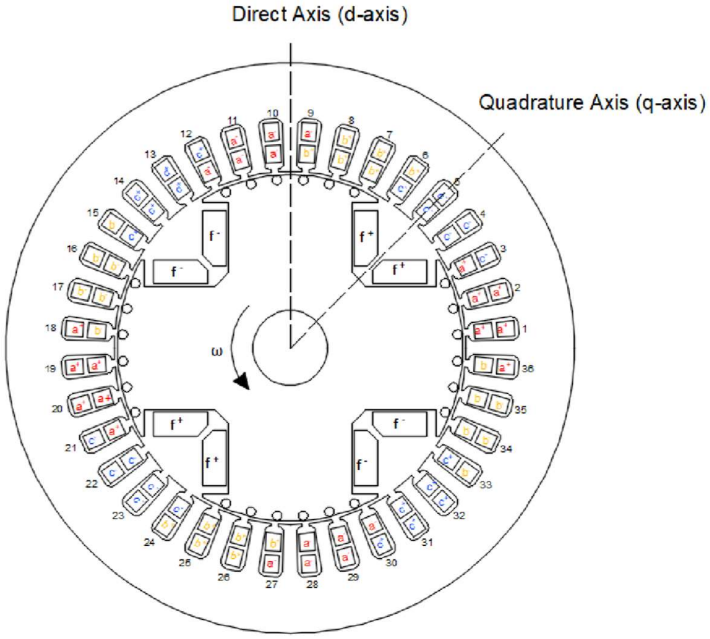

Figure A2: Four-Pole Salient Type Synchronous Generator with Phase Current, d-axis and q-axis presentation

The two orthogonal axis (**d-q**) system of figure A1 is rotating, starting from a point α = 0° around the air gap. Maximum magneto-motive (MMF) occurs at $\alpha_l = 90°$ along phase 'a' axis, while the rotor is also at rotor angle of $\theta_r = 0^\circ$

Direct Axis: MMF (F) component along the direct axis of the rotor $F_d = \mathbf{F}_a \cos \theta_r$

Quadrature Axis: MMF (F) component along the quadrature axis of the rotor $F_q = \mathbf{F}_a \sin \theta_r$

The stator magneto-motive force generated by the armature winding of phase 'a' is represented by a sine waveform ($\mathbf{F}_a \sin \alpha$).

Also, the rotor positions around the machine's circumference determine the MMF distribution around the air gap. The fundamental component of MMF of the stator phase 'a'

MMF will produce air gap magneto-motive force that is a summation of the direct and quadrature axis components. This can be analytically expressed by equations below:

Rotor direct axis component of MMF reference to $\alpha = 0°$ is expressed as $\alpha 1 = \left(\frac{\pi}{2} + \theta_r\right)^{\circ}$

$$F_d(\alpha 1) = -F_d(\theta_r)\cos\left[\alpha + \left(\frac{\pi}{2} + \theta_r\right)\right] \quad \text{A.1}$$

Using trigonometric identity (Vince, J., 2005) below and applying to equation 1

$$\mathbf{cos(A + B) = cos\ A\ cos\ B - sin\ A\ sin\ B} \quad \text{A.2}$$

$$\mathbf{sin(A - B) = sin\ A\ cos\ B - cos\ A\ sin\ B} \quad \text{A.3}$$

Equation A.1 becomes:

$$F_d(\alpha 1) = -F_d(\theta_r)\left[\cos\alpha\cos\left(\frac{\pi}{2} + \theta_r\right) - \sin\alpha\sin\left(\frac{\pi}{2} + \theta_r\right)\right] \quad \text{A.4}$$

$F_d(\theta_r) = \mathbf{F}_a\cos\theta_r$; $F_q(\theta_r) = \mathbf{F}_a\sin\theta_r$;

$$\cos\left(\frac{\pi}{2} + \theta_r\right) = -\sin\theta_r\ ;\ \sin\left(\frac{\pi}{2} + \theta_r\right) = \cos\theta_r$$

Applying the following identity above into equation A.2 makes equation A.3 into equation A.5 and A.6

$$F_d(\alpha 1) = \mathbf{F}_a\cos\theta_r\sin(\alpha + \theta_r) \quad \text{A.5}$$

Likewise, the quadrature axis of the rotor position in reference to $\alpha = 0°$ is expressed as $\alpha 2 = \theta_r^{\circ}$ can also be expressed as

$$F_q(\alpha 2) = -F_q(\alpha 2)\cos(\alpha + \theta_r)$$

or

$$F_q(\theta_r) = -F_q(\theta_r)\cos(\alpha + \theta_r) \quad \text{A.6}$$

Substituting $F_q(\theta_r) = \mathbf{F}_a\sin\theta_r$ into equation 4.6, and it becomes

$$F_q(\theta_r) = -\mathbf{F}_a\cos(\alpha + \theta_r)\sin\theta_r \quad \text{A.7}$$

Therefore, the total armature MMF ($\mathbf{F}_a$) around the generator air gap equals the summation of the direct axis and quadrature axis MMF.

Total MMF ($\mathbf{F}_a$) $= F_d(\alpha 1) + F_q(\alpha 2)$.

This becomes

Total armature MMF $(\mathbf{F}_a) = \mathbf{F}_a \cos\theta_r \sin(\alpha + \theta_r) - \mathbf{F}_a \sin\theta_r \cos(\alpha + \theta_r)$ A.8

Rearranging equation A.8 results in equation A.9

$\mathbf{F}_a[\sin(\alpha + \theta_r)\cos\theta_r - \cos(\alpha + \theta_r)\sin\theta_r]$ A.9

Applying trigonometric identity of equation A.3 into equation A.9 makes total MMF ($\mathbf{F}_a$) to be expressed as

$\mathbf{F}_a[\sin(\alpha + \theta_r - \theta_r)]$ A.10

The total magneto-motive force (MMF) around the generator air-gap becomes

MMF $(\mathbf{F}) = \mathbf{F}_a \mathbf{\sin \alpha}$

Through the above mathematical proof of using armature MMF projection into the two orthogonal (**d** and **q**) axis of the rotor, the armature MMF wave is generated by phase 'a' current into the air gap of the generator.

Appendix B: Computation and Plotting of Generator Power/Angle Curve from ANSYS Maxwell Result and Simulated Parameters

The parameters obtained from Table 4.1 as displayed below, are used for computational verification of Generator Power Angle Curve as obtained from ANSYS Maxwell

$X_d = 7.3\Omega$

$Xq = 4.11\Omega$

$X_d pu = 0.91154pu$

$X_q pu = 0.514203pu$

Power factor angle (θ^o) = 32.14°

Phase voltage (V) = 231Volts

Line-Line Voltage (E) = 400Volts

Phase current (I_a) = 28.86A

Phase Voltage (V)pu = 1pu

Line-Line Voltage (E)pu = 1.73pu

Figure 4.11(a) and figure 4.11(b) power angle curve were plotted from power-angle equation derived from ANSYS Maxwell result. From the ANSYS Maxwell result and the data inserted into equation B.1, the computation of the resultant power is obtained as follows:

$Pe(kW) = 1.90\sin\delta + 0.424\sin 2\delta$

B.1

From the data, $\delta = 18.54^o$

Therefore

Non-Saliency Power = $1.90\sin\delta$ pu = 0.603pu

Reluctance Power = $0.424\sin 2\delta$ = 0.256pu

Resultant Power Due to Saliency = (0.603 + 0.256)pu = 0.8595pu

Converting to real power in kilowatts

Pe(kW) = 0.8595 x 20,000 = 17.19kW

From figure 4.12 (a) the curve shows more power is delivered with minimum power angle for Salient-pole compared to the Cylindrical rotor generator.

Appendix C: Open and Short Circuit Characteristics

The open and short circuit characteristics of Salient-Pole Synchronous Generator plot in figure C1 is also used to obtain the Short Circuit Ratio (SCR) and the value compared with the result in table 4.1.

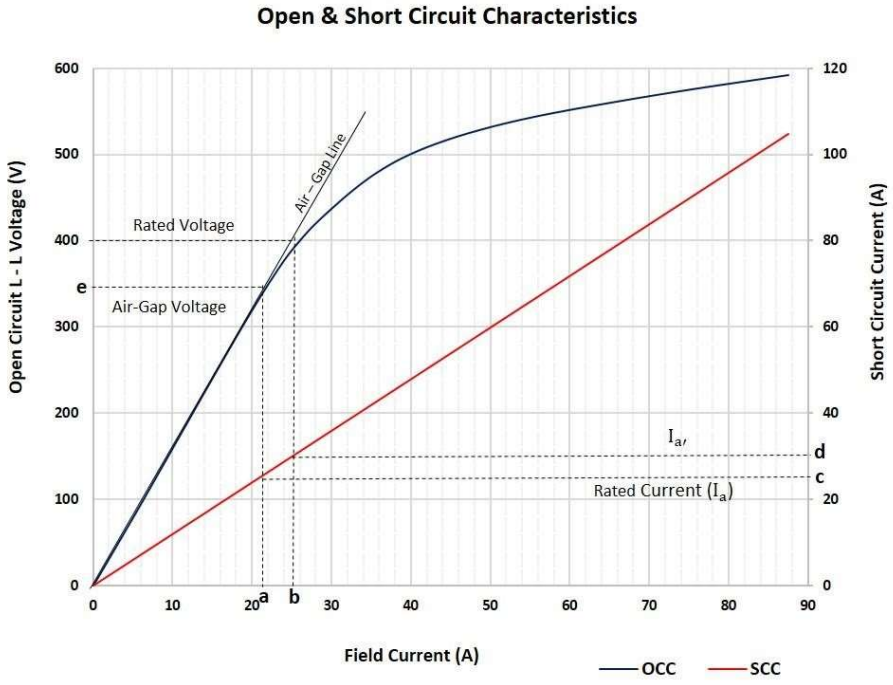

Figure C1: Open and Short Circuit Characteristic of the Salient-Pole Synchronous Generator

Legend a = 21.72 Amps **b** = 25.99 Volts **c** = 26 Amps **d** = 28.86 Amps **e** = 350 Amps The graph shown in figure C1 shows open and short circuit characteristic of the salientpole synchronous generator simulated in this work. The graph was plotted from the data result obtained from the simulation. The graph is essential because of the key performance indicator short circuit ratio (SCR) which is one of the data obtained during simulation and will be computed as below:

Excitation current for rated open circuit voltage = 25.99Amp

Excitation current for rated short circuit current = 21.72Amp

Therefore,

Short circuit ratio (SCR) = $\frac{25.99}{21.72}$ = 1.1965

This value is compared with standard range value of salient-pole generator, which is between 0.9 to 1.3, and it is observed to fall within the acceptable range.

Appendix D: Winding Function Method Result Data: Computation of Direct and Quadrature Axis Reactances

---

The reactances developed in the salient-pole synchronous generator are due to the permeances offered by the gap along the direct and quadrature axis respectively. The self-reactance for the generator phases are expressed as

$$X_{aa} = X_l + X_1 + X_2 \cos 2\theta_r$$

$$X_{bb} = X_l + X_1 + X_2 \cos 2(\theta_r - 120°) \quad \text{D.1}$$

$$X_{cc} = X_l + X_1 + X_2 \cos 2(\theta_r + 120°)$$

Likewise, inductance for phase 'a', 'b' and 'c' become

$$L_{aa} = L_l + L_1 + L_2 \cos 2\theta_r$$

$$L_{bb} = L_l + L_1 + L_2 \cos 2(\theta_r - 120°) \quad \text{D.2}$$

$$L_{cc} = L_l + L_1 + L_2 \cos 2(\theta_r + 120°)$$

The Two-Axis Reactance for Direct and Quadrature Axis are also expressed as

$$\text{D-Axis Reactance } (X_d) = X_l + \frac{3}{2}(X_1 + X_2) \quad \text{D.3}$$

$$\text{Q-Axis inductance } (X_q) = X_l + \frac{3}{2}(X_1 - X_2) \quad \text{D.4}$$

In order to compute the X_1 and X_2 values the value of X_{ad} and X_{aq} given in table 4.1 of ANSYS Maxwell result will be used.

To solve for the value of X_1 and X_2 and neglecting X_l the computation is done with equation

$$X_{ad} = \frac{3}{2}(X_1 + X_2)\ \Omega \quad \text{D.5}$$

$$X_{aq} = \frac{3}{2}(X_1 - X_2)\ \Omega \quad \text{D.6}$$

Direct and Quadrature – axis derived from Winding Function Method for phase 'a' inductance in equation D.2

$L_{aa} = 9.67 + 3.5 \cos 2(\varphi - \theta_r)\text{mH}$ D.7 Thus
$L_1 = 9.67\text{mH}$, $L_2 = 3.50\text{mH}$

$X_1 = 2\pi f L_1 = 3.04\ \Omega$ D.8

$X_2 = 2\pi f L_2 = 1.10\ \Omega$ D.9

From equation D.5 and D.6, X_{ad} and X_{aq} become

$X_{ad} = 6.21\ \Omega$

$X_{aq} = 2.91\ \Omega$

Appendix E: MATLAB Coding for Salient Pole Synchronous Generator – FEMM

Control

```
% Script to Compute the Rotational Characteristics of a 36pole,
4-slots
% electric machine using FEMM/MATLAB
% VERSION: 2 OF 2
close all; clear;
clc
tic % Timing (for code optimization)
addpath('c:\\ femm42\\mfiles'); savepath;
openfemm;
dAlfa = 15; % Degrees of rotor rotation

opendocument('C:\\Users\\user\\Documents\\Clients\\Engr.
paul\\24th October, 2020\\24Oct ArmatureEx Electric Mch
36s4pol siml.FEM');
  mi_saveas('C:\\Users\\user\\Documents\\Clients\\Engr.
paul\\24th October, 2020\\24Oct ArmatureEx TEMPf.fem');
mi_seteditmode('group'); main_maximize; mi_zoomnatural;

% Set figure window in MATLAB
% scrsz = get(0,'ScreenSize');

% Programming for dynamic data gathering begins from here!
```

```
for n = 1:360/dAlfa+1
%     figure('Position',[1 1 1360 676]) % [1366,768]

    mi_analyze(1);
mi_loadsolution();

%     FEMM Magnetics Post-Processor

mo_showdensityplot(0,0,0.390096938358205,6.59221912931063e-
006,'mag');
mo_maximize;
mo_zoomnatural;

        alfa = dAlfa*(n);
    disp(['Current angle is:    ' num2str(alfa) 'degrees'])     %
Control rotation angle    if alfa == 180        break    else
   % Picture Saving     mpx =
strcat('C:\Users\user\Documents\Clients\Engr. paul\24th
Sept2020\Elec 36s 4p mac REx ',num2str(n),'-
',num2str(alfa),'degrees', '.bmp');
mo_savebitmap(mpx);



    % Point Selection for plotting B.n and H.n
mo_selectpoint(3956.0943,1169.1461);
mo_selectpoint(3771.0474,1169.1461);

    mo_addcontour(3956.0943,1169.1461);
mo_bendcontour(180,2)

% %     Create text document     txto1 =
strcat('C:\\Users\\Kuby\\Documents\\Clients\\Engr.
Paul\\Project\\Mar 2019\\Electr 36p4s Bn', num2str(n),'-
',num2str(alfa), 'radians', '.txt');
%
%     % Create text document 2     txto2 =
strcat('C:\\Users\\Kuby\\Documents\\Clients\\Engr.
Paul\\Project\\Mar 2019\\Electr 36p4s Hn', num2str(n),'-
',num2str(alfa), 'radians', '.txt');



%     Plot data from Post-Processor to text file
mo_makeplot(2,2000,txto1,0);  % 2 denotes PlotType; in this
case, B.n
    mo_makeplot(5,2000,txto2,0);  % 5 denotes PlotType; in this
case, H.n
```

```
%     Make plot visible ///Temporarily Disabled///
mo_makeplot(2,2000)     mo_makeplot(5,2000)


     % Next iteration begins here!

    mi_selectgroup(5);

    mi_moverotate(2381.6646,1160.7471,dAlfa);
end end
toc % Timing (for code optimization)
```

Appendix F: MATLAB Coding for Round Rotor Synchronous Generator – FEMM Control

---

```
% Script to Compute the Rotational Characteristics of a 36pole,
4-slots
% Original data was obtained from ANSYS Maxwell design the
further
% processed in AutoCAD and exported to FEMM for Finite Element
Analysis
% electric machine using FEMM/MATLAB
% VERSION: 3 OF 3
close all; clear;
clc
tic % Timing (for code optimization)
addpath('c:\\femm42\\mfiles'); savepath;
openfemm;
dAlfa = 30; % Degrees of rotor rotation

opendocument('C:\Users\user\Documents\Clients\Engr. Paul\14th
October 2021\Round rotor machine_m3.FEM');

mi_saveas('C:\Users\user\Documents\Clients\Engr. Paul\14th
October 2021\Round rotor machine_m3.fem');
mi_seteditmode('group'); main_maximize;
mi_zoomnatural;

% Set figure window in MATLAB scrsz
= get(0,'ScreenSize');
```

```
% Programming for dynamic data gathering begins from here!

F = zeros(2,1); Salfa
= zeros(0,8); mfe =
zeros(0,8); Lfemm =
zeros(0,8);

for n = 1:360/dAlfa+1
%     figure('Position',[1 1 1360 676]) % [1366,768]

    mi_analyze(1);
mi_loadsolution();

%     FEMM Magnetics Post-Processor
%
mo_showdensityplot(0,0,0.00336059500239086,1.39445630041919e-
007,'mag');
mo_maximize;
mo_zoomnatural;

    alfa = dAlfa*(n);
disp(alfa)

   % Picture Saving     mpx =
strcat('C:\Users\user\Documents\Clients\Engr.
Paul\15th December 2021\Bn plots ',num2str(n),'-
',num2str(alfa),'degrees', '.bmp');
mo_savebitmap(mpx);


    % Point Selection for plotting B.n and H.n
mo_selectpoint(93.1375,0)     mo_selectpoint(-93.1375,0)

    mo_addcontour(93.1375,0)
mo_bendcontour(180,2)

%     Create text document     txto1 =
strcat('C:\Users\user\Documents\Clients\Engr.
Paul\15th December 2021\Bn plots ', num2str(n),'-
',num2str(alfa), 'radians', '.txt');

    % Create text document 2
%     txto2 = strcat('C:\Users\user\Documents\Clients\Engr.
paul\20 Mar 2020\PR_Im_36s4p\ANSYS_AD_FM Hn', num2str(n),'-
',num2str(alfa), 'radians', '.txt');
```

```
%     Plot data from Post-Processor to text file
mo_makeplot(2,2000,txto1,0);  % 2 denotes PlotType; in this
case, B.n
%     mo_makeplot(5,2000,txto2,0);  % 5 denotes PlotType; in this
case, H.n

%     Make plot visible ///Temporarily Disabled///
%     mo_makeplot(2,2000)
%     mo_makeplot(5,2000)


  %% Text File Reading to MATLAB for Post-Processing

% Plot Processing for B.n  fileID
= fopen(txto1);
C_hed = textscan(fileID,'%f %f','HeaderLines',2);
Length_mm = C_hed{1,1};
Bn_Tesla = C_hed{1,2};

Deg = (720.*Length_mm)./581.157;
plot(Deg,Bn_Tesla,'b'),xlabel('Rotor Angle, \theta
(radians)'),ylabel('Normal Flux Density (B), Tesla')
set(gca,'xtick',0:90:720,'xticklabel',0:90:720) hold
on; plot(Deg,0,'k'); axis tight
  fig_out =
strcat('C:\\Users\\user\\Documents\\Clients\\Engr.
Paul\\15th December 2021\\Bn plots\\ Bn', num2str(n),'-
',num2str(alfa), 'degrees', '.bmp');
saveas(gcf,fig_out) hold off

%
% % Plot Processing for H.n fileID
= fopen(txto2);
C_hed = textscan(fileID,'%f %f','HeaderLines',2);
Length_mm = C_hed{1,1};
Hn_Ampm = C_hed{1,2};

Deg = (720.*Length_mm)./581.157;

plot(Deg,Hn_Ampm,'r'),xlabel('Rotor Angle, \theta
(radians)'),ylabel('Normal Field Intensity (H), A/m')
set(gca,'xtick',0:90:720,'xticklabel',0:90:720) hold
on; plot(Deg,0,'k'); axis tight
  fig_out =
strcat('C:\\Users\\Kuby\\Documents\\Clients\\Engr.
Paul\\Project\\Mar 2019\\Electr 36p4s Hn', num2str(n),'-
```

```
',num2str(alfa), 'degrees', '.bmp');
saveas(gcf,fig_out) hold off   close
all

%=============================================================

    % Close Magnetics Post-Processor Window %%
Area selection and manipulation
mo_clearcontour

   CP = mo_getcircuitproperties('b+'); % Extract circuit
properties of phase b+
    mo_groupselectblock(10) % selection of areas to compute block
integral



    % Computation of Inductance
    mfe(n) = mo_blockintegral(2); % Magnetic field energy, W
Lfemm(n) = 2*mfe(n)/(CP(1)^2);
    fprintf('Rotor Angle: %d degrees \n', alfa-dAlfa)
disp(['The Inductance is: ' num2str(Lfemm(n)) ' Henries'])

    mo_clearblock

mo_close()

    Salfa(n) = alfa - dAlfa;
    Salfa(1) = 0;

     % Next iteration begins here!

    mi_selectgroup(5);

    mi_moverotate(0,0,dAlfa);

end
% %% Additional plots

figure(1)
plot(Salfa,Lfemm), xlabel('Angle, \alpha'), ylabel('Inductance,
H')

Ld = Lfemm(46); %Inductance @ 45 degrees
Lq = Lfemm(1); % Inductance @ 0 degrees
Ls = (Ld + Lq)/2 + (Ld - Lq)/2*cosd(2*Salfa);

figure(2)
```

```
plot(Salfa,Ls),xlabel('Angle, \alpha'), ylabel('Ls')

%% Write Data to a file
Hd = {'Angle', 'Inductance in FEMM, A.J', 'Calculated
Inductance, Ls'};
A = [Salfa;Lfemm;Ls]';
  xlswrite('C:\Users\Kuby\Documents\Clients\Engr.
Paul\Project\Mar 2019\Electr\Data Points.xlsx',Hd,'A1:C1')
xlswrite('C:\Users\Kuby\Documents\Clients\Engr.
Paul\Project\Mar 2019\Electr\Data Points.xlsx',A,'A2:C74')

toc % Timing (for code optimization)
```

Appendix G: MATLAB Coding of Fourier Analysis on Phase A, B & C Winding Functions

---

```
clear;clc;
%Determination of the Harmonic components of the winding
function.
%The Fourier Series expansion of the function is employed.
%The trapz MATLAB command is used here for integration.

N = [-1.5 -1 0 1 1.5];

h=(pi/12)/10;
% For the intervals in the a-phase function
x1 = 0:h:1.88;    x6 = 6.08:h:6.28; x2 =
1.88:h:2.28; x7 = 5.74:h:6.08; x3 =
2.28:h:2.62; x8 = 5.38:h:5.74; x4 =
2.62:h:2.98; x9 = 5.06:h:5.38; x5 =
2.98:h:5.06;
  k=0;
for n=1:2:99   % Only Odd harmonics are present
k=k+1;
f1a=N(1)*cos(n*x1);f6a=N(1)*cos(n*x6);
f2a=N(2)*cos(n*x2);f7a=N(2)*cos(n*x7);
f3a=N(3)*cos(n*x3);f8a=N(3)*cos(n*x8);
f4a=N(4)*cos(n*x4);f9a=N(4)*cos(n*x9); f5a=N(5)*cos(n*x5);
```

```
f1b=N(1)*sin(n*x1);f6b=N(1)*sin(n*x6);
f2b=N(2)*sin(n*x2);f7b=N(2)*sin(n*x7);
f3b=N(3)*sin(n*x3);f8b=N(3)*sin(n*x8);
f4b=N(4)*sin(n*x4);f9b=N(4)*sin(n*x9); f5b=N(5)*sin(n*x5);


% For the Fourier a-coefficeints of a-phase
a1=trapz(x1,f1a);a6=trapz(x6,f6a);
a2=trapz(x2,f2a);a7=trapz(x7,f7a);
a3=trapz(x3,f3a);a8=trapz(x8,f8a);
a4=trapz(x4,f4a);a9=trapz(x9,f9a); a5=trapz(x5,f5a);
an=(1/pi)*(a1+a6+a2+a7+a3+a8+a4+a9+a5);

%For the Fourier b-coefficients of a-phase
b1=trapz(x1,f1b);b6=trapz(x6,f6b);
b2=trapz(x2,f2b);b7=trapz(x7,f7b);
b3=trapz(x3,f3b);b8=trapz(x8,f8b);
b4=trapz(x4,f4b);b9=trapz(x9,f9b); b5=trapz(x5,f5b);
bn=(1/pi)*(b1+b6+b2+b7+b3+b8+b4+b9+b5);

c=sqrt((an^2)+(bn^2)); ph=atan2(bn,an);
cn(k)=c;         % Each harmonic magnitude
phi(k)=ph;       % Each harmonic phase angle
bnn(k)=bn; end   cn1=cn(1)
phi1=phi(1) % fundamental component phasor
bco=bnn(3) % x=1:2:99; x=1:50; figure(1)
bar(x,cn,0.3) xlabel('Sampled harmonics')
ylabel('Winding Functions Harmonics Amplitude')
figure(2) bar(x,phi,0.5) grid on
xlabel('Sampled harmonics')
ylabel('Harmonic phase value(rad)')
```

Appendix H: MATLAB Coding for Winding Function Fundamental and Harmonics Components

```
 clear; clc

H=1024; % number of samples in 2*pi
dx=2*pi/H; % discretization step i =
1;
%% Phase A winding

    for teta=0:dx:6.28-dx
            if(((teta>=4.19))&(teta<=6.07)) |
(((teta>=3.99))&(teta<=4.19))
naA1(i)=-1.5;              else
naA1(i)=0;             end
theta(i) = teta;
i=i+1;     end  i = 1;
    for teta=0:dx:6.28-dx
            if(((teta>=6.07))&(teta<=6.28)) |
(((teta>=3.65))&(teta<=3.99)) | (((teta>=0))&(teta<=0.19))
naA2(i)=-1.0;              else                naA2(i)=0;
end             theta(i) = teta;             i=i+1;     end
i = 1;
    for teta=0:dx:6.28-dx
            if(((teta>=0.19))&(teta<=0.53)) |
(((teta>=3.29))&(teta<=3.65))
naA3(i)=0;              else
naA3(i)=0;             end
theta(i) = teta;
i=i+1;     end      i = 1;
    for teta=0:dx:6.28-dx
            if(((teta>=0.53))&(teta<=0.89)) |
(((teta>=2.97))&(teta<=3.29))
naA4(i)=1.0;              else
naA4(i)=0;             end
theta(i) = teta;
i=i+1;     end          i = 1;
```

```
    for teta=0:dx:6.28-dx
            if(((teta>=0.89))&(teta<=2.97))
naA5(i)=1.5;             else
naA5(i)=0;             end
theta(i) = teta;             i=i+1;     end

NaA1 = naA1-mean(naA1); NaA2 = naA2-mean(naA2); NaA3 =
naA3mean(naA3); NaA4 = naA4-mean(naA4); NaA5 = naA5-
mean(naA5);
nasumA = sum([NaA1;NaA2;NaA3;NaA4;NaA5],1);
  figure(1)

% subplot(2,1,1);
%
plot(theta,naA1,theta,naA2,theta,naA3,theta,naA4,theta,naA5);x
label('\theta [rad]'), ylabel('N_a [turns]'); axis auto
% legend('show')

% subplot(2,1,2);
plot(theta,nasumA);xlabel('Stator Circumference Angle, \theta
[rad]'), ylabel('Phase A Winding Function'); axis ([0 7 -2 2])

%% Phase B winding i
= 1;
    for teta=0:dx:6.28-dx
            if(((teta>=0))&(teta<=1.88)) |
(((teta>=6.08))&(teta<=6.28))
naB1(i)=-1.5;              else
naB1(i)=0;             end
theta(i) = teta;
i=i+1;     end
i = 1;
    for teta=0:dx:6.28-dx
            if(((teta>=1.88))&(teta<=2.28)) |
(((teta>=5.74))&(teta<=6.08))
naB2(i)=-1.0;             else
naB2(i)=0;             end
theta(i) = teta;
i=i+1;     end    i = 1;
    for teta=0:dx:6.28-dx
            if(((teta>=2.28))&(teta<=2.62)) |
(((teta>=5.38))&(teta<=5.74))
naB3(i)=0;             else
naB3(i)=0;             end
theta(i) = teta;
i=i+1;     end      i = 1;
    for teta=0:dx:6.28-dx
            if(((teta>=2.62))&(teta<=2.98)) |
```

```
(((teta>=5.06))&(teta<=5.38))
naB4(i)=1.0;              else
naB4(i)=0;             end
theta(i) = teta;
i=i+1;     end          i = 1;
    for teta=0:dx:6.28-dx
            if(((teta>=2.98))&(teta<=5.06))
naB5(i)=1.5;             else
naB5(i)=0;             end
theta(i) = teta;             i=i+1;     end

NaB1 = naB1-mean(naB1); NaB2 = naB2-mean(naB2); NaB3 =
naB3mean(naB3); NaB4 = naB4-mean(naB4); NaB5 = naB5-
mean(naB5);
nasumB = sum([NaB1;NaB2;NaB3;NaB4;NaB5],1);
 figure(2)  %
subplot(2,1,1);
%
plot(theta,naB1,theta,naB2,theta,naB3,theta,naB4,theta,naB5);x
label('\theta [rad]'), ylabel('N_b [turns]'); axis auto
% legend('show') %
subplot(2,1,2);
plot(theta,nasumB);xlabel('Stator Circumference Angle, \theta
[rad]'), ylabel('Phase B Winding Function'); axis ([0 7 -2 2
])

%% Phase C winding i
= 1;
    for teta=0:dx:6.28-dx
            if(((teta>=2.09))&(teta<=3.97)) |
(((teta>=1.89))&(teta<=2.09))
naC1(i)=-1.5;              else
naC1(i)=0;             end
theta(i) = teta;
i=i+1;     end      i = 1;
    for teta=0:dx:6.28-dx
            if(((teta>=3.97))&(teta<=4.37)) |
(((teta>=1.55))&(teta<=1.89))
naC2(i)=-1.0;              else
naC2(i)=0;             end
theta(i) = teta;
i=i+1;     end    i = 1;
    for teta=0:dx:6.28-dx
            if(((teta>=4.37))&(teta<=4.71)) |
(((teta>=1.19))&(teta<=1.55))
naC3(i)=0;              else
naC3(i)=0;             end
theta(i) = teta;
i=i+1;     end      i = 1;
```

```
    for teta=0:dx:6.28-dx
            if(((teta>=4.71))&(teta<=5.07)) |
(((teta>=0.87))&(teta<=1.19))
naC4(i)=1.0;              else
naC4(i)=0;             end
theta(i) = teta;
i=i+1;     end          i = 1;
    for teta=0:dx:6.28-dx
            if(((teta>=5.07))&(teta<=6.28)) |
(((teta>=0))&(teta<=0.87))
naC5(i)=1.5;             else
naC5(i)=0;             end
theta(i) = teta;
i=i+1;     end

NaC1 = naC1-mean(naC1); NaC2 = naC2-mean(naC2); NaC3 =
naC3mean(naC3); NaC4 = naC4-mean(naC4); NaC5 = naC5-
mean(naC5);
nasumC = sum([NaC1;NaC2;NaC3;NaC4;NaC5],1);
  figure(3)

% subplot(2,1,1);
%
plot(theta,naC1,theta,naC2,theta,naC3,theta,naC4,theta,naC5);x
label('\theta [rad]'), ylabel('N_c [turns]'); axis auto
% legend('show') %
subplot(2,1,2);
plot(theta,nasumC);xlabel('Stator Circumference Angle, \theta
[rad]'), ylabel('Phase C Winding Function'); axis ([0 7 -2 2
])

%% Phases Comparison
  figure(4)
subplot(3,1,1)

plot(theta,nasumA);xlabel('Stator Circumference Angle, \theta
[rad]'), ylabel('Phase A Winding Function'); axis auto
  subplot(3,1,2)
plot(theta,nasumB);xlabel('Stator Circumference Angle, \theta
[rad]'), ylabel('Phase B Winding Function'); axis auto
subplot(3,1,3)
plot(theta,nasumC);xlabel('Stator Circumference Angle, \theta
[rad]'), ylabel('Phase C Winding Function'); axis auto
```

Appendix I: Phase A, B and C Winding Function generated from MATLAB with Curve Fittings

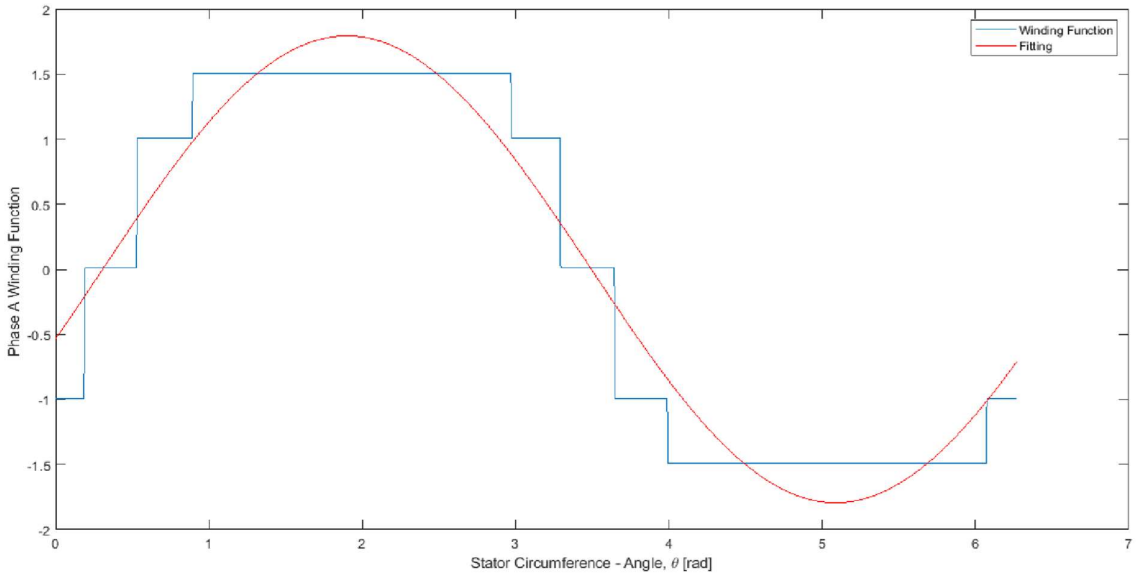

Figure I1: Phase A Winding Function

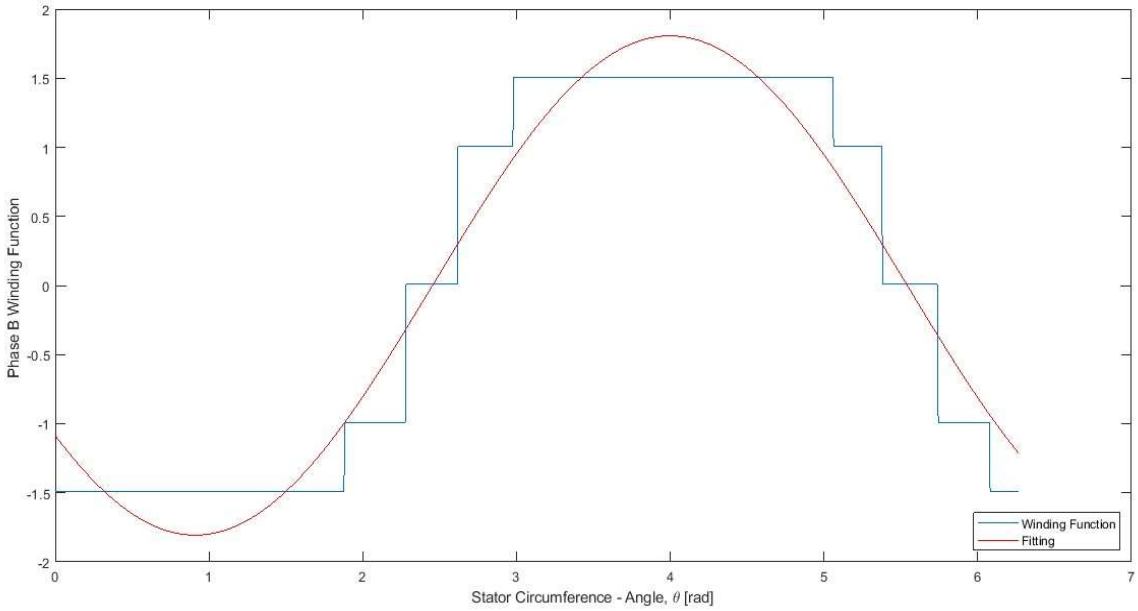

Figure I2: Phase B Winding Function

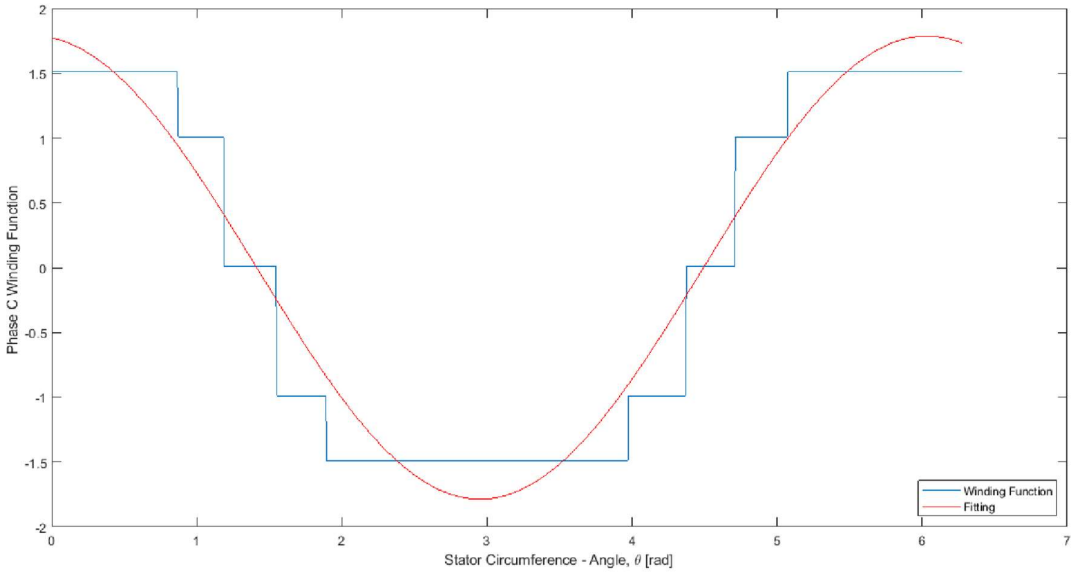

Figure I3: Phase C Winding Function

Appendix J: Fundamental and Harmonic Components of Phase A Winding Function generated from MATLAB

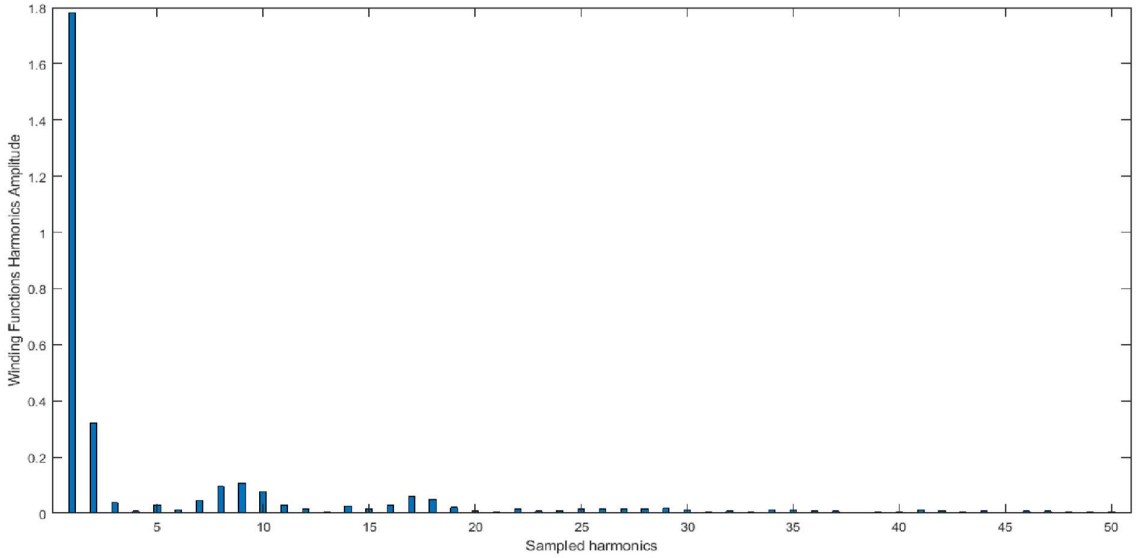

Figure J1: Phase A Fundamental and Harmonic Components

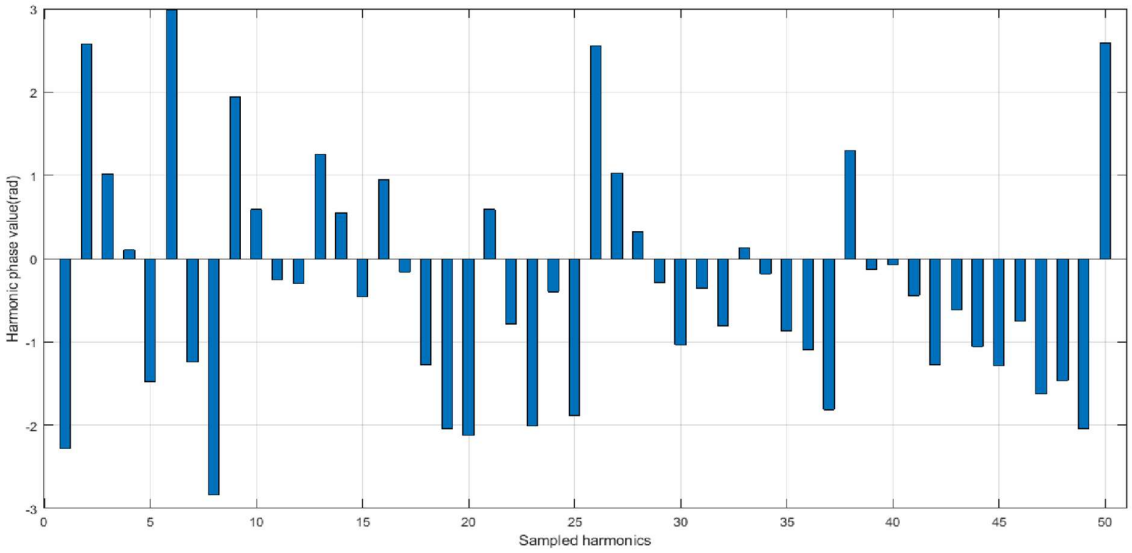

Figure J2: Phase A Phase Angles of Fundamental and Harmonics Components